The role of lipoxygenases in evasion of ferroptotic programmed cell death in ovarian cancer

Rhiannon Gould

Submitted to Swansea University in fulfilment of the requirements for the Degree of Master of Science by Research

Swansea University, 2021

Swansea University Medical School
Ysgol Feddygaeth Prifysgol Abertawe

Swansea University
Prifysgol Abertawe

Abstract

Ovarian cancer is the 6th most common cancer in women in the UK. High-grade serous ovarian carcinomas (HGSOC), the most common and aggressive subtype, account for 90% of epithelial ovarian cancers. Whilst most patients initially respond well to chemotherapy, the majority of cases will develop chemotherapy resistance upon relapse. Recent research has shown chemotherapy resistant cancers to be vulnerable to the induction of ferroptosis, an iron-dependent form of programmed cell death, characterised by the peroxidation of polyunsaturated fatty acids (PUFAs) by lipoxygenases (ALOX) to form lipid peroxides.

Niclosamide, an anthelmintic compound, has been shown to induce cytotoxicity in ovarian cancer cells via mitochondrial uncoupling leading to an increase in arachidonic acid (AA). It was hypothesised that this increase in AA provides for an increase in ALOX activity, allowing for ALOX metabolites to activate the NRF2 pathway, an important antioxidant signalling pathway. Crucial protective proteins (SLC7A11 and GPX4) from ferroptosis are confirmed targets of NRF2, suggesting that this pathway could provide resistance to ferroptotic cell death.

Cell viability data shows that Niclosamide provided resistance to SLC7A11 positive cells from both Erastin- and RSL3-induced cell death; Erastin and RSL3 are inducers of ferroptosis. Here it was confirmed that Niclosamide acts as a mitochondrial uncoupler using the Mito Stress Test. ALOX12 protein expression was implicated in some cell lines but not others, showing other ALOX isomers need to be investigated. GPX4 protein expression was consistent with cell viability data, indicating its activation as a protective mechanism. NRF2 was also shown to be affected by Niclosamide.

The significance of this project is to understand the pathways involving ferroptosis to explore and identify possible targets for novel therapies to induce ferroptosis and treat chemotherapy resistance ovarian cancers.

Declarations

DECLARATION

This work has not previously been accepted in substance for any degree and is not being concurrently submitted in candidature for any degree.

Signed ...[redacted]

Date .....25/09/2021.....

STATEMENT 1

This thesis is the result of my own investigations, except where otherwise stated. Where correction services have been used, the extent and nature of the correction is clearly marked in a footnote(s).

Other sources are acknowledged by footnotes giving explicit references. A bibliography is appended.

Signed .....[redacted]

Date .....25/09/2021.....

STATEMENT 2

I hereby give consent for my thesis, if accepted, to be available for photocopying and for inter-library loan, and for the title and summary to be made available to outside organisations.

Signed .....[redacted]

Date .....25/09/2021.....

Table of Contents

List of Figures……7

List of Tables ……9

List of Abbreviations……9

1. Introduction……11

1.1. Ovarian Cancer……11

1.1.1. Epidemiology……11

1.1.2. Diagnosis……11

1.1.3. Ovarian Cancer Subtypes……11

1.1.3.1. Endometrioid Ovarian Cancer……12

1.1.3.2. Mucinous Ovarian Cancer……12

1.1.3.3. Clear Cell Ovarian Cancer……12

1.1.3.4. Low-Grade Serous Ovarian Cancer……13

1.1.3.5. High-Grade Serous Ovarian Cancer……13

1.1.4. Risk Factors……14

1.1.4.1. Menstrual Age……14

1.1.4.2. Genetics……14

1.1.4.3. Endometriosis……15

1.1.5. Current Therapies……16

1.1.5.1. Angiogenesis Inhibitors……16

1.1.5.2. Poly(ADP-ribose) Polymerase (PARP) Inhibitors……16

1.1.6. Chemotherapy Resistance……17

1.1.6.1. Cancer Stem Cells……17

1.1.6.2. Intra-Tumour Heterogeneity……18

1.1.6.3. Epithelial-Mesenchymal Transition……19

1.2. Ferroptosis……19

1.2.1. Lipid Peroxidation……22

1.2.1.1. Non-Enzymatic Lipid Peroxidation……22

1.2.1.2. Lipoxygenase Enzymes……23

1.2.2. Iron……25

1.2.3. Inducers of Ferroptosis……26

1.2.3.1. Eradicator of RAS- and ST-Expressing Cells (Erastin)……26

1.2.3.2. RAS-Selective Lethal 3 (RSL3)……27
1.2.4. Inhibitors of Ferroptosis……28
1.2.4.1. Radical Trapping Antioxidants (RTAs)……28
1.2.4.2. Iron Chelators……29
1.2.4.3. Ferroptosis Suppressor Protein 1 (FSP1)……30
1.3. Niclosamide……31
1.3.1. Mitochondrial Uncoupling……31
1.4. Signalling Pathways……33
1.4.1. Nuclear Factor E2-Related Factor 2 (NRF2)……33
1.5. Hypothesis……36
1.5.1. Aims and Objectives……36
2. Methods……38
2.1. *In silico* Analysis……38
2.2. Cell Culture……38
2.3. MTT ((3-(4, 5-dimethylthiazol-2-yl)-2, 5-diphenyltetrazolium bromide)) assay……39
2.4. Western Blot Analysis……39
2.4.1. Protein Extraction……39
2.4.2. DC Assay- Protein Concentration……40
2.4.3. SDS-Page……40
2.4.4. Western Blotting……41
2.5. Cell Staining for Flow Cytometry……42
2.6. Flow Cytometry……43
2.7. XF Mito Stress Test……43
2.7.1. Normalisation Using CyQUANT……44
2.8. Statistical Analysis……45
3. Results……46
3.1. *In silico* Analysis……46
3.1.1. Cell lines TOV112D and SKOV3 are most and least sensitive to Niclosamide, respectively……46
3.1.2. Key genes involved in ferroptosis and their relationship with Niclosamide sensitivity ……46

3.2. *In vitro* analyses……47
3.2.1. Fer-1 had no effect on Niclosamide-induced cell death in ovarian cancer cells……47
3.2.2. Niclosamide rescues SKOV3 and TOV112D cells from Erastin-induced ferroptosis……48
3.2.3. Niclosamide rescues SKOV3 and TOV112D cells from RSL3-induced ferroptosis at 6 h……49
3.3. Western Blot Analysis……51
3.3.1. GPX4 expression is affected by Niclosamide in ovarian cancer cells……51
3.3.2. Niclosamide affects ALOX12 expression in ovarian cancer cells……53
3.3.3. NRF2 expression is affected by Niclosamide in ovarian cancer cells……56
3.4. Flow Cytometry Analysis……60
3.4.1. Niclosamide reduced lipid peroxidation in Niclosamide-sensitive cells treated with Erastin……60
3.5. XF Mito Stress Test Analysis……62
3.5.1. Niclosamide affects basal respiration in ovarian cancer cells and is a confirmed mitochondrial uncoupler……62
4. Discussion……65
4.1. Niclosamide Sensitivity……65
4.2. Niclosamide does not use non-enzymatic ferroptosis to induce cell death…66
4.3. Niclosamide rescued SLC7A11 positive cells from ferroptotic cell death……66
4.4. GPX4 protein expression increased in less Niclosamide-sensitive cells when treated with Niclosamide……67
4.5. Niclosamide increased ALOX12 expression in Niclosamide-sensitive cells……68
4.6. NRF2 expression was affected in all cell lines when treated with Niclosamide……69
4.7. Niclosamide reduced lipid peroxidation in SLC7A11 positive cell lines treated with Erastin……70
4.8. Niclosamide is a confirmed mitochondrial uncoupler and effected basal respiration of ovarian cancer cells……72
5. Conclusion……73

6. Appendix……74
7. Bibliography……89

Acknowledgments

I would like to thank Dr James Cronin for his guidance throughout this project, and Dr Nick Jones for all his help. I would also like to thank Carmen Tse, Rhiannon Beadman and the rest of the 4th Floor of ILS1 for all of their support.

List of Figures

Figure 1. The different histological sub-types of epithelial ovarian carcinomas……..12
Figure 2. Suggested mechanisms of CSCs in ovarian cancer chemotherapy resistance……18
Figure 3. The pathway of ferroptosis……..20
Figure 4. Diagram showing the reaction mechanism of GPX4……..21
Figure 5. The mechanism of non-enzymatic lipid peroxidation……23
Figure 6. The structure of mammalian lipoxygenase……..23
Figure 7. (A) The molecular structure of arachidonic acid. (B) The mechanism of ALOX15……24
Figure 8. The Fenton reaction……..25
Figure 9. Structure of Erastin……26
Figure 10. The ferroptotic pathway showing induction of ferroptosis by Erastin and RSL3……27
Figure 11. Structures of A) Ferrostatin-1 and B) Liproxstatin-1……28
Figure 12. Proposed mechanisms of RTAs, in this example, Lip-1……..29
Figure 13. The mechanism of FSP1……..31
Figure 14. A) The structure of Niclosamide. B) The structure of Dinitrophenol……32
Figure 15. Structure of NRF2……34
Figure 16. Proposed pathway induced by Niclosamide effecting ferroptotic cell death……36
Figure 17. Example gating strategy for ovarian cancer cells……..43
Figure 18. Niclosamide sensitivity across ovarian cancer cell lines……46

Figure 19. Relationships between Niclosamide sensitivity and relevant gene effects……47
Figure 20. Cell viability when treated with Niclosamide and Ferrostatin-1……48
Figure 21. Cell viability when treated with Niclosamide and Erastin……49
Figure 22. Cell viability when treated with Niclosamide and RSL3……50
Figure 23. GPX4 expression when SKOV3 cells are treated with Niclosamide and Erastin or RSL3……51
Figure 24. GPX4 expression when OVCAR3 cells are treated with Niclosamide and Erastin or RSL3……52
Figure 25. GPX4 expression when TOV112D cells are treated with Niclosamide and Erastin or RSL3……53
Figure 26. ALOX12 expression when SKOV3 cells are treated with Niclosamide and Erastin or RSL3……54
Figure 27. ALOX12 expression when OVCAR3 cells are treated with Niclosamide and Erastin or RSL3……55
Figure 28. ALOX12 expression when TOV112D cells are treated with Niclosamide and Erastin or RSL3……56
Figure 29. NRF2 expression when SKOV3 cells are treated with Niclosamide, MG-132 and Erastin or RSL3……57
Figure 30. NRF2 expression when OVCAR3 cells are treated with Niclosamide, MG-132 and Erastin or RSL3……58
Figure 31. NRF2 expression when TOV112D cells are treated with Niclosamide, MG-132 and Erastin or RSL3……59
Figure 32. Lipid peroxidation levels when cells are treated with Niclosamide and Erastin……61
Figure 33. Oxygen consumption rate when cells are treated with Niclosamide and Erastin……63

List of Tables

Table 1. Reagents used for running gels for SDS-Page……40

Table 2. Reagents used for stacking gels for SDS-Page……..41

Table 3. Antibodies used for Western Blotting……42

Table 4. Concentrations of compounds used for Mito Stress Test……44

List of Abbreviations

AA: Arachidonic Acid

ABAM: Antibiotic Antimycotic Solution

AIFM1: Apoptosis-Inducing Factor Mitochondria-Associated 1

ALOX: Arachidonate Lipoxygenase

ATP: Adenosine Triphosphate

APS: Ammonium Persulfate

ARE: Antioxidant Response Element

AR-V7: Androgen Receptor Variant 7

CaLB: Cytosolic Phospholipase A_2

CoQ_{10}-H_2: Ubiquinol

$cPLA_2$: Cytosolic Phospholipase A_2

CSC: Cancer Stem Cell

DFO: Deferoxamine

DNP: Dinitrophenol

EMT: Epithelial-Mesenchymal Transition

Erastin: Eradicator of RAS and ST-expressing Cells

FBS: Foetal Bovine Serum

FCCP: Carbonyl Cyanide-4 (trifluoromethoxy) Phenylhydrazone

Fer-1: Ferrostatin-1

FSP1: Ferroptosis Suppressor Protein 1

FTH1: Ferritin Heavy Chain 1

GPX4: Glutathione Peroxidase 4

GSH: Glutathione

GSTA2: Glutathione S-Transferase A2

HGSOC: High Grade Serous Ovarian Carcinoma

HETE: Hydroxyeicosatetraenoic Acid

HPETE: Hydroperoxyeicosatetraenoic Acid

IL-6: Interleukin-6

IL-8: Interleukin-8

KEAP1: Kelch-like ECH Associated Protein 1

Lip-1: Liproxstatin-1

MCP-1: Monocyte Chemoattractant Protein-1

MTT: ((3-(4,5-dimethylthiazol-2-yl)-2, 5-diphenyltetrazolium bromide))

MUFA: Monounsaturated Fatty Acid

NQO1: NADPH: Quinone Oxidoreductase I

PARP: Poly(ADP-ribose) Polymerase

PBS: Phosphate Buffered Saline

PUFA: Polyunsaturated Fatty Acid

ROS: Reactive Oxygen Species

RSL3: Ras-Selective Lethal 3

SDS: Sodium Dodecyl Sulfate

sMaf: Small Musculoaponeurotic Fibrosarcoma

STIC: Serous Tubal Intraepithelial Carcinomas

VDAC: Voltage-Dependent Anion Channel

VEGF: Vascular Endothelial Growth Factor

1. Introduction

1.1. Ovarian Cancer

1.1.1. Epidemiology

Ovarian cancer is the 6th most common cancer in women in the UK, with over 7,400 cases per year (Cancer Research UK, 2019). The UK has the second highest rate of ovarian cancer at 12.5 per 100,000 women per year (Coburn, Bray, Sherman, & Trabert, 2017). Globally, incidence rates are highest in North America and Central and Eastern Europe, and lowest in Asia and Africa (Reid, Permuth, & Sellers, 2017).

1.1.2. Diagnosis

Nearly 60% of all ovarian cancer cases in the UK are diagnosed at a late stage of disease (stages III-IV), wherein the cancer has already metastasised to surrounding organs, resulting in the current 10-year survival rate of only 35% (Cancer Research UK, 2019).

1.1.3. Ovarian Cancer Subtypes

The three main types of ovarian cancers are epithelial, mesenchymal and germ cell (Rosen et al., 2009). Epithelial ovarian cancers account for 90% of ovarian carcinomas, with the most common and aggressive subtype being high-grade serous ovarian carcinoma (HGSOC; Labidi-Galy et al., 2017; Figure 1). Other subtypes of epithelial carcinomas include low-grade serous ovarian cancer, endometrioid, mucinous and clear cell (Figure 1; Rosen et al., 2009; Vaughan et al., 2011)

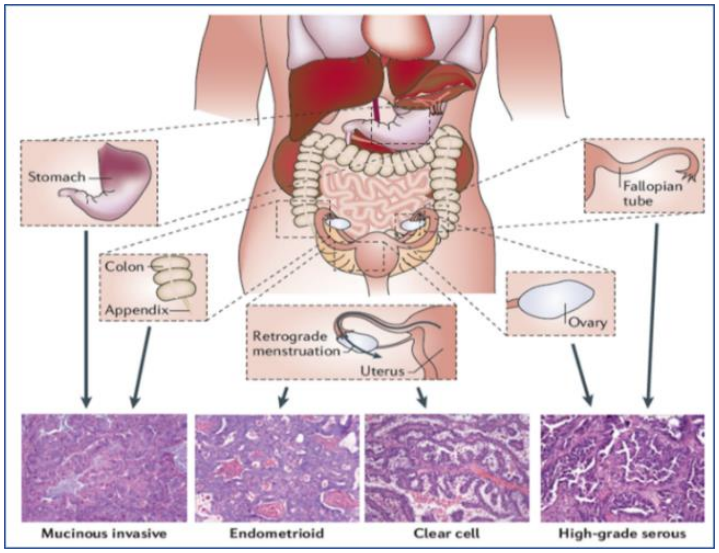

Figure 1. The different histological subtypes of epithelial ovarian carcinomas (Vaughan et al., 2011).

1.1.3.1. Endometrioid Ovarian Cancer

Many women with endometrioid ovarian cancer have a previous diagnosis of endometriosis. This type of ovarian cancer accounts for approximately 10% of all ovarian cancers (Lim et al., 2016). Endometrioid ovarian cancer is often diagnosed at early stages, therefore has a better prognosis than other subtypes (Cont et al., 2015). A common biomarker used for diagnosis is the dysregulation of β-catenin, a gene that controls signal transduction and transcription activation (Moreni-Bueno et al., 2001).

1.1.3.2. Mucinous Ovarian Cancer

Mucinous ovarian cancer can be classified as benign, borderline, or malignant and can be endocervical-like, intestinal-like or a mixture of the two. Intestinal-like epithelium are recognised by their goblet cells and are more often malignant or borderline (Tenti et al., 1992). Malignant mucinous ovarian cancer account for approximately 3% of ovarian carcinomas and 80% of these are stage I at diagnosis, leading to a better overall prognosis (Babaier & Ghatage, 2020).

1.1.3.3. Clear Cell Ovarian Cancer

Clear cell ovarian cancers account for fewer than 5% of ovarian carcinomas and are often diagnosed in early stages due to the presence of large pelvic masses (Tan &

Kaye, 2007). There is a correlation between clear cell ovarian cancer and endometriosis, but it is unclear why. There are very few *TP53* mutations in clear cell ovarian cancers, implying a p53 independent pathway is used to avoid apoptosis (Okuda et al., 2003).

1.1.3.4. Low-Grade Serous Ovarian Cancer

Low-grade serous ovarian cancers are differentiated from HGSOC by nuclear atypia and mitosis. Low-grade serous ovarian cancers have minimal nuclear atypia and mitoses are rare, while HGSOC are the opposite (Malpica et al., 2004). HGSOC commonly express mutations in *TP53* and *BRCA1/2*, while low grade serous ovarian cancers are characterised by mutations in the *KRAS* or *BRAF* pathways (Jacobs & Lancaster, 1996; Singer et al., 2003). Low-grade serous ovarian cancers are sometimes described as type I tumours as they form from adenoma to a borderline tumour, resulting in a carcinoma. Conversely, HGSOC are type II tumours and develop on the surface epithelium (Singer et al., 2005).

1.1.3.5. High-Grade Serous Ovarian Cancer

HGSOC often originate in the fallopian tube, metastasising to the ovaries (Kim et al., 2018). Serous tubal intraepithelial carcinomas (STICs) within the fallopian tube are caused by a mutation in *TP53*. Ovulation may result in the incorporation of STICs into the ovary, resulting in type II carcinomas (Labidi-Galy et al., 2017).

HGSOC can also metastasise further to the omentum (a fat rich layer that lies over the peritoneal organs) via ascites; a fluid that accumulates in the peritoneum in some ovarian cancer cases (McHutchison, 1997). This has been shown to be driven by adipokines released by the omentum such as interleukin (IL)-6, IL-8 and monocyte chemoattractant protein-1 (MCP-1). Furthermore, fatty acids released by adipocytes situated at the omentum are an energy source for ovarian tumour cells (Di Nicola, 2019; Nieman et al., 2011).

1.1.4. Risk Factors

There are a number of risk factors associated with ovarian cancer, such as age (mainly menopausal women), family history of breast and ovarian cancer, particularly due to *BRCA1* or *BRCA2* mutations, endometriosis and being overweight or obese (Cancer Research UK, 2019). The risks associated with ovarian cancer can be reduced by breast-feeding and pregnancy or contraception, resulting in a reduced rate of ovulation (Momenimovahed, Tiznobaik, Taheri, & Salehiniya, 2019).

1.1.4.1. Menstrual Age

There are conflicting studies on the effect of puberty and menopause and the risks of developing ovarian cancer, resulting in two main theories; the incessant ovulation hypothesis or the gonadotrophin hypothesis (Casagrande, Louie, Pik, Ross, & Henderson, 1979; Cramer & Welch, 1983). Incessant ovulation describes the lowered risk of ovarian cancer from anovulation, associated with lower rates of cellular division and surface epithelium repair (Casagrande et al., 1979). The gonadotrophin hypothesis highlights the increased risk of ovarian cancer from hormones such as luteinizing hormone and follicle-stimulating hormone (Cramer & Welch, 1983). Some studies show that reaching puberty later lowers risk whilst others show it increases risk (Apter & Vihko, 1983; Jordan, Webb, & Green, 2005). It is the same situation with menopause. If menopause is reached earlier, the number of ovulatory cycles decreases, reducing risk. On the other hand, if menopause is reached later, that delays the post-menopausal gonadotrophin hormones being released (Reid et al., 2017).

1.1.4.2. Genetics

The breast cancer susceptibility genes *BRCA1* and *BRCA2* both code for proteins that are involved in the DNA break repair pathway and act as tumour suppressor genes. Most *BRCA1/2* mutations in ovarian cancers are deletions or small insertions which result in frameshifts. These mutations can lead to inherited cases of ovarian cancer with the overall lifetime risk of 40-53% for *BRCA1* or 20-30% for *BRCA2* mutations, respectively (Ramus & Gayther, 2009).

Mutations in *KRAS* are common in low-grade ovarian cancers such as endometrioid and mucinous cancers. RAS molecules are involved in signalling downstream of receptors, such as the endothelial growth factor receptors, activating a mitogenic response resulting in cell proliferation and differentiation (Auner et al., 2009). A 2010 study found that *KRAS* mutations occur in approximately 25% of non-selected ovarian cancer cases (Ratner et al., 2010). *BRAF*, a downstream target of *KRAS*, codes for a RAF protein, a serine/threonine protein kinase (Turashvili et al., 2018). Mutations in this gene lead to the activation of the RAF/MEK signalling pathway which regulate carcinogenesis (El-Osta et al., 2011).

Normally, p53 regulates cell cycle arrest, apoptosis, and differentiation (Y. Zhang, Cao, Nguyen, & Lu, 2016). p53 also sensitises cells to ferroptotic cell death, a type of programmed cell death reliant on iron metabolism and lipid peroxide formation, through the suppression of amino acid antiporter SLC7A11 (Jiang et al., 2015). However, mutations in *TP53* occur in nearly all high-grade ovarian tumours at an early stage of tumour development, driving carcinogenesis possibly via avoidance of ferroptosis (Jiang et al., 2015; Y. Zhang et al., 2016).

1.1.4.3. Endometriosis

Endometriosis is a disease involving the growth of endometrium tissue in areas other than the uterine cavity. The current theory is that atypical endometriosis could be a stepping-stone to a malignant tissue, implying that endometriosis could be a pre-malignant condition. Ovarian cancers are present in 5-10% of endometriosis cases. The proposed mechanisms of transformation from endometriosis to ovarian cancer include genomic alterations, oxidative stress and inflammatory processes (Kralickova, Lagana, Ghezzi, & Vetvicka, 2020). Clear cell ovarian cancers are thought to arise through the haemorrhages that are caused by endometriosis providing more iron, leading to an increase in oxidative stress and therefore more genetic mutations (Brilhante et al., 2017).

1.1.5. Current therapies

The current standard therapy for ovarian cancer involves surgical debulking and platinum-based chemotherapy. Debulking may include a hysterectomy, oophorectomy or an omentectomy depending on the stage of the cancer. The aim is to remove all of the tumour to improve patient survival, however in late stages this is not always possible (du Bois et al., 2009). After surgery, patients are treated with platinum/taxane regimes. The tumour is then reassessed and interval debulking surgery can be performed before continuing with chemotherapy (Basta et al., 2015). This method does lead to a complete response in most patients, however many will relapse (Foley, Rauh-Hain, Del Carmen, & Marcela, 2013).

1.1.5.1. Angiogenesis Inhibitors

Angiogenesis inhibitors have been found to successfully treat epithelial ovarian cancers by inhibiting vascular endothelial growth factor (VEGF) and its receptors. This was thought to cause tumour shrinkage, although they may also facilitate drug delivery through normalisation of vasculature (Jain, 2014). These drugs include VEGF inhibitor bevacizumab and VEGF receptor inhibitors cediranib, pazopanib and nintedanib. However, these drugs are not economically viable and have a higher degree of side effects than standard chemotherapy (Cortez, Tudrej, Kujawa, & Lisowska, 2018).

1.1.5.2. Poly(ADP-ribose) Polymerase (PARP) Inhibitors

PARP inhibitors have been found to cause DNA damage and cell death in *BRCA1/2* mutated cancer cells. This is due to the synthetic lethality where two genetic mutations are harmless when they occur separately but are lethal when combined. PARPs are a family of enzymes who have a wide variety of functions. PARP1 and PARP2 are involved in DNA repair and inhibiting these PARPs has been found to induce cancer cell death (Yap, Shandu, Carden, & de Bono, 2011). PARP inhibitors include olaparib and niraparib (J. F. Liu, Konstantinopoulos, & Matulonis, 2014). These have become a standard of care for individuals with *BRCA* mutations; however,

new therapies need to be developed as only 5-15% of all ovarian cancer cases have *BRCA* mutations (Ramus & Gayther, 2009).

All these therapies are promising; however, novel therapies need to be developed that could be applied to a wider number of patients with more tolerable side effects.

1.1.6. Chemotherapy Resistance

Ovarian cancer patients initially respond well to chemotherapy, however the majority often relapse within 18 months, commonly with therapy-resistant disease, particularly patients with HGSOC (Kurman & Shih, 2010). Chemotherapy resistance in ovarian cancer is mostly due to cancer stem cells (CSCs), intra-tumour heterogeneity and epithelial-mesenchymal transition (EMT) (Testa, Petrucci, Pasquini, Castelli, & Pelosi, 2018).

1.1.6.1. Cancer Stem Cells

The current CSC model shows that differentiated cells can de-differentiate into CSCs, acquiring the ability to self-renew (Friedmann-Morvinski & Verma, 2014). CSCs have the ability to repair their DNA and persist as inactive dormant cells with asymmetric cell division which brings about relapse in patients (Markowska, Sajdak, Huczyński, Rehlis, & Markowska, 2018). The markers used to identify CSCs in ovarian cancers include CD44, CD133, CD177, CD24, ALDH1A1 and EpCAM. A correlation has been found between the presence of these markers and chemotherapy resistant tumours (Meng et al., 2012; Silva et al., 2011; J. Zhang et al., 2012). These CSCs can regenerate into tumours that are metastatically aggressive and chemotherapy resistant after first line therapy. The mechanism of this resistance is not yet fully understood. Although, it is thought to involve the CSC's slow proliferation rate, their effective DNA repair and protection, and altered stem cell signalling pathways (Deng et al., 2016; Figure 2).

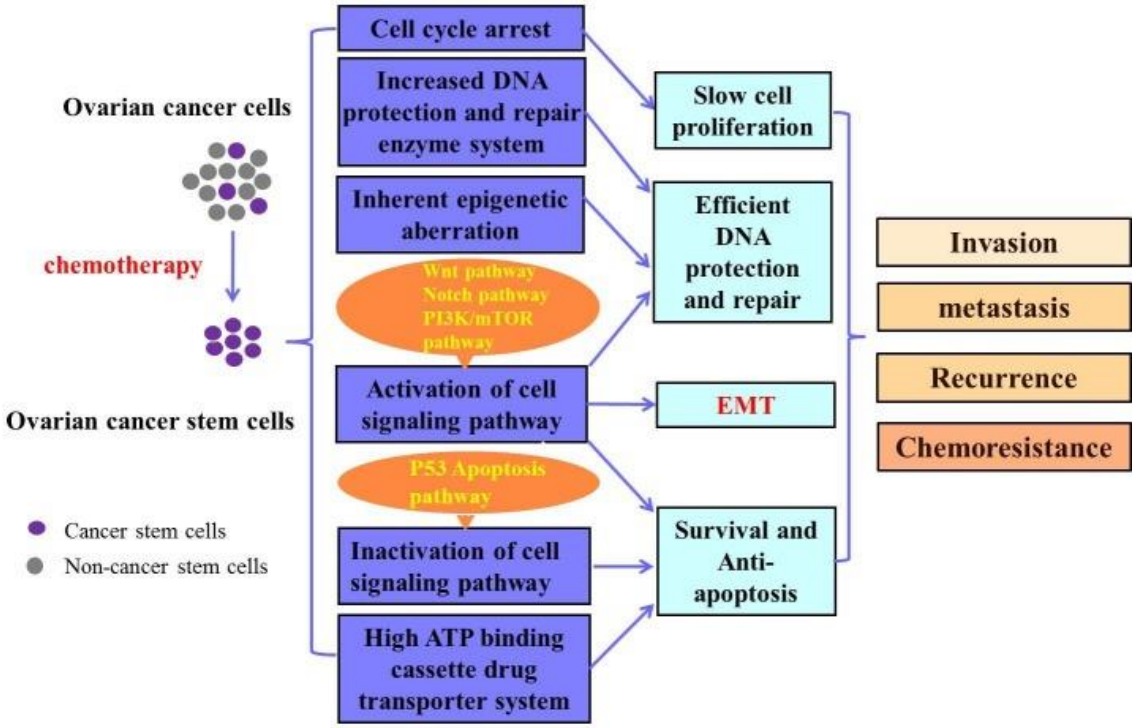

Figure 2. Suggested mechanisms of CSCs in ovarian cancer chemotherapy resistance (Deng et al., 2016). Chemotherapy fails to kill cancer stem cells allowing for a recurrence in disease. The shown attributes of CSCs all contribute to their progression and resistance to chemotherapy.

1.1.6.2. Intra-Tumour Heterogeneity

CSCs are only a small sub-set of cell types in ovarian cancers due to intra-tumour heterogeneity. Intra-tumour heterogeneity is the variability of the ovarian cancer cells' genome in the same patient. These genomic changes are due to chromosomal instability leading to ploidal changes and structural rearrangements (Bayani et al., 2008). This variability can change within different regions of the body (spatially due to metastasis) or over time (Bashashati et al., 2013). This is caused by tumour evolution leading to the development of resistant tumours following chemotherapy. Variability can also be a result of CSCs and can also be influenced by different tumour microenvironments within the body. For example the omentum provides elevated levels of adipocytes and adipokines, which lead to an increase in proliferation, migration and therapy resistance (Nowicka et al., 2013).

1.1.6.3. Epithelial-Mesenchymal Transition

Epithelial-Mesenchymal Transition (EMT) is associated with chemotherapy resistance in ovarian cancer. EMT involves the epithelial cells developing mesenchymal characteristics, allowing the cells to move through the extracellular matrix and settle in new areas. EMT is key to wound healing, stem cell behaviour and cancer progression (Lamouille, Xu, & Derynck, 2014). Chemoresistance and EMT share many markers in ovarian cancer (Haslehurst et al., 2012). The full mechanisms for EMT involvement in chemoresistance have yet to be discovered; however, SLUG and SNAIL signalling pathways (markers of EMT) have been shown to allow the development of CSC like properties in ovarian cancer, reducing p53-mediated apoptotic programmed cells death (Kurrey et al., 2009).

Therapy-resistant ovarian cancer cells have also been shown to be vulnerable to the induction of ferroptosis, a newly described form of non-apoptotic programmed cell death, potentially providing the opportunity to find novel therapies for chemotherapy resistant cancers (Dixon et al., 2012).

1.2. Ferroptosis

Ferroptosis is an iron-dependent programmed cell death characterised by the accumulation of toxic lipid peroxides. Tumour cells are able to evade ferroptotic cell death by upregulating glutathione peroxidase 4 (GPX4), an enzyme that converts toxic lipid peroxides to their non-toxic alcohol equivalents. System Xc^- is a cystine/glutamate antiporter, providing cysteine for the synthesis of glutathione (GSH), a cofactor of GPX4 to eliminate lipid peroxides (Figure 3; Dixon et al., 2012).

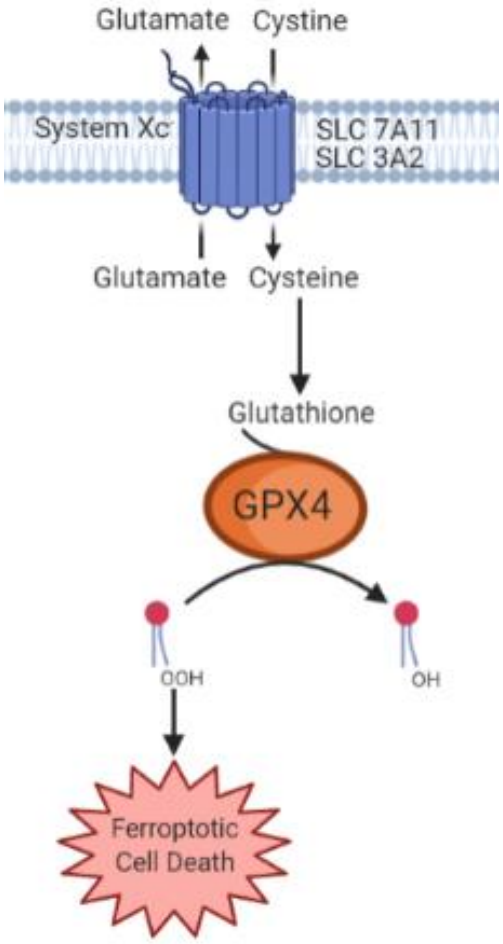

Figure 3. GPX4 is utilised by cells to evade Ferroptosis as it converts the toxic-lipid peroxides to non-toxic lipid alcohols. System Xc^- is a key antiporter involved in GPX4 regulation as it transports the cysteine into the cell which is crucial in the formation of glutathione, a co-factor of GPX4.

GPX4 is part of the glutathione peroxidase family which catalyse reduction of various peroxide groups, protecting cells from oxidative stress. GPX4 has a preference for lipid hydroperoxides, protecting cells from excessive lipid peroxidation in the membrane, which could lead to cell death (Li et al., 2018). The *GPX4* gene contains a UGA codon which translates to a selenocysteine active site. This is a rare amino acid as UGA usually acts as a stop codon; however, in this case it does not due to the conserved stem-loop structure (Latreche, Duhieu, Touat-Hamici, Jean-Jean, & Chavatte, 2012). GPX4 is essential to life due to its reducing abilities with GSH being the reducing cofactor of GPX4. The cationic area of GPX4 undergoes electrostatic binding to polar heads of phospholipids in the plasma membrane. The hydroxy groups of the phospholipids then interact with the active site of GPX4. Redox

reactions then produce two -OH groups that face each other and allow access for GSH to the active site. A second GSH molecule is brought in due to a disulfide bond that undocks GPX4 from the membrane surface. The oxidation of both GSH reducing agents displaces the peroxidase and regenerates the reduced catalyst (Figure 4; Cozza et al., 2017).

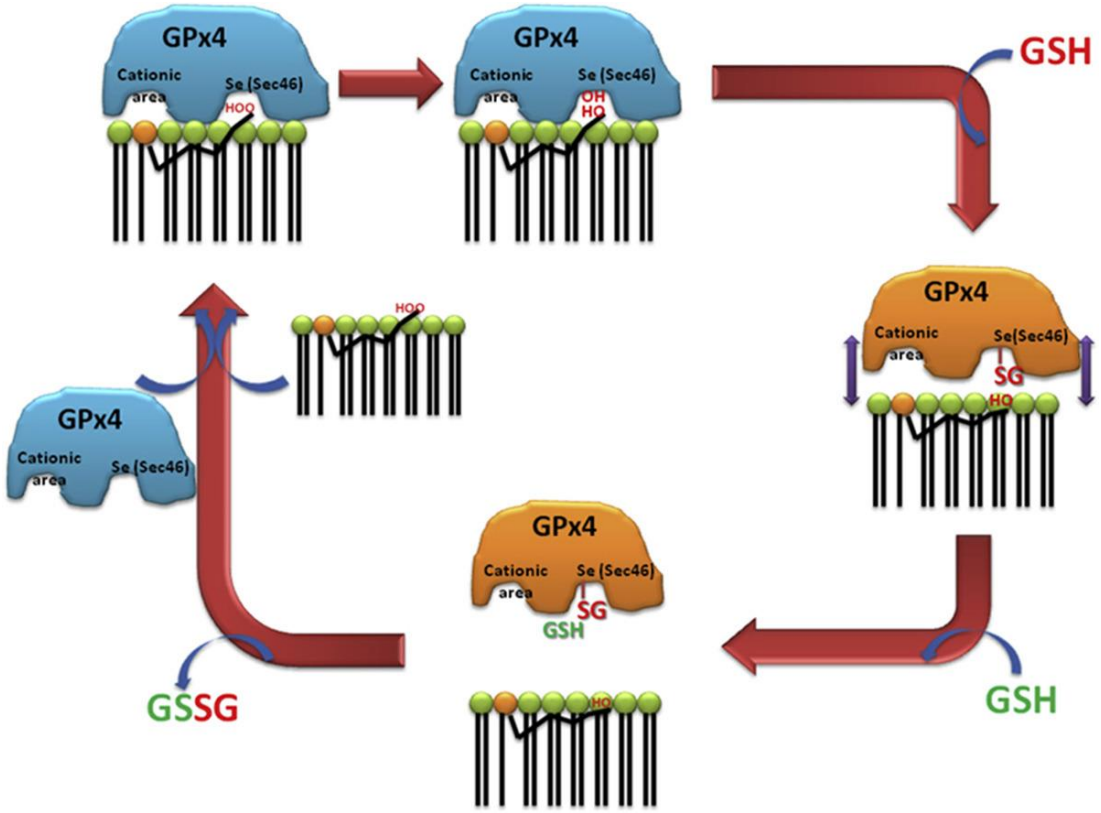

Figure 4. Diagram showing the reaction mechanism for the reduction of phospholipids by GPX4 (Cozza et al., 2017). GPX4 binds to the membrane, interacting with the hydroxy group of the phospholipids. Glutathione acts as a reducing cofactor, producing an alcohol group and allowing for the generation of the reduced form of GPX4. Abbrev: GS, SG; glutathione, GSSG; glutathione disulfide Sec; selenocysteine, OH; hydroxy group, OOH; peroxy group.

System Xc^- is an amino acid antiporter that is found in plasma membranes of mammalian cells. There is an exchange of cystine entering the cell and glutamate exiting the cell at a ratio of 1:1 (Bannai, 1986). The cystine that is imported is rapidly reduced to cysteine which is then used for protein and GSH synthesis (Christensen, 1990). This GSH can then be utilised as a cofactor for GPX4.

1.2.1. Lipid Peroxidation

Lipid peroxidation is the degradation of lipids by radicals, most often hydroxyl or hydroperoxyl (Ayala, Munoz, & Arguelles, 2014). Lipids that contain polyunsaturated fatty acids (PUFAs), such as arachidonic acid (AA), are more susceptible to lipid peroxidation than those with monounsaturated fatty acids (MUFAs) due to the bis-allylic hydrogen atoms (Gaschler & Stockwell, 2017). MUFAs do not have bisallylic carbons where the hydrogen is easily abstracted. This explains why PUFAs are the family of lipids that are most heavily involved in ferroptosis. The production of lipid peroxides by ferroptosis is lethal to cells due to the breakdown of lipids in the cell and mitochondrial membranes (Conrad et al., 2018; Yang et al., 2016). A 2019 study showed that MUFAs actually provide resistance to cells from ferroptosis by displacing PUFAs in the plasma membrane, allowing for less peroxidation, and therefore damage, within the membrane (Magtanong et al., 2019).

1.2.1.1. Non-Enzymatic Lipid Peroxidation

There are three steps in non-enzymatic lipid peroxidation: initiation, propagation, and termination. Initiation is the formation of a carbon-centred lipid radical on the allylic carbon using a prooxidant to abstract the hydrogen. During propagation, the lipid radical reacts with oxygen to form a lipid peroxy radical which in turn takes a hydrogen from another allylic carbon from another lipid, propagating the chain and producing another lipid radical and a lipid hydroperoxide. Termination involves antioxidants donating hydrogens to the lipid peroxy radical, forming an antioxidant radical that reacts with lipid peroxy radical to form a nonradical product (Figure 5; Ayala et al., 2014; Yin, Xu, & Porter, 2011).

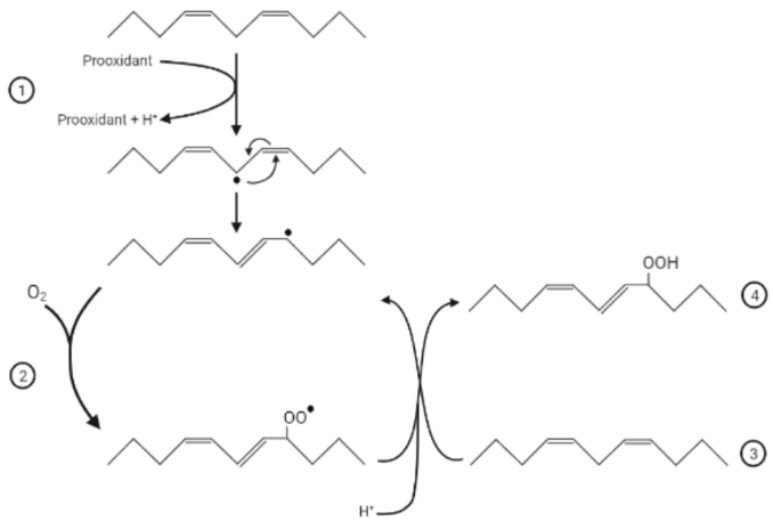

Figure 5. The mechanism of lipid peroxidation, showing (1) initiation, (2,3) propagation and (4) termination. During initiation, the radical is stabilised by forming a conjugate diene due to rearrangement. This means when the peroxyl radical is formed during propagation, the peroxyl group attaches to C_4.

1.2.1.2. Lipoxygenase Enzymes

Lipid peroxidation can also be catalysed by lipoxygenase enzymes. Lipoxygenase enzymes have a conserved core (Figure 6), with additional groups that lead to specificity (Newcomer & Brash, 2015). Lipoxygenase enzymes are found in mammals, plants, and bacteria. Plant lipoxygenases are the largest while bacteria are the smallest as they lack a terminal amino beta barrel (Mashima & Okuyama, 2015).

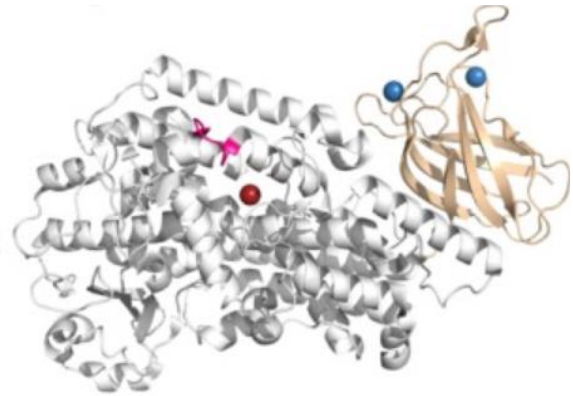

Figure 6. The structure of mammalian lipoxygenase. The helices form the surrounding of the iron-containing active site. A terminal amino beta-barrel (beige) possibly contains Ca^{2+} binding sites. The pink alpha helix forms an arch over the active site in red (Newcomer & Brash, 2015).

In humans, there are six variations of arachidonate lipoxygenase (ALOX) enzymes; ALOX5, ALOX12, ALOX12B, ALOX15, ALOX15B and ALOXE3. The most researched and prevalent of these enzymes are ALOX5, ALOX12 and ALOX15. The generalised mechanism of ALOX involves the abstraction of hydrogen by iron at the catalytic site and the addition of a peroxyl group (Kuhn, Banthiya, & van Leyen, 2014).

The active site of the enzyme acts upon the bis-allylic carbons, similar to non-enzymatic peroxidation. Specificity between the different ALOX enzymes depends on which carbon the hydrogen is abstracted from. For example, ALOX15 can produce 15-hydroperoxy-5,8,11,13-eicosatetraenoic acid (15-HPETE) as well as 12-Hydroperoxy-5,8,10,14-eicosatetraenoic acid (12-HPETE), but to a lesser extent. This is due to the non-haem iron being in close proximity to both C13 and C10 bis-allylic carbons in AA. More 15-HPETE is produced as the iron is closer to C13 (Ivanov, Kuhn, & Heydeck, 2015; Figure 7).

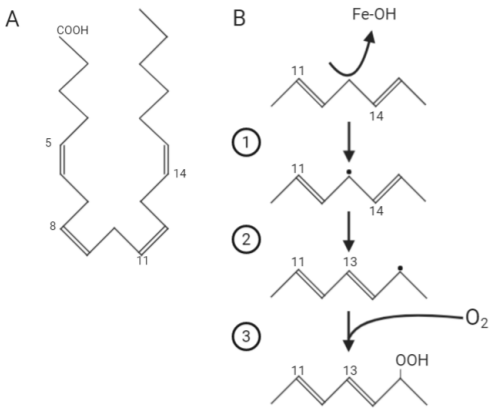

Figure 7. (A) The molecular structure of arachidonic acid. (B) The mechanism of ALOX15: 1) The iron group of the enzyme abstracts a H, forming a radical; 2) +2 radical rearrangement occurs; 3) The peroxyl group is added at C15 forming 15-HPETE. For the formation of 12-HPETE, the same mechanism occurs however the H is abstracted from C10.

It has been shown that lipoxygenase enzymes, including ALOX12, are involved in ferroptosis. This study showed that ALOX12 is required for p53-mediated ferroptosis as p53 downregulates SLC7A11 which binds to ALOX12, repressing its enzymatic function. The downregulation of SLC7A11 allows for more ALOX12 activity, thus

increasing ferroptotic cell death (Chu et al., 2019). Another study showed that both ALOX12 and ALOX15 were utilised during Erastin- and RSL3-induced ferroptosis. This was shown by using ALOX12/15 inhibitors which prevented cell death induced by Erastin and RSL3 (Shintoku et al., 2017). Based on this data, it was decided that ALOX12 was to be investigated during this project as it is involved in both p53-mediated and Erastin- and RSL3-induced ferroptosis.

1.2.2. Iron

Ferroptosis is an iron-dependent process. As previously discussed, the lipoxygenase enzymes contain an iron group; however, there is still much to learn with regards to how free cellular iron affects ferroptotic cell death.

Iron is required for non-enzymatic lipid peroxidation to provide reactive oxygen species (ROS) such as hydroxyl radicals from the Fenton reaction (Figure 8; Latunde-Dada, 2017). The Fenton reaction involves the production of hydroxyl and hydroperoxyl radicals from hydrogen peroxide (H_2O_2) and a ferrous ion (Fe^{2+}). The ROS produced from these iron-dependent reactions can initiate lipid peroxidation by acting as a pro-oxidant (Ayala et al., 2014).

$$H_2O_2 + Fe^{2+} \longrightarrow HO^{\bullet} + HO^{-} + Fe^{3+}$$

$$Fe^{3+} + H_2O_2 \longrightarrow Fe^{2+} + HOO^{\bullet} + H^{+}$$

Figure 8. Fenton reaction. Iron dependent production of hydroxyl and hydroperoxyl radicals.

Cellular iron homeostasis has also been showed to be involved in ferroptosis. The genetic inhibition of ferritin heavy chain 1 (FTH1), a protein that stores excess iron, has been shown to promote Erastin-induced ferroptosis, and expression of FTH1 was upregulated in response to Erastin (Sun et al., 2016). It has also been demonstrated that an increase in the expression of transferrin receptor 1 and a decrease in the

expression of ferritin occurs in ferroptosis sensitive cells. This implies that there is an abundance of free cellular iron in ferroptotic cells (Yang & Stockwell, 2008).

1.2.3. Inducers of Ferroptosis

1.2.3.1. Eradicator of RAS- and ST-Expressing Cells (Erastin)

Erastin was first discovered in 2003 and, as the name suggests, selectively kills tumour cells that express RAS and ST proteins (Figure 3; Dolma, Lessnick, Hahn, & Stockwell, 2003). It was this discovery that led to the detection of ferroptosis as it was seen that Erastin caused a non-apoptotic cell death (Yang & Stockwell, 2008).

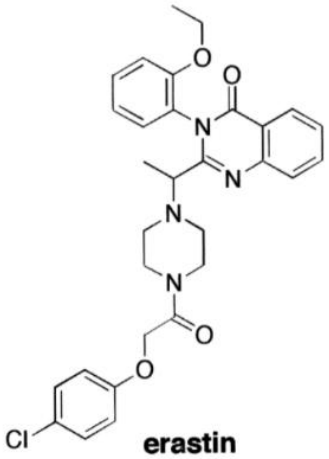

Figure 9. Structure of Erastin (Dolma et al., 2003).

Erastin induces ferroptosis by inhibiting System Xc^- (Dixon et al., 2012). System Xc^- is a disulfide-linked heterodimer made up of the components SLC7A11 and SLC3A2 (H. Sato, Tamba, & Bannai, 1999). SLC7A11 is the component that gives System Xc^- its specificity as an amino acid transporter, and it is this component that Erastin directly inhibits (M. Sato et al., 2018). This inhibition decreases cystine import, and therefore GSH synthesis, leading to reduced GPX4 activation. This indirect inhibition of GPX4 leads to build up of toxic lipid peroxides and ferroptotic cell death.

Erastin is also associated with the opening of voltage-dependent anion channels (VDAC). VDAC are a family of intramembrane protein channels that are involved in metabolic flux and signal transduction (Colombini, 2004). It has been shown that Erastin also binds directly to VDAC2 (Yagoda et al., 2007). This binding of Erastin to

VDAC has also been shown to antagonise the inhibition of VDAC by tubulin. The role of Erastin opening VDAC and increasing mitochondrial metabolism and therefore ROS production can lead to cell death (DeHart et al., 2018)

1.2.3.2. Ras-Selective Lethal 3 (RSL3)

RSL3 directly inhibits GPX4, resulting in the accumulation of toxic lipid peroxides and consequently ferroptotic cell death (Sui et al., 2018). The chloroacetamide group on (1S, 3R)-RSL3 diastereomer covalently binds to the nucleophilic selenocysteine active site of GPX4. Alternative diastereomers of RSL3 such as (1R, 3R) are inactive as an inhibitor of GPX4 (Yang et al., 2016).

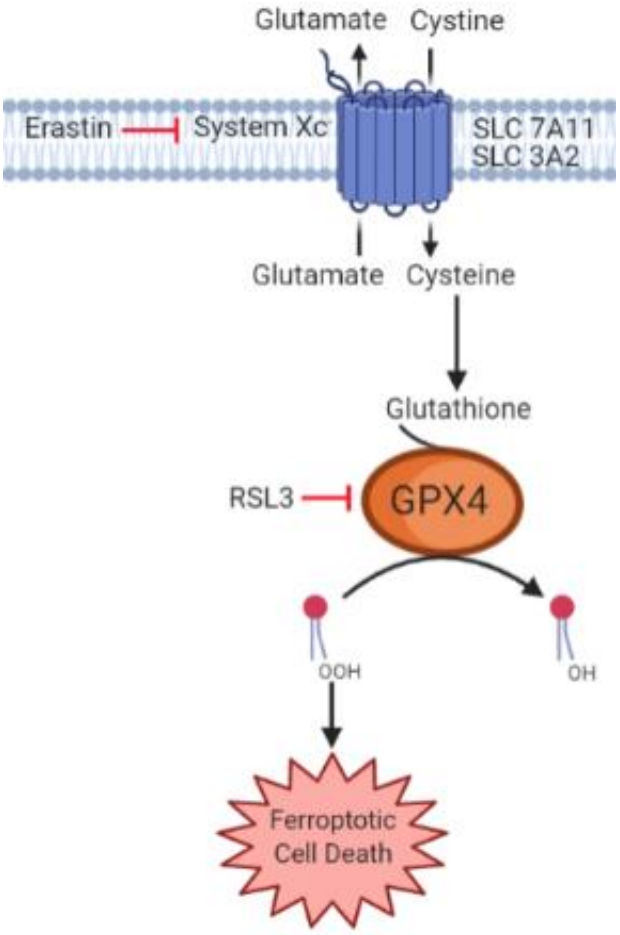

Figure 10. The ferroptotic pathway showing induction of ferroptosis by Erastin and RSL3. RSL3 directly induces ferroptotic cell death by the direct inhibition of GPX4, while Erastin induces ferroptosis by inhibiting System Xc^-, preventing the synthesis of glutathione that acts as an essential cofactor of GPX4. This inhibition of GPX4 leads to the accumulation of toxic lipid peroxides, causing ferroptotic cell death.

1.2.4. Inhibitors of Ferroptosis

1.2.4.1. Radical Trapping Antioxidants (RTAs)

Ferroptosis can be inhibited using radical trapping antioxidants (RTAs), such as the small molecules Ferrostatin-1 (Fer-1) and Liproxstatin-1 (Lip-1; Figure 11; Angeli et al., 2014; Dixon et al., 2012). This is due to their ability to inhibit lipid peroxidation directly by trapping chain-carrying radicals, as they are arylamines making them weak H bond donors, therefore they are more reactive to radicals (Skouta et al., 2014).

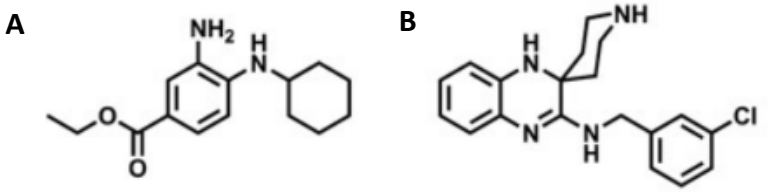

Figure 11. Structures of A) Ferrostatin-1 and B) Liproxstatin-1 (Zilka et al., 2017).

The current proposed mechanism of RTAs involves the abstraction of a hydrogen atom from the RTA by a peroxyl radical (Figure 12). The aminyl radical intermediate that is produced then reacts with a second peroxyl radical to produce an alkoxyl radical containing nitroxide. This nitroxide can trap radicals in a catalytic way. It reacts with a third peroxyl radical to produce an oxoammonium ion which then reacts with an alkyl radical to renew the nitroxide (Zilka et al., 2017).

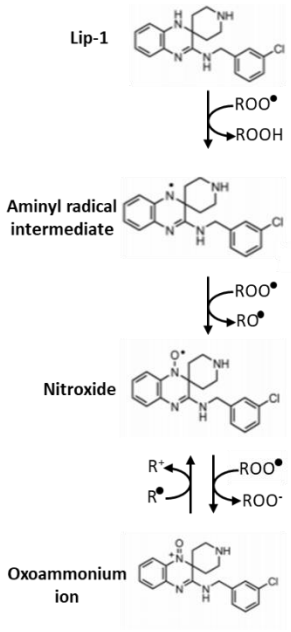

Figure 12. Proposed mechanisms of RTAs, in this example, Liproxstatin-1. A peroxyl radical abstracts hydrogen from Lip-1. A second peroxyl radical then reacts with the intermediate compound to produce a nitroxide which has the ability to act as a regenerative catalyst in order to trap radicals.

Fer-1 and Lip-1 were only effective in inhibiting non-enzymatic peroxidation, and had nearly no effect on ALOX15, showing non-enzymatic peroxidation has a role in ferroptosis (Zilka et al., 2017).

1.2.4.2. Iron Chelators

As an iron-dependent mechanism, it has been shown that iron chelators such as deferoxamine (DFO) and ciclopirox (CPX) can inhibit ferroptosis. This is achieved by decreasing the amount of iron available for both non-enzymatic and enzymatic lipid peroxidation, which are iron-dependent mechanisms (Stockwell et al., 2017).

DFO is a hexadentate allowing for a 1:1 binding ratio between iron and DFO and allows for an increased excretion of iron through urine (Naser et al., 2016). DFO is membrane impermeable and chelates lysosomal iron as it enters the cell via endocytosis (Hao et al., 2018). It has been shown that lysosomal iron accounts for the majority of free cellular iron. This leads to a reduction in iron that would be used to make lipid-based ROS. However, due to DFO being impermeable to membranes, it can act as an iron sink and cause autophagy (Kurz, Gustafsson, & Brunk, 2006).

CPX is a lipophilic chelator so can cross membranes and chelate iron in the labile pool. This means it can chelate free iron and reduce the level of iron available for lipid peroxidation and, due to the lipophilic nature of CPX, it doesn't stay in cells for long as it can move freely across the membranes. This means once it has chelated the redox-active iron it can leave the cell without causing any extra oxidative stress, unlike DFO (Kurz et al., 2006).

1.2.4.3. Ferroptosis Suppressor Protein 1 (FSP1)

FSP1, previously known as apoptosis-inducing factor mitochondria-associated 1 (AIFM1), was renamed after it was discovered to complement the loss of GPX4 in a genetic screen. It was found that FSP1 was independent of glutathione levels as well as oxidisable fatty acid content. FSP1 has a myristoylation motif at the N terminus which appears to be essential in its ability to suppress ferroptosis due to the increased association with lipid bilayers that the myristoyl terminus provides (Doll et al., 2019). Myristoylation is the covalent addition of a 14-carbon myristoyl group from myristoyl-coenzyme A to an NH_2 terminal glycine (Borgese, Aggujaro, Carrera, Pietrini, & Bassetti, 1996). This myristoyl group anchors FSP1 to the plasma membrane to allow it to act as a ferroptosis inhibitor (Bersuker et al., 2019)

In the same study that discovered FSP1's role in ferroptosis, they showed that it prevents lipid peroxidation by reducing ubiquinone to ubiquinol using NAD(P)H as a reducing co-substrate. The ubiquinol that is generated acts as an RTA (Figure 13; Doll et al., 2019).

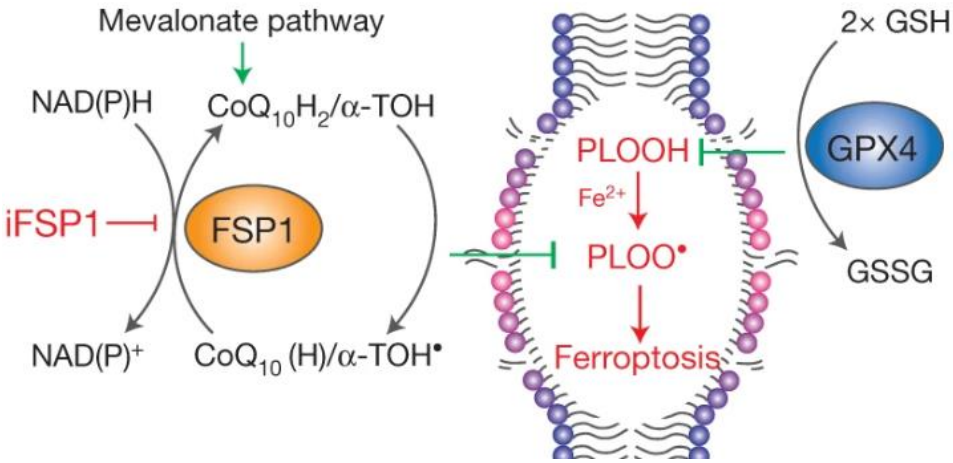

Figure 13. The mechanism of FSP1 facilitating the regeneration of ubiquinol from ubiquinone to inhibit the lipid peroxide radicals undergoing non-enzymatic peroxidation within the lipid bilayer and how this pathway is independent of GPX4 (Doll et al., 2019).

1.3. Niclosamide

Niclosamide is a chlorinated salicylanilide which acts as an antihelminth. It is currently used for the treatment of tapeworms. It is known as a STAT3 inhibitor due to its ability to degrade androgen receptor variant 7 (AR-V7) which prevents AR-V7-mediated STAT3 phosphorylation and therefore activation, preventing expression of STAT3 target genes (C. Liu et al., 2014; Ren et al., 2010). STAT3 can activate diverse targets, many of them oncogenes, including *VEGF*, *MCL1* and *MYC* (Gu, Mohammad, & Liu, 2020). This has identified STAT3 as a possible target for novel therapies, however this is not relevant to the scope of this project.

1.3.1. Mitochondrial Uncoupling

As well as a STAT3 inhibitor, Niclosamide also has the ability to cause mitochondrial uncoupling of the electron transport chain (ETC) (Tao, Zhang, Zeng, Shulman, & Jin, 2014). This is crucial to its use as a drug in the treatment of tapeworms due to the reduced production of adenosine triphosphate (ATP) and therefore disturbed metabolic function (Frayha, Smyth, Gobert, & Savel, 1997).

Mitochondrial uncoupling is the disturbance of the membrane potential across the inner mitochondrial membrane, leading to a reduction in the number of protons that

move through ATP synthase. This decreases the amount of ATP produced. It was initially thought that this was a mitochondrial dysfunction, however uncoupling has been shown to be involved with many biological processes, such as thermogenesis, protein secretion and macroautophagy (Demine, Renard, & Arnould, 2019).

Niclosamide has a similar structure, and therefore mechanism, to the uncoupling reagent 2,4 dinitrophenol (DNP) which was used as a treatment for obesity in the 1930s but was discontinued due to the occurrence of hypothermia at high doses (Frayha, Smyth, Gobert, & Savel, 1997; Paranscandola, 1974; Figure 14). DNP is a protonophore that allows the movement of protons across a membrane. The protonated form of DNP passes through the membrane as it is lipophilic and deprotonates in the mitochondrial matrix before passing back through the membrane (Blaikie et al., 2006). This reduces the membrane potential and decreases the amount of ATP being produced by protons moving through ATP synthase. It has previously been shown that Niclosamide is a proton carrier, demonstrating that it has a similar mode of action to DNP (Jurgeit et al., 2012). However, Niclosamide is a mild mitochondrial uncoupler compared to DNP (Amara et al., 2007). This is the reason Niclosamide has a much better safety profile compared to DNP.

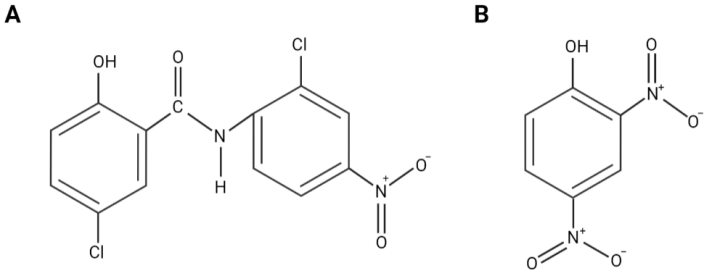

Figure 14. A) The structure of Niclosamide. B) The structure of Dinitrophenol.

Calcium is stored in the mitochondria as it is a cofactor to enzymes such as ATP synthase and dehydrogenases that lead to the production of ATP (Tarasov, Griffiths, & Rutter, 2012). Calcium flux is dependent on the membrane potential of the inner mitochondrial membrane. The decrease in membrane potential by Niclosamide leads to an efflux of Ca^{2+} into the cytosol (Horvath, Diano, & Barnstable, 2003). Ca^{2+} can be

transported across the outer mitochondrial membrane by VDAC which, as previously discussed, can be opened by Erastin (Rosencrans, Rajendran, Bezrukov, & Rostovtseva, 2021).

An increase in cytosolic calcium allows for an increase in calcium dependent phospholipid binding (CaLB) of cytosolic phospholipase A_2 ($cPLA_2$). $cPLA_2$ contains a calcium dependent 140 amino acid fragment that translocates to natural membrane vesicles. Here, $cPLA_2$ cleaves AA; $cPLA_2$ preferentially hydrolyses arachidonyl phospholipids compared to other phospholipids (Clark et al., 1991). There are two amino acids in the $cPLA_2$ structure that are required for it to be catalytically active: Ser-228 and Asp-549. Ser-228 is the nucleophilic active site while Asp-549 is part of a motif that matches catalytic aspartic acid residues in proteases (Kramer & Sharp, 1997).

The effect of mitochondrial uncoupling by Niclosamide causes this efflux of calcium into the cytosol, activating the translocation of phospholipase to membranes and producing AA (Kumar et al., 2018). It has previously been mentioned that AA is the substrate for ALOX which produces HPETEs and therefore toxic lipid peroxides. However, ALOX enzymes also have an effect on signalling pathways such as those involving Nuclear Factor E2-Related Factor 2 **(**NRF2).

1.4. Signalling Pathways

1.4.1. Nuclear Factor E2-Related Factor 2 (NRF2)

NRF2, first isolated in 1994, is a transcription factor with a basic leucine zipper DNA binding domain (Moi, Chan, Asunis, Cao, & Kan, 1994). NRF2 contains 7 distinct domains (Neh1-7), each one playing a different role in NRF2 function (Figure 15; Tonelli, Chio, & Tuveson, 2018). This signalling pathway controls the expression of genes which produce proteins that are involved in antioxidative and reducing electrophilic agents. This is a major mechanism in cellular defence (Nguyen, Nioi, & Pickett, 2009).

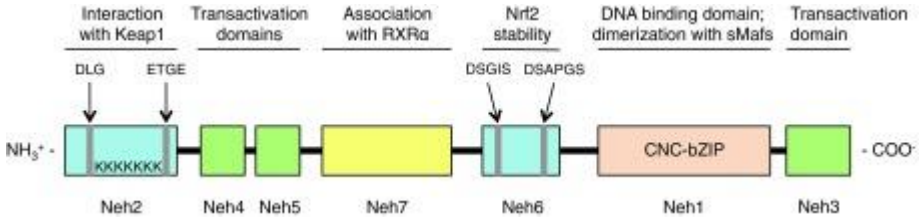

Figure 15. Structure of NRF2. Of particular note, Neh1 contains the region necessary for DNA binding and Neh2 contains amino acid sequences that mediate NRF2 regulation (Tonelli et al., 2018).

NRF2 is regulated by redox-sensitive E3 ubiquitin ligase substrate adaptor Kelch-like ECH associated protein 1 (KEAP1). The double glycine repeat domain of KEAP1 binds to the Neh2 domain of NRF2, causing a sequestering of NRF2 in the cytoplasm (Itoh et al., 1999). KEAP1 also acts as an adaptor protein for Cul3 E3 ubiquitin ligase which is responsible for the proteasomal degradation of NRF2, keeping basal levels of NRF2 low (Cullinan, Gordan, Jin, Harper, & Dielh, 2004). NRF2 activation occurs by the reaction of thiol groups with cysteine residues on KEAP1, leading to the disassociation of the KEAP1-NRF2 complex when the cell is exposed to stress such as ROS (Dinkova-Kostova et al., 2002). Upon activation and release from KEAP1, NRF2 translocates from the cytoplasm to the nucleus (Itoh et al., 1999).

Once NRF2 has reached the nucleus, it dimerizes with small musculoaponeurotic fibrosarcoma (sMaf) proteins. This heterodimer then acts as a transcription factor and binds to the antioxidant response element (ARE) which is a regulatory enhancer region within the promoting region of genes coding for proteins such as glutathione S-transferase A2 (*GSTA2*) and NADPH: quinone oxidoreductase 1 (*NQO1*), two major detoxication enzymes (Itoh et al., 1997; Nguyen et al., 2009). This response to oxidative stress controls over 200 genes involved in antioxidant and anti-inflammatory processes, not just *GSTA2* and *NQO1* (Petri, Korner, & Kiaei, 2012).

As NRF2 is activated in the presence of ROS, it was shown that the metabolic products of a lipoxygenase enzyme activated NRF2: 5-hydroxyeicosatetraenoic acid (5-HETE), a downstream metabolite of AA when broken down by ALOX5, has been shown to

induce increased nuclear translocation of NRF2 (Nagahora, Yamada, Kikuchi, Hakozaki, & Yano, 2017).

The gene encoding for SLC7A11, a sub-unit of the amino acid antiporter system Xc-, has been shown to have ARE in its promoter region (Habib, Linher-Melville, Lin, & Singh, 2015). This means that NRF2 activation leads to an upregulation of *SLC7A11*, allowing an increase in activity of System Xc^-. This in turn could increase the levels of intracellular cysteine, upregulating the synthesis of GSH, providing more cofactor for GPX4, increasing its activity. It has been found that the gene encoding for GPX4 is also regulated by NRF2. This means that, as with *SLC7A11*, if NRF2 is activated *GPX4* is upregulated allowing for an increase in GPX4 activity (Shin, Kim, Lee, & Roh, 2018). Thus, knocking down NRF2 has been shown to sensitise cells to ferroptotic cell death (Dodson, Castro-Portuguez, & Zhang, 2019).

Overall, Niclosamide may result in increased AA via mitochondrial uncoupling, providing an increase in substrate for lipoxygenase enzymes. The metabolites from these enzymes then activate NRF2, leading to an increase in *GPX4* and *SLC7A11* expression. Here, this is the proposed mechanism of rescue from ferroptosis that Niclosamide provides to ovarian cancer cells (Figure 16).

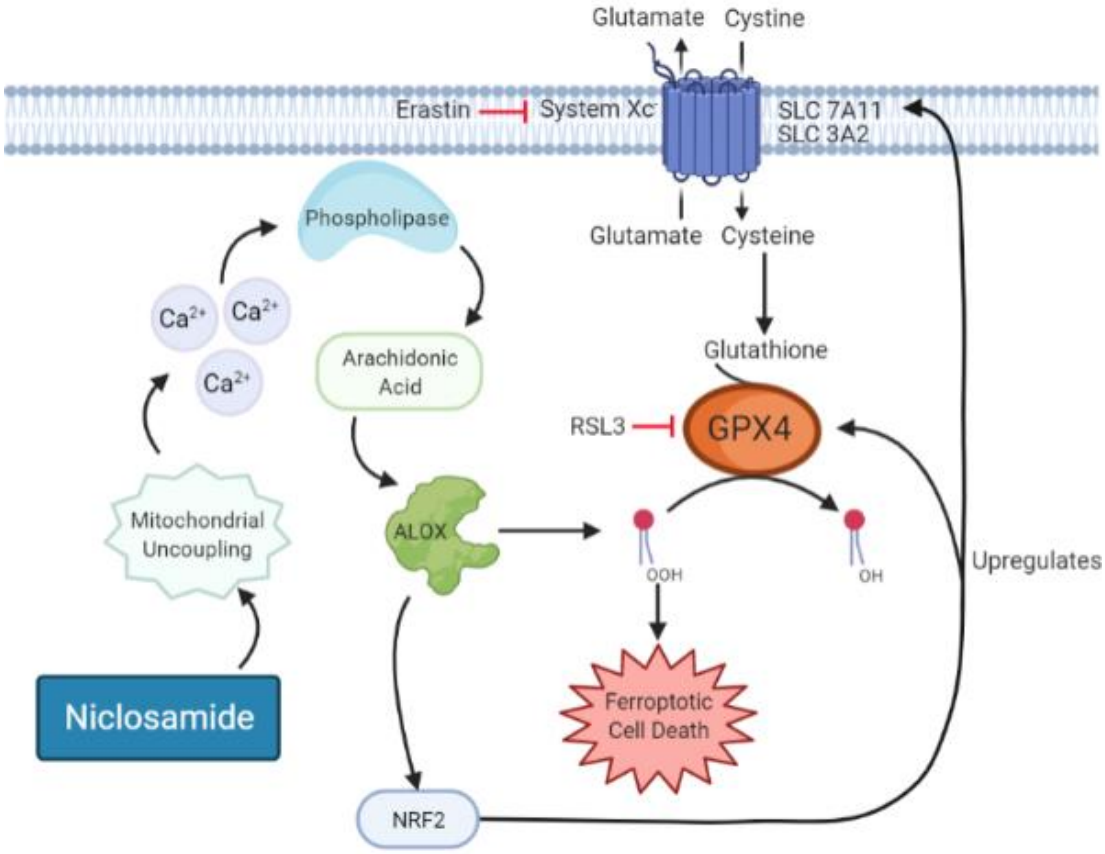

Figure 16. Proposed pathway induced by Niclosamide effecting ferroptotic cell death. Niclosamide induces mitochondrial uncoupling, causing an efflux in Ca^{2+} which allows for an increase in calcium dependent phospholipase binding, cleaving more AA from the membrane. An increase in AA causes an increase in ALOX activity which could either provide more toxic lipid peroxides, or trigger the NRF2 signalling pathway, inducing an upregulation of *GPX4* and *SLC 7A11*.

1.5. Hypothesis

Niclosamide activates the NRF2 signalling pathway via ALOX metabolites to rescue cells from Erastin- and RSL3-induced ferroptotic cell death.

1.5.1. Aims and Objectives

This project will establish the sensitivity of ovarian cancer cell lines to Niclosamide, Erastin or RSL3, and the effect these molecules on different target proteins associated with ferroptosis will be monitored. Candidate ovarian cancer cell lines will be selected using *in silico* analysis of data archived in databases, such as DepMap. Cell viability in cells treated with Niclosamide, Erastin or RSL3 will be monitored using the MTT assay. Whilst Western blotting will be utilised to assess

expression of key proteins including GPX4, ALOX12 and NRF2. To confirm that Niclosamide is acting as a mitochondrial uncoupler, the Mito Stress Test will be performed on cells treated with Niclosamide. Flow cytometry following staining with Liperfluo will be used to assess lipid peroxidation in cells treated with Niclosamide and Erastin or RSL3. The data found from these assessments should hopefully give an understanding of how these molecular pathways are linked.

2. Methods

2.1. *In silico* Analyses

Depmap, an online platform (https://depmap.org/portal/), was used to identify genetic and pharmacological dependencies in ovarian cancer cell lines relating to Niclosamide and genes that are relevant to ferroptosis. The dataset used to analyse Niclosamide sensitivity, measured in area under curve (AUC), across different cell lines was PRISM Repurposing Secondary Screen 19Q4 (Corsello et al., 2020). A second data set, DepMap 21Q2 Public CERES, was also used to compare the effect of loss of relevant genes with Niclosamide sensitivity using CRISPR data (Dempster et al., 2019; Depmap & Broad, 2021; Meyers et al., 2017). This data was collected by using CRISPR to identify the effect of loss-of-function over a wide variety of genes. The CERES method was developed to reduce the false positives produced during the Cas-9 DNA cleavage in copy number-amplified areas. It involves the use of single guide DNA depletion, copy number data and a guide activity score to calculate a more accurate gene knockout effect value (Meyers et al., 2017).

2.2. Cell Culture

Three cell lines that represent ovarian cancers were used; SKOV3, OVCAR3 and TOV112D. OVCAR3 are representative of HGSOC, while SKOV3 and TOV112D cells are representative of endometrioid carcinomas. OVCAR3 and TOV112D express a mutated *TP53* gene (Coscia et al., 2016), however the protein is not expressed in SKOV3 due to partial deletion or rearrangement in one of the alleles (Yaginuma & Westphal, 1992).

SKOV3 cells were routinely subcultured in McCoys 5A media (Gibco, Cat#26600-023), supplemented with 10% foetal bovine serum (FBS; Biosera, Cat#FB-1001/500) and 1% Antibiotic Antimycotic solution (ABAM; 100 U/ml penicillin, 0.1 mg/ml streptomycin, 0.25 µg/ml amphotericin B; Sigma, Cat#A5955-100). OVCAR3 cells were routinely subcultured in RPMI 1640 media (Gibco, Cat#31870-025) supplemented by 20% FBS, 1% ABAM, 1% L-Glutamine (Gibco, Cat#25030-024) and 0.1% insulin solution from bovine pancreas (Sigma, Cat#10516-5). TOV112D cells

were routinely subcultured in DMEM media (Gibco, Cat#41965-039) supplemented with 10% FBS and 1% ABAM.

All cell lines were maintained in an air incubator at 37°C, with 5% CO_2 and 18% O_2 and were cultured to 80% confluency in 75 cm^2 flasks (T-75; Corning, Cat#430641U) before being seeded for treatment. To avoid becoming over-confluent, cells were split every 2-3 days. This involved removing the media from the flasks, adding 5 ml of phosphate buffered saline (PBS; Gibco, Cat#10010-015), gently swirling the flask and removing the PBS. Then, 2 ml of accutase was added (Sigma, Cat#A6964-500) and the flask was incubated for 5 min. To inactivate the accutase, 8 ml of media was added then the cells were mixed to form a suspension. An appropriate volume of cell suspension was removed from the flask depending on the confluency, then media was added up to 20 ml.

Cells were treated with varying concentrations of Niclosamide (Abcam, Cat#ab120865), Erastin (Tocris Bioscience, Cat#5449), RSL3 (Selleckchem, Cat#S8155), or MG-132 (Merck, Cat#474790-1MG), as stated in *Results*.

2.3. MTT ((3-(4,5-dimethylthiazol-2-yl)-2, 5-diphenyltetrazolium bromide)) assay

Cells were seeded at $5x10^3$ cells in 100 µl media per well in a 96-well plate (TPP, Cat#92096) 24 h prior to treatment. After treatment, cells were incubated for 2 h with 50 µl of a 1 in 10 dilution of 0.5mg/ml MTT (Sigma, Cat#M2128-5) per well. The MTT was then removed and 100 µl of dimethyl sulfoxide (DMSO) was added to dissolve the formazan crystals formed. The plate was then incubated for 15 min at room temperature. Absorbance was then measured at 570 nm using the microplate spectrophotometer system; POLARstar Omega (BMG Labtech).

2.4. Western Blot Analysis

2.4.1 Protein Extraction

Cells were seeded in 3 ml of their recommended media at $5x10^4$ cells per ml in a 6-well plate (TPP, Cat#92006) 24 h prior to treatment. After treatment, supernatants

were removed, cells gently washed with PBS, and 100 µl of radioimmunoprecipitation assay (RIPA; Millipore, Cat#20-188) buffer with 0.1% protease inhibitor cocktail (PIC; Sigma, Cat#P1860-1) was added to each well. RIPA buffer was used as a lysis buffer as most of the target proteins are found in the mitochondria. The cells were then scraped and centrifuged to form a cell pellet. The waste pellet was removed leaving the protein in the supernatant.

2.4.2 DC Assay- Protein Concentration

For the DC-assay, 5 µl of BSA (Sigma, Cat#A7906) standards or the cell samples were loaded into a 96-well plate in duplicate. To each well, 25 µl of reagent A/S (2 ml/40 µl; Biorad, Cat#500-0113/Cat#500-0115) was added and subsequently 200 µl of reagent B (Biorad, Cat#500-0114). Absorbance was measured at 750 nm and a standard curve was made with an r^2 value more than 0.99.

The linear regression average for each sample in duplicate was calculated and 10 was divided by this average to find the volume of sample needed for 10 µg of protein. Equal parts of samples and 2x Laemmli buffer (Sigma, Cat#S3401-10VL) were added to a fresh PCR tube.

2.4.3. SDS-PAGE

Running gels were cast at 10% acrylamide using the reagents found in Table 1.

Table 1: Volumes of reagents used for running gels for SDS-Page.

Reagent	Volume (ml)
Water	4.2
30% Acrylamide (Sigma, Cat#A3449-100)	3.3
4 x TRIS and SDS (Separating buffer; Melford, Cat#MEL-S28100-500.0)	2.5
10% APS (Thermo, Cat#HC2005)	0.1
TEMED (Biorad, Cat#161-0800)	0.01

2-Propanol (Sigma, Cat#19516-500) was added, to ensure a clean interface between resolving and stacking gels, and the gel was left for 30 min to set. The 2-Propanol was

removed before adding the stacking gel. The stacking gel was made using the reagents found in Table 2.

Table 2: Volumes of reagents used to make stacking gels for SDS-Page.

Reagent	Volume (ml)
Water	1.75
30% Acrylamide	0.5
4 x TRIS and SDS (Stacking buffer; Melford, Cat#MEL-S28200-500.0)	0.75
10% APS	0.05
TEMED	0.003

The 15 well comb was placed in the gel and left to set for 20 min. The samples with equal parts 2x Laemmli buffer were heated at 95°C for 5 min before being loaded into the gel. The first and last lanes contained a dual colour protein ladder (Biorad, Cat#1610374). The gels were then run in 1x running buffer at 120 V for 60 min.

2.4.4. Western Blotting

After running a suitable distance, the proteins from SDS-PAGE gels were transferred onto a polyvinylidene difluoride (PVDF; Biorad, Cat#1620177) membrane using the trans-blot turbo transfer system running at 25 V for 30 min. The membrane was then placed in blocking buffer (as specified by the manufacturer) for 60 min before the primary antibody was added at the recommended dilution. The membrane was left overnight at 4°C. The membrane was then washed with TBS-Tween 3 times for 5 min each before adding the secondary antibodies in blocking buffer for 90 min at room temperature at the recommended dilution, and finally washed again. The membranes were then imaged using Image J version 2,0, after exposure with low intensity ECL solution (Biorad, Cat#170-5061). Membranes were stripped for re-probing by being placed in stripping buffer (Thermo, Cat#46430) for 10 min before being washed in dH_2O for 2 min then TBS-Tween for 5 min.

Table 3: Antibodies used during Western Blotting.

Antibody	Catalogue number
Anti-GPX4	Abcam, ab125060
Anti-ALOX12	Abcam, ab211506
Anti-NRF2	Cell Signalling Technologies, 12721S
Anti-α-tubulin	Cell Signalling Technologies, 2144S
Anti-β-actin	Abcam, ab8227
Anti-Rabbit	Cell Signalling Technologies, 7074P2

2.5. Cell Staining for Flow Cytometry

Cells were seeded in 1 ml of complete media at $5x10^4$ cells per ml in a 24 well plate (TPP, Cat#92024) 24 h prior to treatment. The positive control, cumene hydroperoxide (Sigma, Cat#247502-5) was added to one well and incubated for 2 h before the end of the treatments. Liperfluo solution was prepared by dissolving 50 µg of Liperfluo (Dojindo, Cat#L248) in 60 µl of DMSO. As Liperfluo is light sensitive it must be protected using aluminium foil and must be used within one day of preparation. The media from all wells were then changed and 5 µl of Liperfluo solution was added to each well except the blank. The cells were then incubated at 37°C for 15 min. The media was then replaced with 1 ml of PBS, to gently wash the cells, and then removed. Cells were then detached by adding 200 µl of accutase to each well and incubating the plate at 37°C for 5 min. Then, 1 ml of FACS buffer was added to each well and the suspension was transferred to FACS tubes. The tubes were centrifuged for 7 min at 290 RCF at 4°C. The supernatant was discarded, and the cells resuspended in 100 µl of FACS buffer. Then, 5 µl of a 1 in 15 dilution of DRAQ7 (Biostatus, Cat#DR71000) was added to the samples. The samples were incubated in the dark for 15 min. Then, 1 ml of FACS buffer was added to the samples before centrifugation for 10 min at 290 RCF. The FACS buffer was then removed, and the pellet was gently resuspended in 200 µl of FACS buffer. Samples were then analysed by flow cytometry.

2.6. Flow Cytometry

Median fluorescence intensity (MFI) for Liperfluo was recorded for both live cells and all cells in a sample. The viability was also calculated using DRAQ7. To assess Liperfluo MFI in live cells, dead cells were gated out using DRAQ7 data (Figure 17).

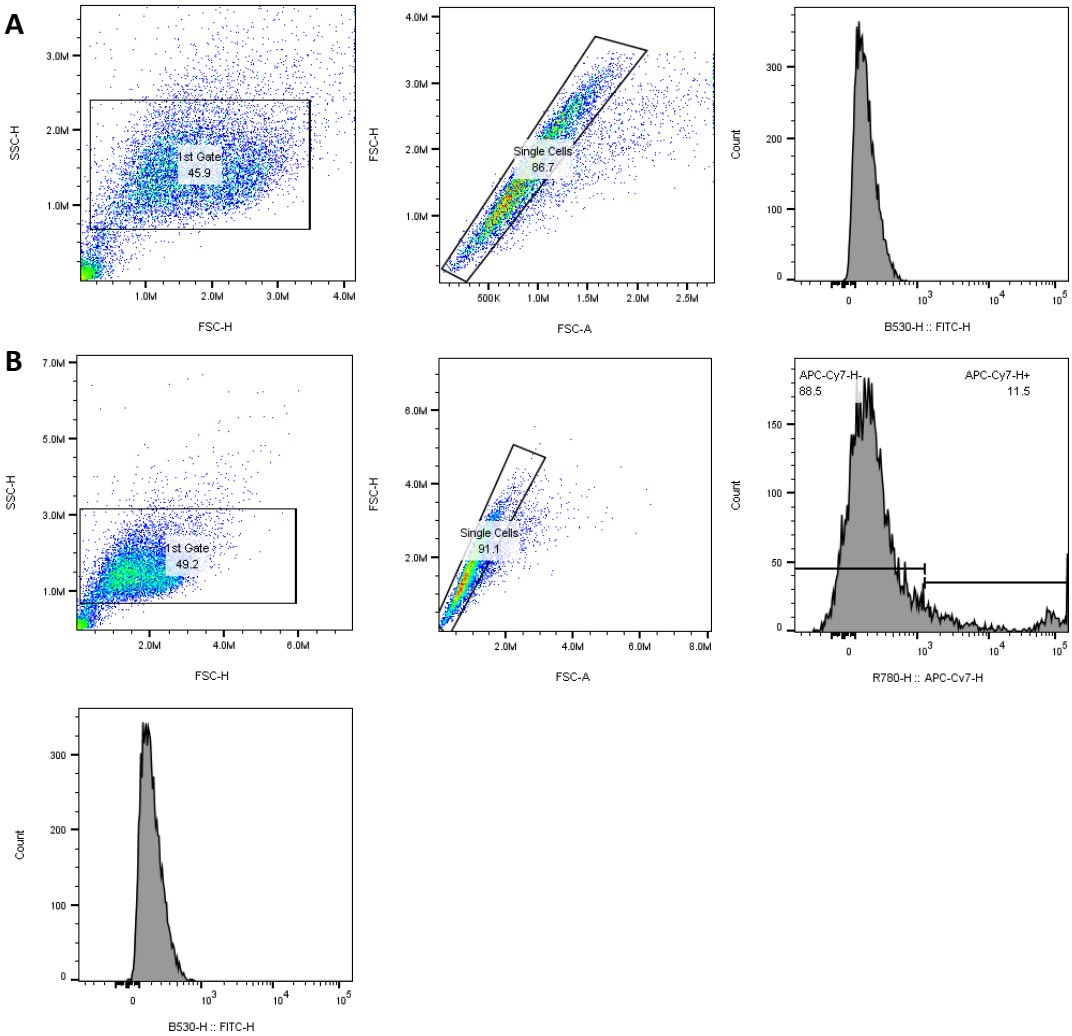

Figure 17. Example gating strategy for ovarian cancer cells. A) Gating strategy to find Liperfluo MFI for all cells. B) Gating strategy to find Liperfluo MFI for live cells.

2.7. XF Mito Stress Test

Cells were seeded in 100 µL media at a suitable density for each cell line in a 96-well plate (Agilent, Cat#101085-004) 24 h prior to treatment. The day before the assay was run 200 µl of Seahorse calibrant (Agilent, Cat#100840-000) was added to each well of a calibration plate (Agilent, Cat#102416-100) and the plate placed in a 37°C non-CO_2 incubator. The day of the assay, the Seahorse assay media (Agilent, Cat#103576-100) was supplemented with 1% 200 mM L-Glut, 0.4% Glucose (Sigma, Cat#G8769-100) and adjusted to pH 7.4. The injections oligomycin, carbonyl cyanide-

4 (trifluoromethoxy) phenylhydrazone (FCCP), rotenone and antimycin A were prepared to the manufacturer's recommended concentrations. Rotenone and antimycin A were injected together so were prepared at half volume with double concentration.

Table 4: Concentrations of compounds used for injections for the Mito Stress Test.

Compounds	Well Volume (µl)	Injection Volume (µl)	Working Concentration (µM)	Final Concentration (µM)
Oligomycin	150	25	17.5	2.5
FCCP	175	25	16	2
Rotenone	200	25	18	1
Antimycin A	225	25	18	1

The growth media was replaced with pre-warmed assay media and the Seahorse plate was incubated in a 37°C non-CO_2 incubator for 45-60 min. Whilst the plate was incubating, the injection ports were then loaded with appropriate inhibitor on the calibration plate. The machine was then calibrated using the calibration plate before the assay was run with the Seahorse cell culture plate.

2.7.1. Normalisation using CyQUANT

After plates had been run on the Seahorse Bioanalyzer the cell culture plates were prepared for CyQUANT (ThermoFisher, Cat#C7026) analysis by removing all liquid and placing plates in a -80°C freezer upside down. The CyQUANT mastermix was prepared by diluting the CyQUANT GR stock solution 400-fold in 1x cell-lysis buffer solution. Then, 100 µl of the mastermix was added to each sample well and incubated for 15 min protected from light. A standard curve was made using serially diluted samples of bacteriophage λ DNA using the mastermix, with concentrations ranging from 16 ng/ml to 1 µg/ml of DNA. All samples and standards were transferred to a black half area plate to be read on the fluorescent microplate reader with an excitation of 480 nm and emission of 520 nm.

This data was then used to normalise Seahorse data according to DNA content which is relevant to number of cells.

2.8. Statistical Analysis

Statistical analyses were performed on GraphPad Prism. Normal distribution was tested with Shapiro-Wilks. The data was then analysed using either one-way ANOVA or two-way ANOVA.

3. Results

3.1. *In silico* analyses

3.1.1. Cell lines TOV112D and SKOV3 were the most and least sensitive to Niclosamide, respectively

An *in silico* analysis was performed using the DepMap database to assess the sensitivity of a range of ovarian cancer cell lines to Niclosamide. DepMap reports the area under the curve (AUC) value, which represents the sensitivity of cells to a given drug. The lower the AUC value the higher the sensitivity (Pozdeyev et al., 2016). Of the 11 ovarian cancer cell lines analysed, TOV112D had the lowest AUC and SKOV3 had the highest AUC (Figure 18).

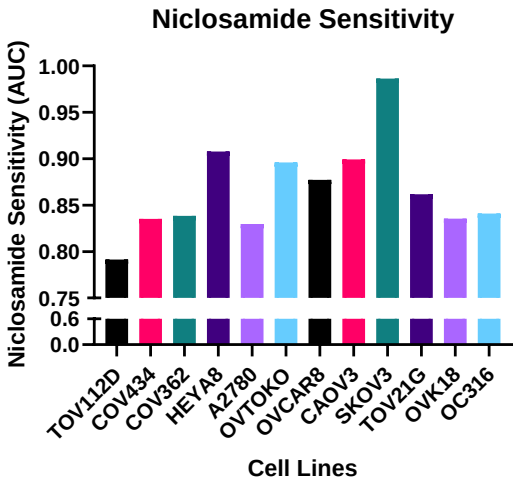

Figure 18. Area under the curve (AUC) values for ovarian cancer cells lines showing differences in sensitivity to Niclosamide. Data obtained from DepMap (Corsello et al., 2020).

3.1.2. Key genes involved in ferroptosis and their relationship with Niclosamide sensitivity

The relationship between Niclosamide sensitivity and relevant gene effect was also investigated using DepMap. Gene effect describes the extent to which the loss-of-function of a gene affects the cell. It was found that an increase in the gene effect of *GPX4*, *SLC7A11*, *SLC3A2* or *ALOX12* was positively correlated with an increase in Niclosamide sensitivity (Figure 19A-D). Whereas an *ALOX5* gene effect showed a negative correlation with Niclosamide sensitivity and there seemed to be no overall correlation with *NRF2* gene effect (Figure 19E, F).

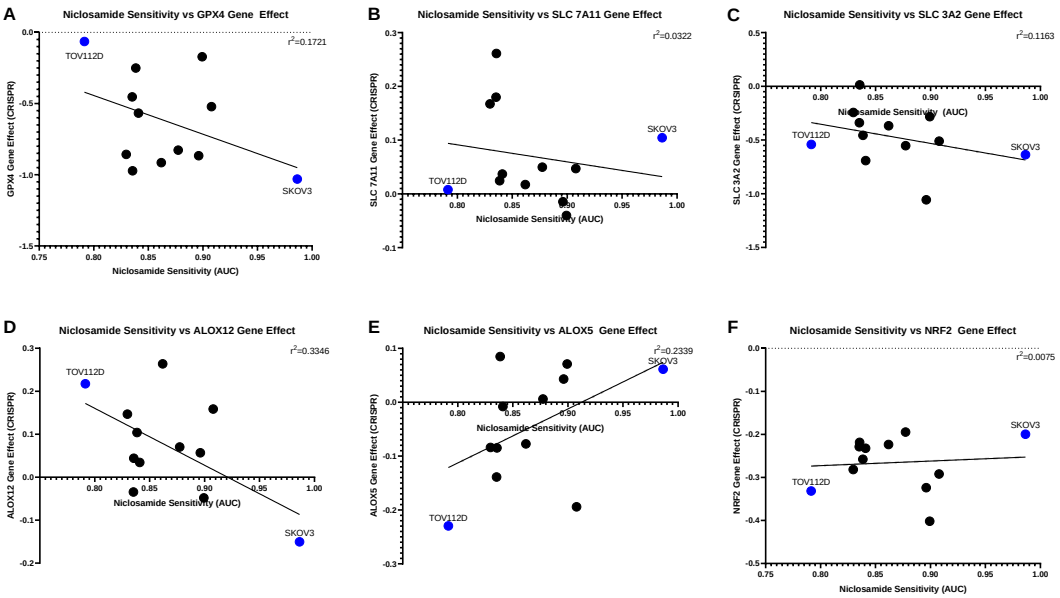

Figure 19. Ovarian cancer cell lines analysed to investigate relationships between gene effect and Niclosamide sensitivity. TOV112D and SKOV3 are highlighted as they are the ends of the spectrum of Niclosamide sensitivity (Corsello et al., 2020; Dempster et al., 2019; Depmap & Broad, 2021; Meyers et al., 2017).

3.2. *In vitro* analyses

3.2.1. Fer-1 had no effect on Niclosamide-induced cell death in ovarian cancer cells

The SKOV3, OVCAR3 and TOV112D ovarian cancer cells were treated with Niclosamide (0 – 5 µM), Fer-1 (0 – 1 µM) for 24 or 48 h (Figure 20A-F). Across all three cell lines, Niclosamide alone significantly reduced cell viability, although the largest reduction in cell viability was in TOV112D cells (Figure 20E, F), which supports *in silico* data, suggesting these cells are more sensitive to Niclosamide. Fer-1 alone had little to no effect on cell viability across 24 and 48 h and had no effect on Niclosamide-induced cell death (Figure 20).

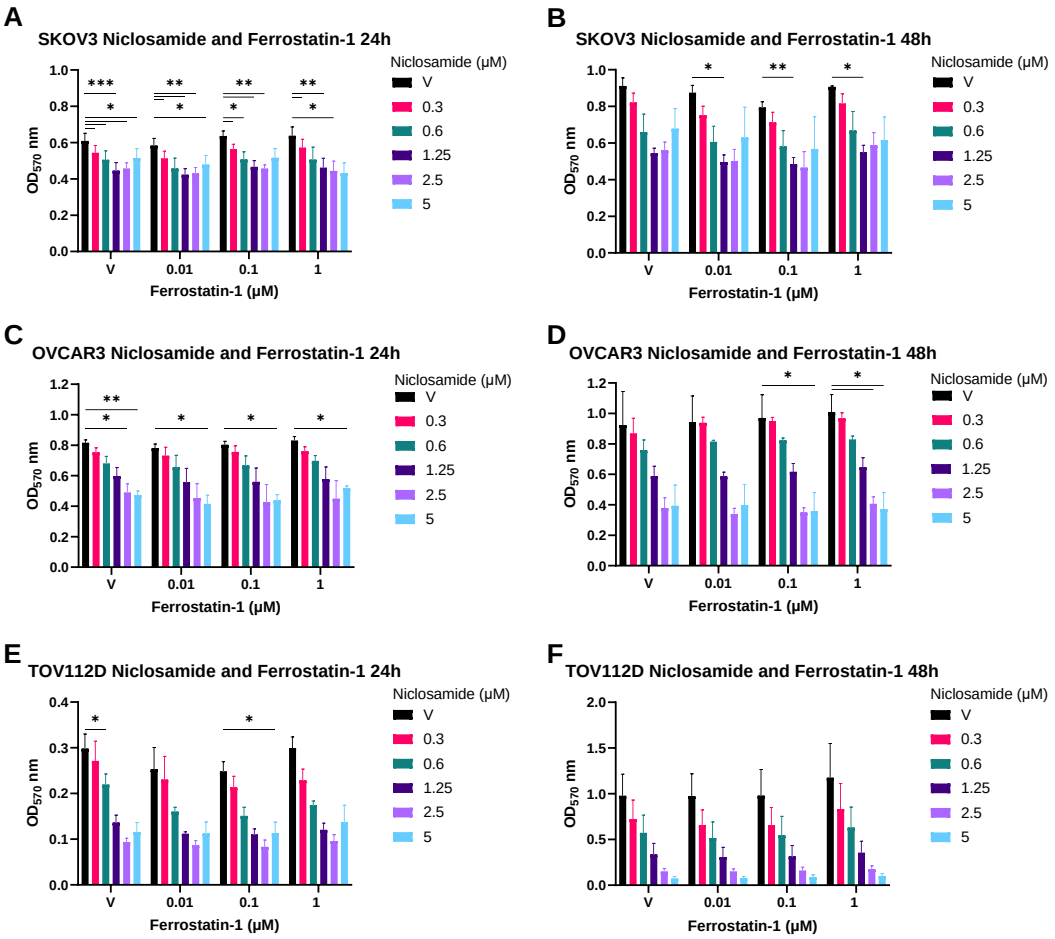

Figure 20. Effect of Niclosamide alone or in combination with Fer-1 in SKOV3 cells for A) 24 h or B) 48 h, OVCAR3 cells for C) 24 h or D) 48 h and TOV112D cells for E) 24 h or F) 48 h. Cell viability was evaluated using the MTT assay. Data is presented as + mean of the standard error (SEM) indicated by error bars from 3 independent biological experiments and analysed using two-way ANOVA, $^{*}p<0.05$, $^{**}p<0.01$, $^{***}P<0.001$.

3.2.2. Niclosamide rescues SKOV3 and TOV112D cells from Erastin-induced ferroptosis

Ovarian cancer cell lines were treated with Niclosamide (0 – 5 μM) and Erastin (0 – 10 μM) over 24 and 48 h. Erastin at 0.1 and 1 μM had little effect on cell viability, however increased ferroptotic cell death can be seen at 10 μM in all cell lines at both 24 and 48 h, although this data is not statistically significant (Figure 21A-F). It is at this concentration of Erastin where the trend of a rescuing effect can be seen with an increase in cell viability with 0.3 – 1.25 μM Niclosamide in SKOV3 cells at 24 and 48 h

and in TOV112D cells at 24 h (Figure 21A, B, E). This increase in cell viability is not statistically significant, however the trend is very prominent.

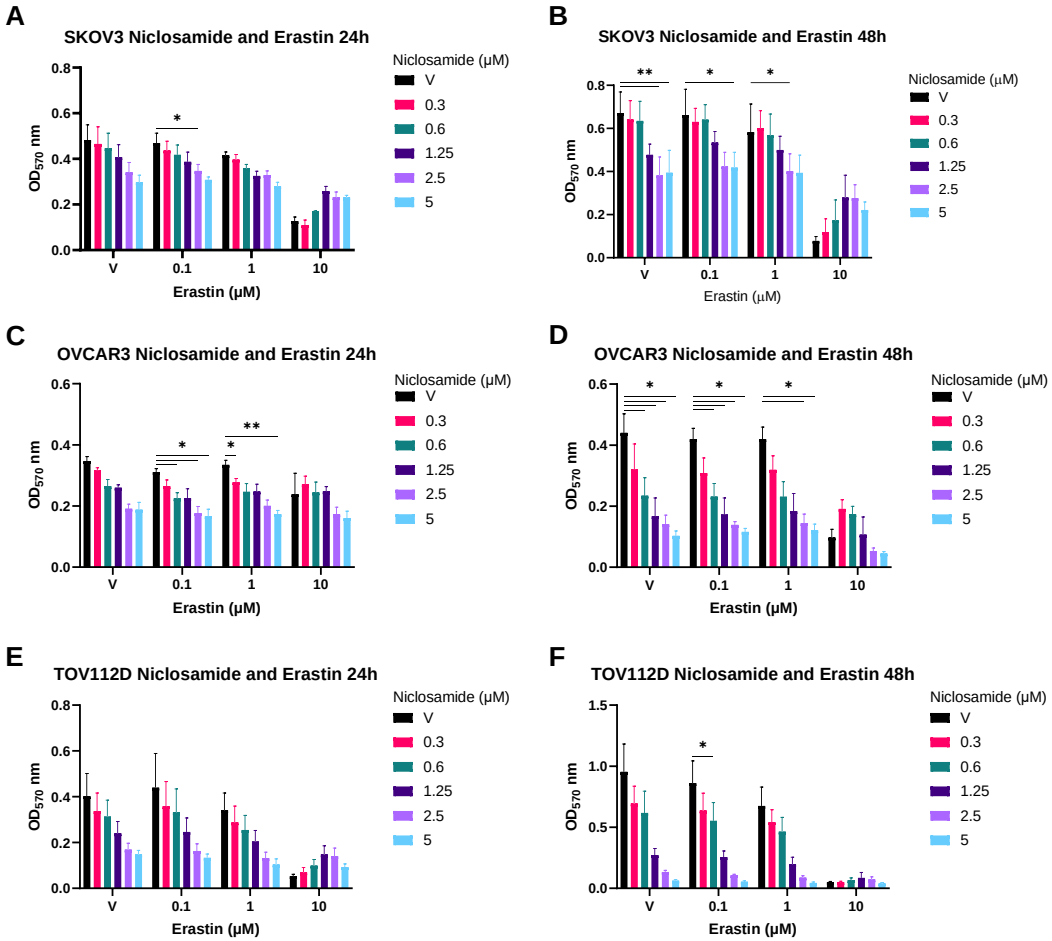

Figure 21. Effect of Niclosamide in combination with Erastin in SKOV3 cells for A) 24 h and B) 48 h, OVCAR3 cells for C) 24 h and D) 48 h and TOV112D cells for E) 24 h and F) 48 h. Cell viability was evaluated using MTT assay. Data is presented as + standard error of the mean (SEM) indicated by error bars from 3 independent biological experiments and analysed by two-way ANOVA, $^{*}p<0.05$, $^{**}p<0.01$.

3.2.3. Niclosamide rescues SKOV3 and TOV112D cells from RSL3-induced ferroptosis at 6 h

Next, SKOV3, OVCAR3 or TOV112D cells were treated with Niclosamide (0 – 5 µM) for 24 h and RSL3 (0 – 5 µM) for either 6 or 24 h. At 6 h, RSL3 induced ferroptotic cell death at 0.5 and 5 µM in all three cell lines (Figure 22A, C, E). At 24 h 0.5 and 5 µM of RSL3 induced cell death in all cell lines, but to a greater extent than at 6 h (Figure 21B, D, F). RSL3 at 0.05 µM caused cell death, but only in SKOV3 and TOV112D at 24 h

(Figure 22B, F). RSL3 induced cell death can be seen in the trend of the data, however this is not statistically significant.

In SKOV3 cells at 6 h, all concentrations of Niclosamide showed a trend of rescuing cells from RSL3 at 0.5 – 5 µM of RSL3 (Figure 21A). There was no rescue effect in OVCAR3 cells at 6 h (Figure 21C). Niclosamide provided rescue from 0.5 – 5 µM of RSL3 in TOV112D cells at 6 h (Figure 21E). However, there was no rescue effect at 24 h across all three cell lines (Figure 22B, D, F). The rescuing effect of Niclosamide against RSL3 is also not statistically significant, however can be observed as trends in the data.

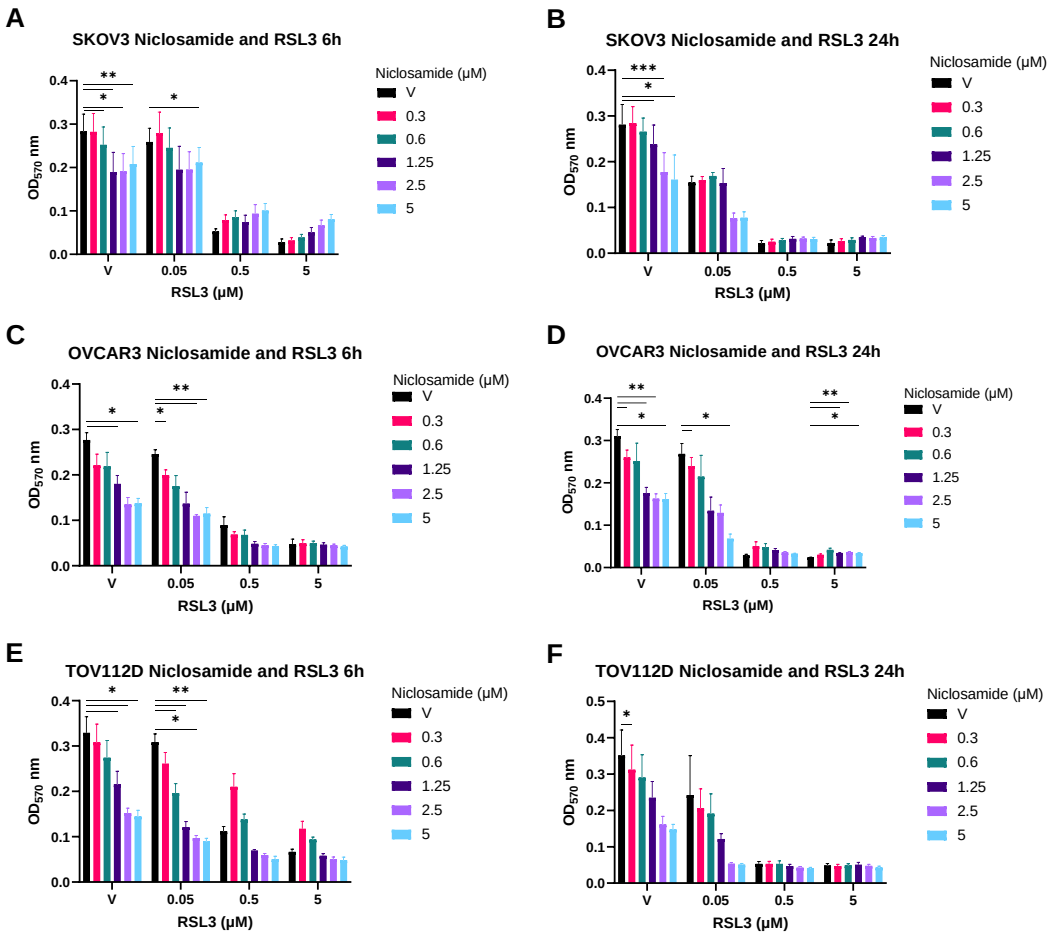

Figure 22. Effect of Niclosamide in combination with RSL3 in SKOV3 cells for A) 6 h and B) 24 h, OVCAR3 cells for C) 6 h and D) 24 h and TOV112D cells for E) 6 h and F) 24 h. Cell viability was evaluated using MTT assay. Data is presented as + standard error of the mean (SEM) indicated by error bars from 3 independent biological experiments and analysed by two-way ANOVA, $^{*}p<0.05$, $^{**}p<0.01$, $^{***}P<0.001$.

3.3. Western Blot Analysis

3.3.1. GPX4 expression is affected by Niclosamide in ovarian cancer cells

Cells were treated with Niclosamide (2.5 and 5 µM) and Erastin (10 µM) for 24 h and Niclosamide (2.5 and 5 µM) for 24 h with RSL3 (5 µM) for 6 h.

In SKOV3 cells, Niclosamide induced an increase in GPX4 expression over 24 h (Figure 23A, B). Erastin induced a depletion of GPX4 and β-actin, which was rescued with increasing concentrations of Niclosamide.

RSL3 also caused a decrease in GPX4 expression (Figure 23C, D). However, β-actin was also affected by RSL3 treatment affecting densitometry data. Niclosamide at 5 µM showed a slight increase in both GPX4 and β-actin, but to a much lesser extent than was seen with Erastin.

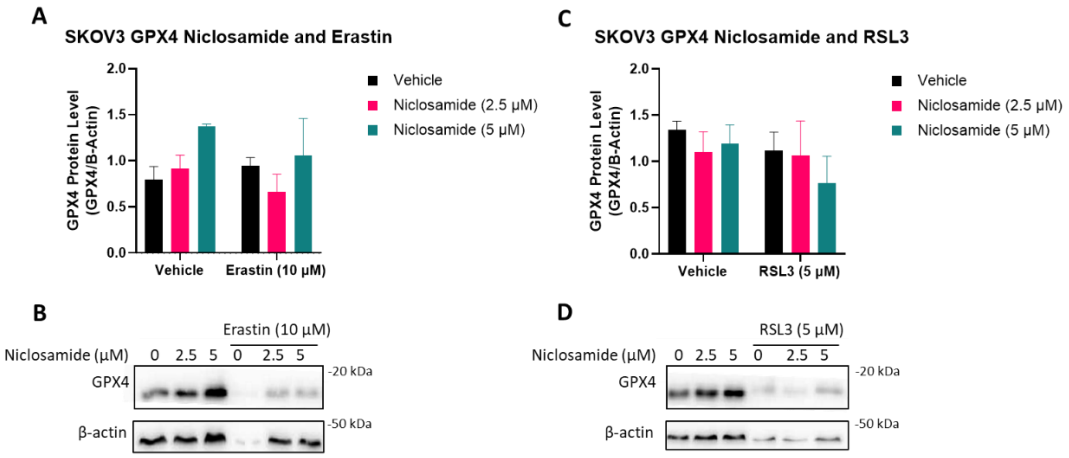

Figure 23. GPX4 protein expression was assessed in SKOV3 cells by Western Blotting. Cells were treated with Niclosamide and Erastin for 24 h and data is presented as A) densitometry values and B) representative Western Blot. Cells were treated with Niclosamide for 24 h and RSL3 for 6 h and data is presented as C) densitometry values and D) representative Western Blot. Densitometry data is presented as + standard error of the mean (SEM) indicated by error bars from 3 independent biological experiments and analysed by two-way ANOVA.

Converse to that observed in SKOV3 cells, Niclosamide induced a decrease in GPX4 expression or had little effect in OVCAR3 cells (Figure 24A, B, D).

Erastin also caused a decrease in GPX4 expression in OVCAR3 cells, but to a lesser extent than seen in SKOV3 cells (Figure 24A, B). Erastin also did not affect β-actin in

OVCAR3 cells as it did in SKOV3 cells (Figure 24B). When OVCAR3 cells were treated with both Erastin and Niclosamide, there was an increase in GPX4 expression (Figure 24A). This can also be seen in the representative Western Blot, however, there appears to be a larger increase at 2.5 µM Niclosamide (Figure 24B).

RSL3 also caused a decrease in GPX4 expression in OVCAR3 cells, but, as with Erastin, to a lesser extent than in SKOV3 cells (Figure 24C, D). β-actin expression was unaffected by RSL3, unlike in SKOV3 cells (Figure 24D). When cells were treated with RSL3 in combination with Niclosamide, there was a decrease in GPX4 expression (Figure 24C, D).

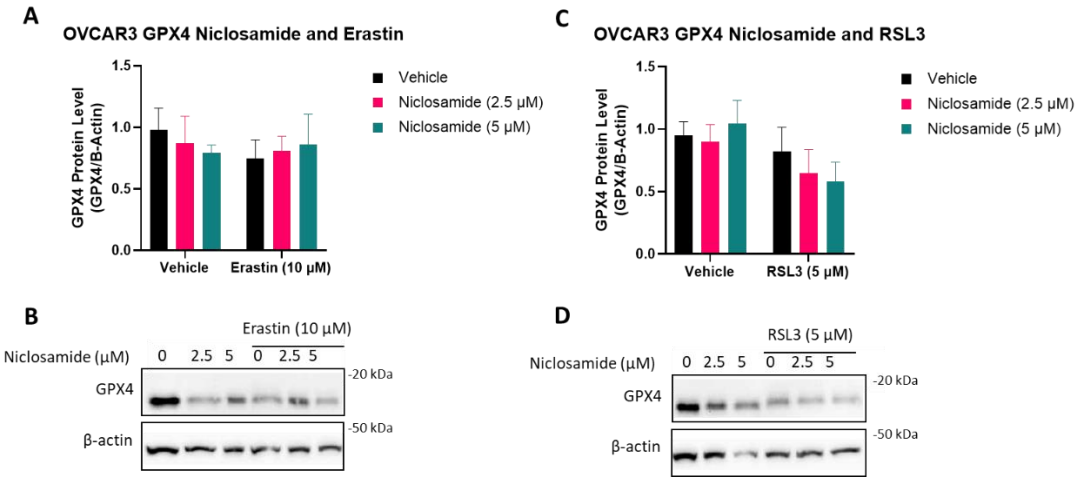

Figure 24. GPX4 protein expression was assessed in OVCAR3 cells by Western Blotting. Cells were treated with Niclosamide and Erastin for 24 h and data is presented as A) densitometry values and B) representative Western Blot. Cells were treated with Niclosamide for 24 h and RSL3 for 6 h and data is presented as C) densitometry values and D) representative Western Blot. Densitometry data is presented as + standard error of the mean (SEM) indicated by error bars from 4 independent biological experiments and analysed by two-way ANOVA.

In TOV112D cells, Niclosamide induced a decrease in GPX4 expression (Figure 25). This can be seen consistently across the densitometry data and the representative Western Blots as Niclosamide had no effect on β-actin expression.

Erastin decreased GPX4 expression in TOV112D cells (Figure 25A, B). β-actin is also affected by Erastin in this cell line. However, when the cells were treated with Erastin and Niclosamide together, GPX4 expression returned to levels seen in the vehicle, as did β-actin expression (Figure 25A, B).

When TOV112D cells were treated with RSL3, GPX4 expression decreased (Figure 25C, D). When Niclosamide was added alongside RSL3, GPX4 expression decreased and at 5 µM Niclosamide, β-actin expression was also decreased (Figure 25C, D).

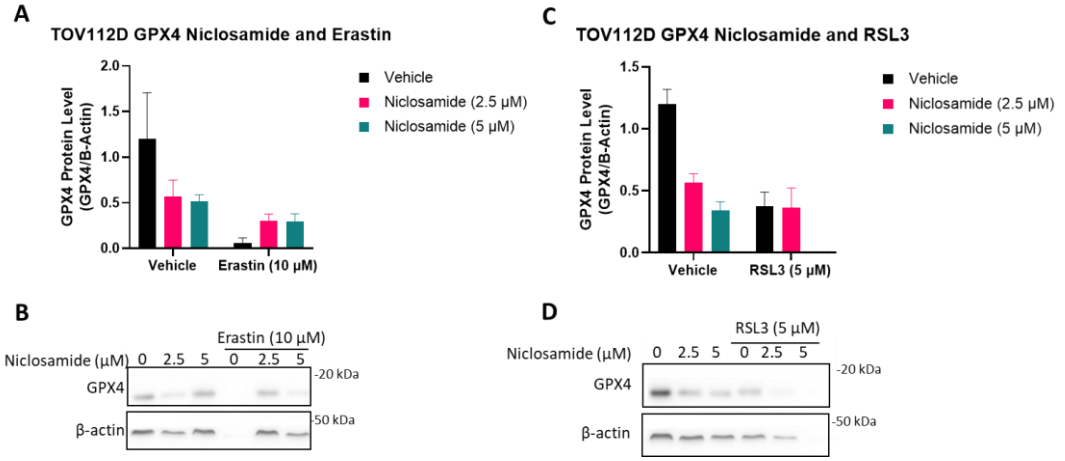

Figure 25. GPX4 protein expression was assessed in TOV112D cells by Western Blotting. Cells were treated with Niclosamide and Erastin for 24 h and data is presented as A) densitometry values and B) representative Western Blot. Cells were treated with Niclosamide for 24 h and RSL3 for 6 h and data is presented as C) densitometry values and D) representative Western Blot. Densitometry data is presented as + standard error of the mean (SEM) indicated by error bars from 3 independent biological experiments and analysed by two-way ANOVA.

3.3.2. Niclosamide affects ALOX12 expression in ovarian cancer cells

Cells were treated with Niclosamide (2.5 and 5 µM) and Erastin (10 µM) for 24 h and Niclosamide (2.5 and 5 µM) for 24 h with RSL3 (5 µM) for 6 h.

Niclosamide caused a decrease in ALOX12 expression in SKOV3 cells (Figure26A, C). However, a trend is not discernible in the representative Western Blots (Figure 26B, D).

An increase in ALOX12 expression can be seen when SKOV3 cells are treated with Erastin (Figure 26A). When SKOV3 cells were treated with Erastin in combination with Niclosamide, there was a decrease in ALOX12 expression (Figure 26A, B).

RSL3 induced an increase in ALOX12, but to a lesser extent than Erastin (Figure 26C). However, as with Erastin, this change is indiscernible on the representative Western Blot (Figure 26D). RLS3 and Niclosamide together caused an increase then decrease

in ALOX12 expression with increasing concentrations of Niclosamide (Figure 26C). However, it can be seen on the representative Western Blot that this might not be the case due to β-actin expression decreasing at 2.5 µM Niclosamide. The Western Blot shows that ALOX12 expression decreases when cells were treated with RSL3 and 2.5 µM Niclosamide, then increases at 5 µM Niclosamide (Figure 26D).

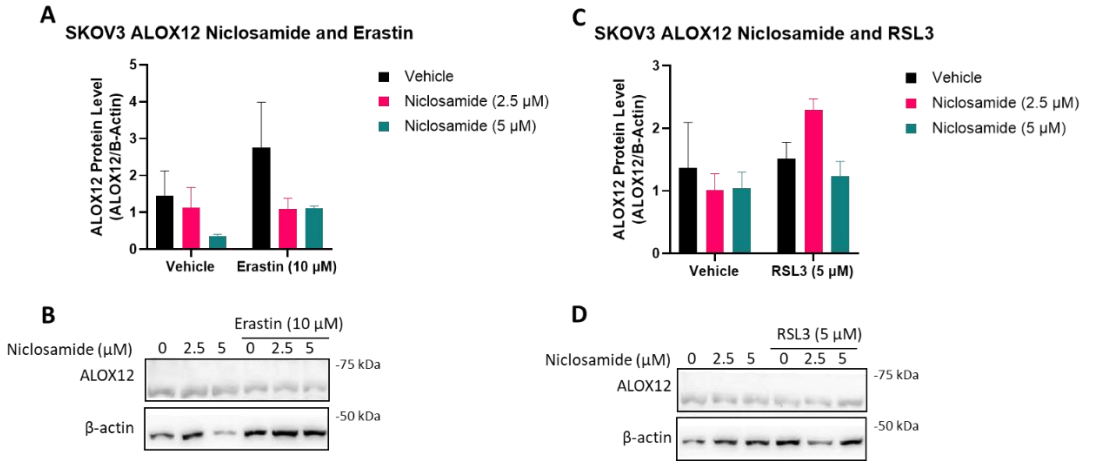

Figure 26. ALOX12 protein expression was assessed in SKOV3 cells by Western Blotting. Cells were treated with Niclosamide and Erastin for 24 h and data is presented as A) densitometry values and B) representative Western Blot. Cells were treated with Niclosamide for 24 h and RSL3 for 6 h and data is presented as C) densitometry values and D) representative Western Blot. Densitometry data is presented as + standard error of the mean (SEM) indicated by error bars from 3 independent biological experiments and analysed by two-way ANOVA.

Niclosamide induced an increase in ALOX12 expression in OVCAR3 cells (Figure 27). This can be seen in both densitometry data and representative Western Blots.

ALOX12 expression is increased in OVCAR3 cells when treated with Erastin (Figure 27A). This is shown in the densitometry data but is indiscernible in the representative Western Blot. This increase is to a lesser extent than that caused by Erastin in SKOV3 cells (Figure 26A). When OVCAR3 cells were treated with Erastin and Niclosamide, the densitometry data shows a small decrease in ALOX12 expression with increasing concentrations of Niclosamide (Figure 27A). The densitometry data is representative of the trends in ALOX12 expression as the β-actin expression is consistent between each treatment (Figure 27B).

RSL3 caused an increase in ALOX12 expression in OVCAR3 cells (Figure 27C, D). When the cells were treated with RSL3 in combination with Niclosamide, there was an increase in ALOX12 expression (Figure 27C). This increase is questionable as there was also a decrease in β-actin expression when Niclosamide was added alongside RSL3, as seen in the representative Western Blot (Figure 27D)

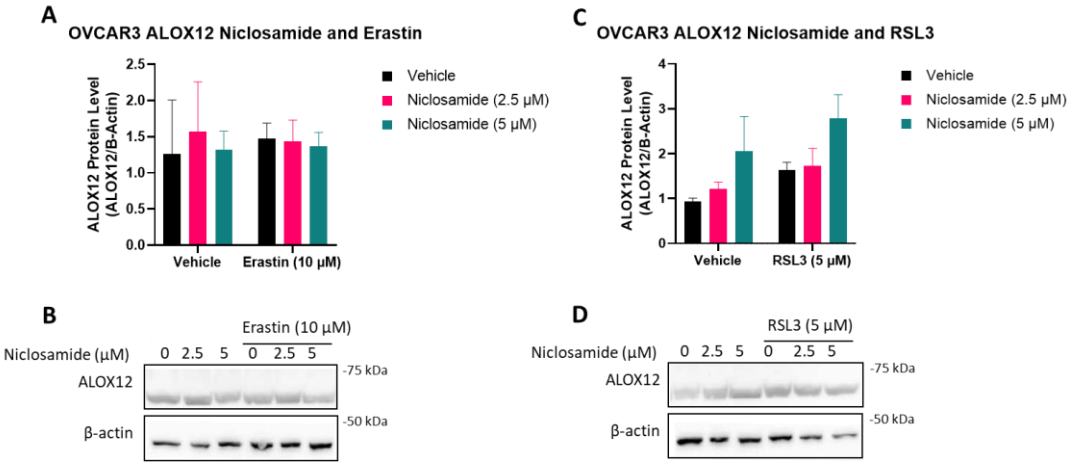

Figure 27. ALOX12 protein expression was assessed in OVCAR3 cells by Western Blotting. Cells were treated with Niclosamide and Erastin for 24 h and data is presented as A) densitometry values and B) representative Western Blot. Cells were treated with Niclosamide for 24 h and RSL3 for 6 h and data is presented as C) densitometry values and D) representative Western Blot. Densitometry data is presented as + standard error of the mean (SEM) indicated by error bars from 4 independent biological experiments and analysed by two-way ANOVA.

In the Niclosamide sensitive TOV112D cell line, Niclosamide induced an increase in ALOX12 expression (Figure 28). This can be seen in the representative blots, as well as the densitometry data as β-actin is unaffected by Niclosamide.

When the cells were treated with Erastin there was an increase in ALOX12 expression (Figure 28A, B). However, this increase was exaggerated in the densitometry data due to Erastin decreasing the expression of β-actin, as seen in the representative Western Blot (Figure 28B). The densitometry data shows that treating the cells with Erastin and Niclosamide causes a decrease in ALOX12 expression, however, these values are also exaggerated by the effect of depletion on β-actin (Figure 28B).

RSL3 caused an increase in ALOX12 expression in TOV112D cells (Figure 28C, D). When cells were treated with RSL3 and Niclosamide in combination, there was a

further increase in ALOX12 expression (Figure 28C, D). However, the densitometry values are exaggerated due to the decrease in β-actin expression seen in the representative blot (Figure 28D). The effect of RSL3 with 5µM Niclosamide is statistically significant, however this is most likely due to the skew caused by the decrease in β-actin expression.

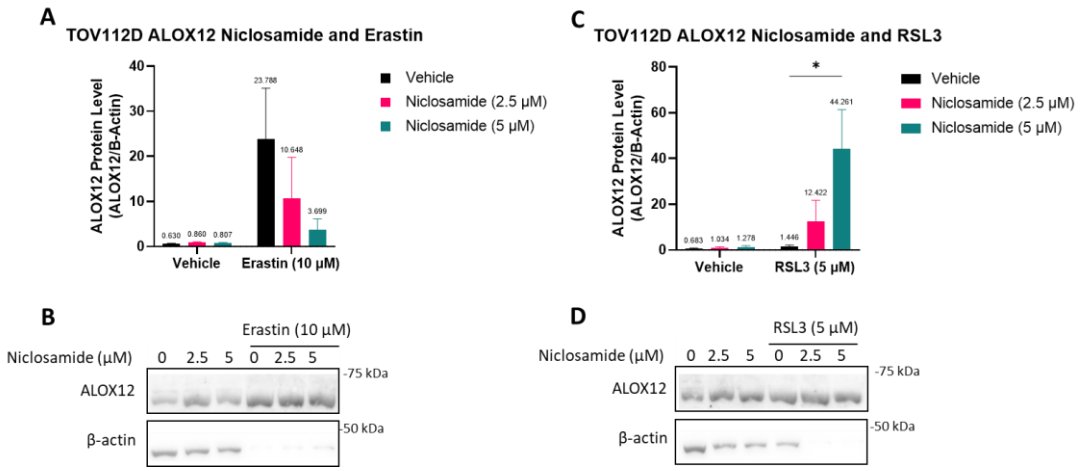

Figure 28. ALOX12 protein expression was assessed in TOV112D cells by Western Blotting. Cells were treated with Niclosamide and Erastin for 24 h and data is presented as A) densitometry values and B) representative Western Blot. Cells were treated with Niclosamide for 24 h and RSL3 for 6 h and data is presented as C) densitometry values and D) representative Western Blot. Densitometry data is presented as + standard error of the mean (SEM) indicated by error bars from 3 independent biological experiments and analysed by two-way ANOVA, *P<0.05.

3.3.3. NRF2 expression is affected by Niclosamide in ovarian cancer cells

Cells were treated with Niclosamide (2.5 and 5 µM), Erastin (10 µM) and MG-132 (25 µM) for 24 h, and Niclosamide (2.5 and 5 µM) and MG-132, a proteasome inhibitor used to stabilise NRF2 and prevent it being degraded, for 24 h with RSL3 (5 µM) for 6 h.

SKOV3 cells have an increased expression of NRF2 when treated with Niclosamide, which is further increased when cells are also treated with MG-132 (Figure 29A, B; Huang, Liang, Qing, Chen, & Shi, 2019).

Erastin induced an increase in NRF2 expression in SKOV3 cells (Figure 29A, B). An alternative housekeeping protein (α-tubulin) was used in this experiment as it was affected less than β-actin, however Erastin still decreased the expression of α-tubulin (Figure 29B). When SKOV3 cells were treated with Erastin and Niclosamide, NRF2 expression decreased. When MG-132 was also added, NRF2 expression decreased but to a lesser extent (Figure 29A, B).

NRF2 expression was increased when SKOV3 cells were treated with RSL3 and expression increased further when Niclosamide was also added and further again when MG-132 was added (Figure 29C, D). The densitometry data is representative of the trend as α-tubulin was consistent between the different treatments (Figure 29D).

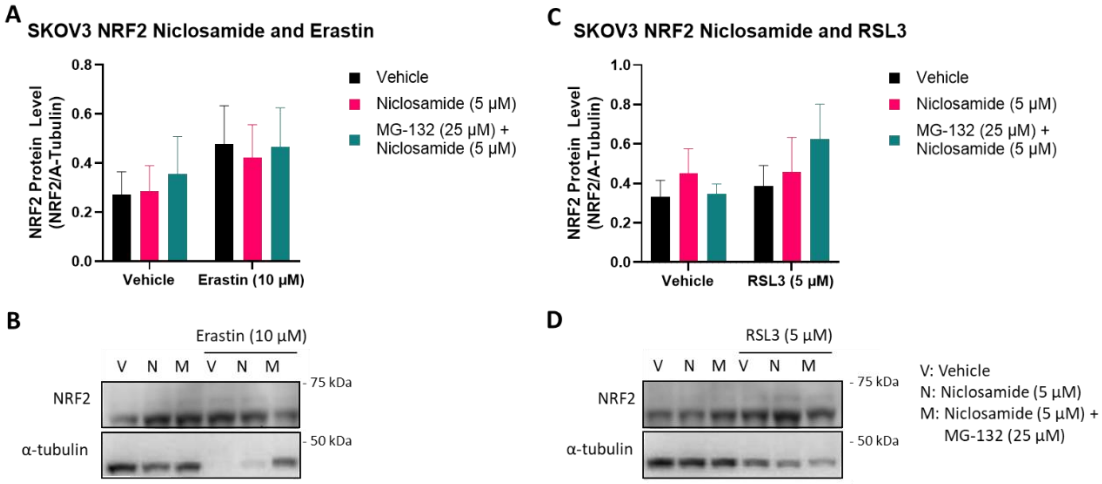

Figure 29. NRF2 protein expression was assessed in SKOV3 cells by Western Blotting. Cells were treated with Niclosamide, Erastin and MG-132 for 24 h and data is presented as A) densitometry values and B) representative Western Blot. Cells were treated with Niclosamide and MG-132 for 24 h and RSL3 for 6 h and data is presented as C) densitometry values and D) representative Western Blot. Densitometry data is presented as + standard error of the mean (SEM) indicated by error bars from 4 independent biological experiments and analysed by two-way ANOVA.

In OVCAR3 cells, Niclosamide caused a decrease in NRF2 expression, which was further decreased when MG-132 was added (Figure 30). The densitometry data is consistent with the representative Western Blots in showing this.

Erastin induced an increase in NRF2 expression in OVCAR3 cells (Figure 30A, B). When the cells were treated with Erastin and Niclosamide in combination there was a

decrease in NRF2 expression that was further decreased by the addition of MG-132 (Figure 30A, B).

In OVCAR3 cells, RSL3 caused an increase in NRF2 expression (Figure 30C, D). When RSL3 and Niclosamide were added to the cells in combination, the densitometry data showed a decrease in NRF2 expression (Figure 30C). However, the representative Western Blots show that this combination decreased the expression of α-tubulin, so the densitometry data is skewed. The Western Blot data indicates that the combination of RSL3 and Niclosamide increases NRF2 expression which decreased with the addition of MG-132 (Figure 30D).

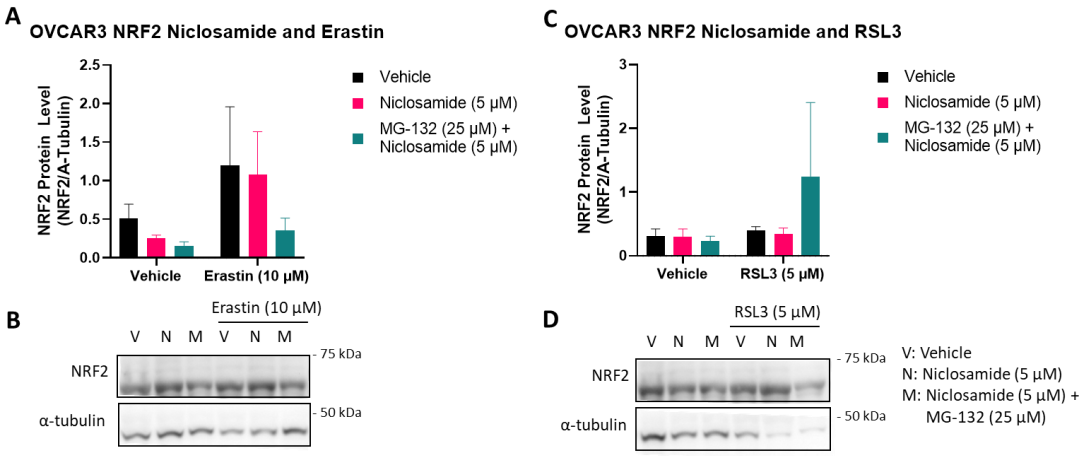

Figure 30. NRF2 protein expression was assessed in OVCAR3 cells by Western Blotting. Cells were treated with Niclosamide, Erastin and MG-132 for 24 h and data is presented as A) densitometry values and B) representative Western Blot. Cells were treated with Niclosamide and MG-132 for 24 h and RSL3 for 6 h and data is presented as C) densitometry values and D) representative Western Blot. Densitometry data is presented as + standard error of the mean (SEM) indicated by error bars from 3 independent biological experiments and analysed by two-way ANOVA. Mean values plotted above bars for clarity.

Niclosamide induced decreased NRF2 expression in TOV112D cells. According to the densitometry data this was further decreased when MG-132 was added, which also decreased the expression of α-tubulin so this is not accurate. The representative blot showed an increase with MG-132 (Figure 31A, B).

An increase in NRF2 expression can be seen in both the densitometry data and the representative Western Blot when TOV112D cells are treated with Erastin (Figure

31A, B). This also affects the expression of α-tubulin, so the densitometry values are not accurate. When the cells were treated with a combination of Erastin and Niclosamide there was an increase in NRF2 expression which was further increased by adding MG-132 (Figure 31A).

NRF2 expression is decreased when TOV112D cells are treated with RSL3 (Figure 31C, D). However, when the cells were treated with both RSL3 and Niclosamide there was an increase in NRF2 expression even though this treatment decreased the expression of α-tubulin (Figure 31CD). Adding MG-132 increased NRF2 expression but to a lesser extent than just treating the cells with RSL3 and Niclosamide (Figure 31D).

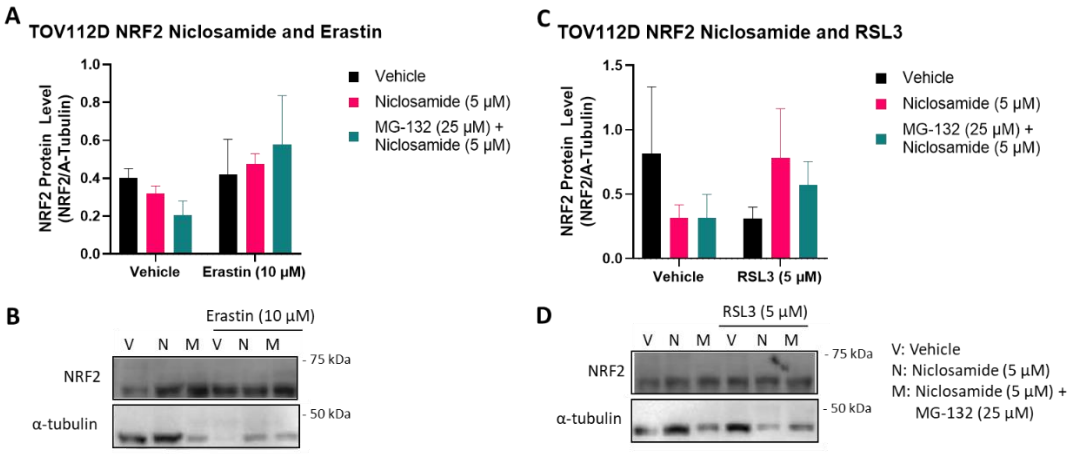

Figure 31. NRF2 protein expression was assessed in TOV112D cells by Western Blotting. Cells were treated with Niclosamide, Erastin and MG-132 for 24 h and data is presented as A) densitometry values and B) representative Western Blot. Cells were treated with Niclosamide and MG-132 for 24 h and RSL3 for 6 h and data is presented as C) densitometry values and D) representative Western Blot. Densitometry data is presented as + standard error of the mean (SEM) indicated by error bars from 3 independent biological experiments and analysed by two-way ANOVA.

The conclusions derived from the western blot data have been from the trends the data have shown as there was no statistical significance. This could be due to issues with housekeeping proteins being affected by the treatments.

So far the data implies that Niclosamide is having a rescuing effect from both Erastin- and RSL3-induced ferroptotic cell death. This can be seen in the trends in the MTT analysis. The western blot data indicated that all 3 proteins of interest are affected by the treatments across all three cell lines, however the results are inconsistent

between the cells. It is important to note the use of SKOV3 cells as they are the least Niclosamide-sensitive ovarian cancer cell line available, and they have highlighted the effect of Niclosamide sensitivity and how it plays an important role in the molecular pathway being unravelled.

3.4. Flow Cytometry Analysis

Lipid peroxidation levels in ovarian cancer cells were assessed using Liperfluo staining and flow cytometry as an indicator of ferroptosis. Cells were also stained with DRAQ7 to assess the viability of the cells. Median fluorescence intensity (MFI) of Liperfluo was calculated for both live and all cells for each sample. Cells were treated with Niclosamide (2.5 and 5 μM) and Erastin (10 μM).

3.4.1. Niclosamide reduced lipid peroxidation in Niclosamide-sensitive cells treated with Erastin

In SKOV3 cells, when analysing all cells, lipid peroxidation increased when the cells were treated with Erastin. There was a small increase in lipid peroxidation when Niclosamide was added; however, when the cells were treated with Erastin and Niclosamide the lipid peroxidation decreased when compared to the Erastin treatment alone. When SKOV3 cells were analysed using only live cells, there was little to no effect on lipid peroxidation when the cells were treated with Erastin. There appeared to be no difference in lipid peroxidation between live cells and all cells in samples treated with Niclosamide (Figure 32A, B).

In OVCAR3 cells, lipid peroxidation increased when the cells were treated with Erastin. This was seen in total cells and when gating for live cells only. In all cells, Niclosamide also caused lipid peroxidation but to a lesser extent than Erastin. In live cells, 2.5 μM caused less lipid peroxidation than Erastin, whereas 5 μM induced slightly more lipid peroxidation than Erastin. In live cells, treating samples with Erastin and Niclosamide (2.5 and 5 μM) had no effect on lipid peroxidation when compared with samples treated with just Erastin. In all cells, this was the case with treating cells with Erastin and 2.5 μM Niclosamide, however there was an increase in lipid peroxidation when treating with 5 μM Niclosamide and Erastin (Figure 32C, D).

When TOV112D cells were treated with Erastin, there was an increase in lipid peroxidation when all cells were analysed, however there was a decrease when only live cells were analysed. Niclosamide appeared to decrease lipid peroxidation; however, there were no differences between the two concentrations, or between live and total cells. In all cells, when Erastin was treated with Niclosamide, there was a decrease in lipid peroxidation when compared to Erastin-only treated cells. In live cells, there was more lipid peroxidation in Niclosamide-only treated cells when compared to the Erastin-treated samples. When the cells were treated with Niclosamide and Erastin in combination, there was a decrease in lipid peroxidation compared to both Niclosamide- and Erastin-only treated samples (Figure 32E, F).

No data retrieved from this analysis was statistically significant, so all interpretations have been based on the trends seen in the data.

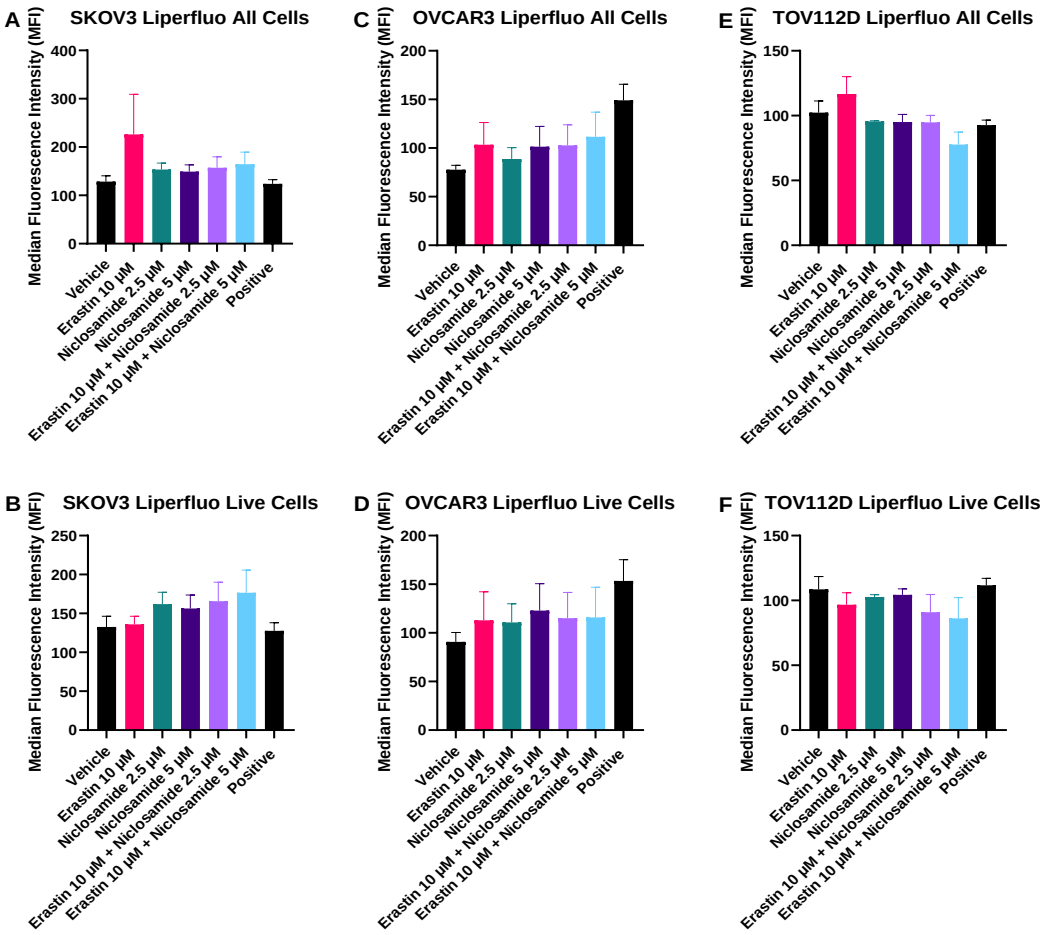

Figure 32. Mean MFI of ovarian cancer cells treated with Niclosamide and Erastin and stained with Liperfluo and DRAQ7 to assess lipid peroxidation and cell death. Data is

presented as mean and standard error (SEM) indicated by error bars from 3 independent biological experiments and analysed using one-way ANOVA.

3.5. XF Mito Stress Test Analysis

Oxygen consumption rates (OCR) were measured using a Seahorse XFe96 analyser. OCR was measured every 7 min and a different injection was added every 18 min. The first three time points show the basal respiration of the cells. Oligomycin was then injected and inhibits ATP synthase. The next three time points show ATP-linked respiration. FCCP is a mitochondrial uncoupler (similar to Niclosamide). After this was injected the time points show the maximal respiration possible by the cells. The last injection was a mix of Rotenone and Antimycin A, inhibitors of complex I and II, respectively. The last three time points show non-mitochondrial oxygen consumption. Cells were treated 24 h before the assay with Niclosamide (0.3 and 0.6 µM) and Erastin (10 µM). The 'normal' response of cells to the Mito Stress Test is a decrease in OCR when Oligomycin is added, an increase when FCCP is added, and a decrease when Rotenone and Antimycin A are added.

3.5.1. Niclosamide affects basal respiration in ovarian cancer cells and is a confirmed mitochondrial uncoupler

Across all three cell lines, the addition of Niclosamide, Erastin or a combination of the two had a statistically significant effect on OCR when compared to the vehicle.

SKOV3 cells responded as expected to Oligomycin and Rotenone/Antimycin A, however there was a weaker response than expected to FCCP, the expected response being an increase in OCR due to FCCP being a mitochondrial uncoupler. When the cells were treated with Niclosamide there was an increase in basal respiration. There was no response to FCCP in SKOV3 cells that had been treated with Niclosamide (Figure 33A). When SKOV3 cells were treated with Erastin, there was a slight increase in basal respiration. There was also a decreased response to FCCP in these cells when treated with Erastin. When cells were treated with Erastin and Niclosamide, there was an increase in basal respiration when compared to cells just treated with Erastin (Figure 33B).

OVCAR3 cells showed a normal response to the Mito Stress Test. As with SKOV3 cells, Niclosamide increased the basal respiration of OVCAR3 cells, and FCCP induced a decrease in OCR in these cells when treated with Niclosamide (Figure 33C). Erastin induced a decrease in basal respiration in OVCAR3 cells, however adding Niclosamide as well increased the basal respiration (Figure 33D).

Like OVCAR3 cells, TOV112D cells showed an expected response to the Mito Stress Test. However, unlike the other two cell lines used, Niclosamide induced a decrease in basal respiration in TOV112D. FCCP had no effect on any of the samples that had been treated with Niclosamide (Figure 33E). When the cells were treated with Erastin, there was a decrease in basal respiration and cells did not respond to FCCP. Adding Erastin and Niclosamide to the cells induced an increase in basal respiration at 0.3 µM Niclosamide and a decrease at 0.6 µM Niclosamide (Figure 33F).

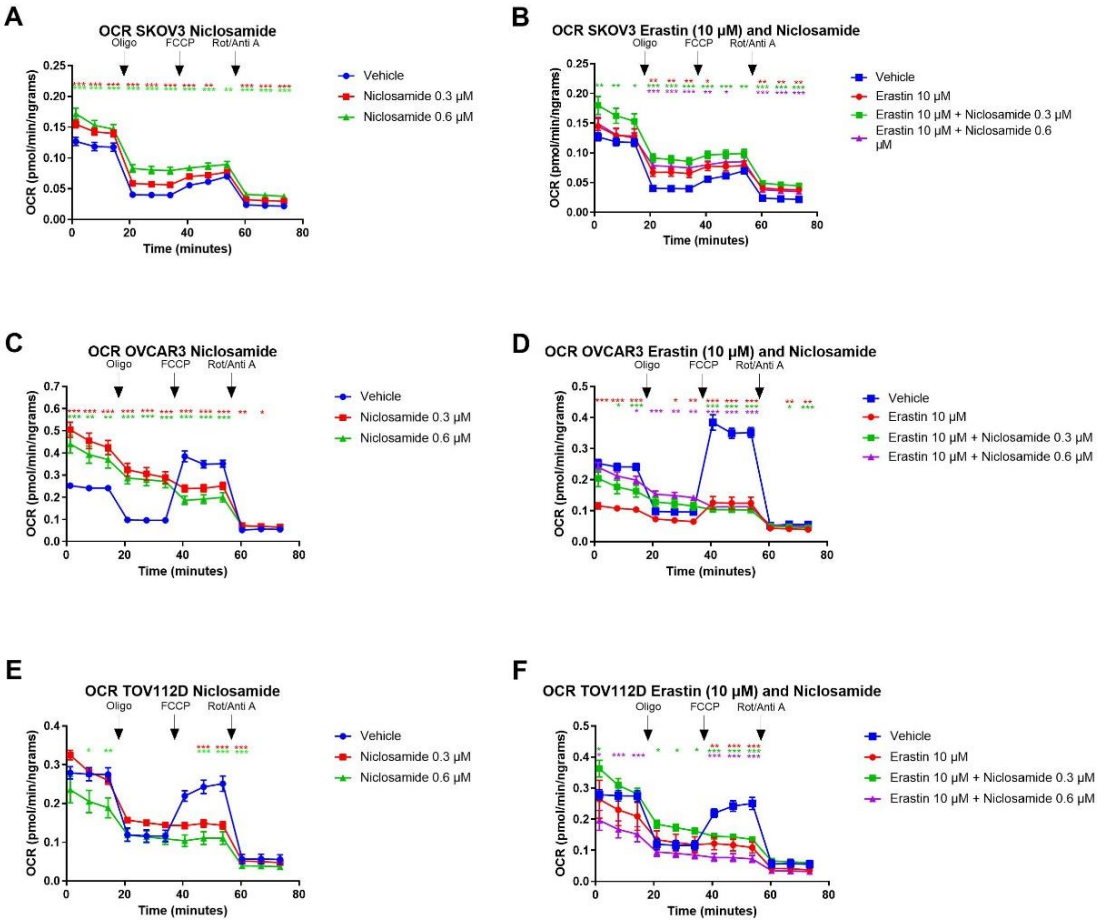

Figure 33. Effect of Niclosamide on OCR in A) SKOV3 cells, C) OVCAR3 cells and E) TOV112D cells and the effect of Niclosamide treated with Erastin on B) SKOV3 cells, D) OVCAR3 cells and F) TOV112D cells. OCR was evaluated using the Mito Stress Test.

Data is presented as mean and standard error (SEM) indicated by error bars from 3 independent experiments and analysed using two-way ANOVA, *P<0.05, **<0.01, ***P<0.001.

4. Discussion

The high occurrence of chemo-resistance in ovarian cancer makes finding novel treatments a priority (Cancer Research UK, 2019). The susceptibility of chemo-resistant cells to ferroptosis has identified this cell death process as a possible target for novel therapies (Dixon et al., 2012). If this form of programmed cell death can be utilised, the prognosis for many women worldwide could improve. However, in order to achieve this, we must first understand fully the pathways involved in ferroptosis.

This project aimed to assess the effects of Niclosamide as a mitochondrial uncoupler on lipoxygenase enzymes and the signalling pathway NRF2 and its downstream targets. It was hypothesised that Niclosamide would increase intracellular AA as a substrate for ALOX, increasing its enzymatic activity and activating NRF2. NRF2 would then increase expression of its downstream targets *SLC7A11* and *GPX4*, rescuing cells from ferroptotic cell death.

4.1. Niclosamide Sensitivity

In silico analysis using DepMap identified SKOV3 and TOV112D as the least and most sensitive ovarian cancer cells to Niclosamide, respectively. This data was used when selecting which cell lines to use throughout the investigation to highlight the differences that Niclosamide sensitivity would present. OVCAR3 cells were also chosen as they are representative of HGSOC and do not express *SLC7A11,* while SKOV3 and TOV112D cells do (Coscia et al., 2016).

DepMap was also used to look for correlations between Niclosamide sensitivity and gene effect. CRISPR/Cas9 loss of function screening was used to analyse gene effect across cell lines. Positive correlations between sensitivity to Niclosamide and gene effect in ovarian cancer cell lines were found with *GPX4*, *SLC7A11*, *SLC3A2* and *ALOX12*. If the hypothesised pathway is correct and Niclosamide induces an increase in NRF2 activation, this data concurs with it as *GPX4* and *SLC7A11* are target genes of NRF2. However, there was no correlation between *NRF2* gene effect and sensitivity. While *ALOX12* gene effect was positively correlated with Niclosamide sensitivity, there was a negative correlation with ALOX5. This was surprising as it has been

previously shown that *ALOX5* expression can be induced by Niclosamide (Kumar et al., 2018). Due to this, it was decided that ALOX12 was to be investigated in this project.

4.2. Niclosamide does not use non-enzymatic ferroptosis to induce cell death

All three cell lines displayed reduced viability when treated with Niclosamide: TOV112D showed the biggest decrease in viability. This correlated with TOV112D cells being the most sensitive cell line to Niclosamide. Fer-1 had no effect on cell viability when treated with Niclosamide. This would imply that Niclosamide does not cause cell death using non-enzymatic Ferroptosis as Fer-1 only inhibits non-enzymatic Ferroptosis. ALOX enzymes could still be utilised during Niclosamide-induced cell death. This was the case across all three cell lines.

4.3. Niclosamide rescued SLC7A11 positive cells from Ferroptotic cell death

Erastin induced cell death in all three cell lines at 10 µM. OVCAR3 was the most resistant to Erastin-induced cell death, possibly due to the fact it does not express *SLC7A11*. This could also explain why OVCAR3 cells did not show the rescuing effect of Niclosamide as *SLC7A11* cannot be upregulated as it is in TOV112D and SKOV3. Niclosamide protected SKOV3 cells and TOV112D cells from Erastin-induced cell death from 0.3 to 1.25 µM at 24 h. This shows that Niclosamide could be utilising the proposed pathway involving ALOX and NRF2 to upregulate *SLC7A11*, counteracting Erastin's inhibition of the amino acid antiporter. At 2.5 and 5 µM of Niclosamide, it protected cells to a lesser extent than lower concentrations from Erastin-induced ferroptotic cell death in SKOV3 and TOV112D cells at 24 and 48 h. This implies there is a balance between the protective action of Niclosamide and its ability to cause cell death through mitochondrial uncoupling.

RSL3 induced cell death at 0.5 and 5 µM across all 3 cell lines at 6 and 24 h and at 0.05 µM at 24 h but only in SKOV3 and TOV112D. It is a much more potent inducer of Ferroptosis than Erastin as it directly inhibits GPX4 while Erastin achieves this indirectly through System Xc^- inhibition. As with Erastin-induced ferroptotic cell death, Niclosamide did not provide resistance to RSL3-induced cell death in OVCAR3

cells. At 24 h with RSL3 and Niclosamide, there was no rescue in SKOV3 or TOV112D cells either. This is most likely due to RSL3's potency. All concentrations of Niclosamide used provided resistance in a dose dependent manner in SKOV3 cells at both 0.5 and 5 µM of RSL3 at 6 h. However, in TOV112D lower concentrations of Niclosamide provided resistance (0.3 – 0.6 µM) whilst increased concentrations of Niclosamide (1.25 – 5 µM) caused cell death at 6 h. This is much like the case with resistance to Erastin-induced cell death, where there may be a balance between ferroptotic- resistance and Niclosamide-induced cell death.

4.4. GPX4 protein expression increased in less Niclosamide-sensitive cells when treated with Niclosamide

SKOV3 cells showed an increase in GPX4 expression when treated with Niclosamide, while TOV112D and OVCAR3 cells showed a decrease (Figure 23-25). This increase in GPX4 could be a protective mechanism in SKOV3 cells to provide an increased resistance to Niclosamide. This is concurrent with the sensitivity data which showed SKOV3 as being the least sensitive ovarian cancer cell line in those analysed and also agrees with the proposed hypothesis that GPX4 can be induced by Niclosamide via ALOX enzymes and the NRF2 pathway. The decrease in GPX4 expression in TOV112D cells when treated with Niclosamide could be due to an increase in cell death as these cells are the most sensitive to Niclosamide. OVCAR3 cells also showed a decrease in GPX4 expression, likely due to their lack of expression of SLC7A11.

Both Erastin and RSL3 caused a decrease in GPX4 expression across all three cell lines. This result was expected as Erastin and RSL3 are indirect and direct inhibitors, respectively, of GPX4. This shows that all three cell lines used are susceptible to ferroptotic cell death.

When compared to samples just treated with Erastin, cells treated with Erastin and Niclosamide showed an increase in GPX4. This implies that even in the presence of Erastin, Niclosamide increases GPX4 expression. This effect was also seen in TOV112D and OVCAR3 cells where Niclosamide-only treatments caused a decrease in GPX4 expression. This aligns with cell viability data which showed that Niclosamide is lethal

on its own, but can rescue cells from Erastin-induced ferroptotic cells death. It is important to note that an increase in GPX4 expression in OVCAR3 when treated with Erastin and Niclosamide is interesting as this would imply that there would be a protective response however that was not seen in the viability data.

SKOV3 cells showed an increase in GPX4 expression when treated with RSL3 and Niclosamide, while the same treatments caused a decrease in GPX4 expression in TOV112D and OVCAR3 cells. The response in SKOV3 cells again showed the protective mechanism being utilised in the least-sensitive cell lines. The decrease in GPX4 in TOV112D cells was likely due to the sensitivity of the cells to Niclosamide. At such concentrations Niclosamide was too toxic to the cells to be able to provide rescue from RSL3-induced cell death. This can also be seen in the cell viability data as lower concentrations of Niclosamide provided rescue. In OVCAR3 cells, a decrease in GPX4 expression was expected as Niclosamide does not provide this cell line any rescue. However, it is interesting that Niclosamide did not show any rescue from RSL3 and RSL3 is SLC7A11 independent. It is possible that RSL3 is just too potent for this cell line.

4.5. Niclosamide increased ALOX12 expression in Niclosamide-sensitive cells

Niclosamide decreased ALOX12 expression in SKOV3 cells. This could be an alternative protective mechanism of SKOV3 cells to reduce toxic lipid peroxides being formed. As GPX4 expression was increased in these cells when treated with Niclosamide, the proposed mechanism of this project could still be happening, but possibly with an alternative ALOX enzymes such as ALOX15 which has also been shown to be involved in Ferroptosis (Shintoku et al., 2017). ALOX12 might not be the ALOX used to activate NRF2 in this cell line as it has been shown that ALOX12 is required for p53-dependent ferroptosis and SKOV3 cells do not express *TP53* (Chu et al., 2019).

TOV112D and OVCAR3 cells both express *TP53* and Niclosamide induced an increase in ALOX12 expression in both of these cell lines, possibly by Niclosamide's function as a mitochondrial uncoupler. GPX4 expression was decreased in these cell lines

when treated with Niclosamide. However, this could be due to TOV112D's sensitivity to the cells. It could also show that ALOX12 can be increased in OVCAR3 but does not take part in any protective mechanism, instead contributing to cell death by increasing levels of toxic lipid peroxides.

All three cell lines experienced an increase in ALOX12 expression when treated with Erastin. This is likely due to the nature of Erastin-induced cell death utilising ALOX12 enzymes to produce toxic lipid peroxides, causing ferroptotic cell death. The same response was seen when the cells were treated with RSL3.

When the cells were treated with Erastin and Niclosamide, all three cell lines saw a decrease in ALOX12 expression. This does not concur with the proposed mechanism of an increased activity of ALOX enzymes activating NRF2, in turn increasing expression of GPX4 and SLC7A11. However, this could still be a protective mechanism, decreasing ALOX12 expression, allowing for fewer toxic lipid peroxides to be produced.

An increase in ALOX12 expression was seen when all three cell lines were treated with RSL3 and Niclosamide. This could be due to the nature of RSL3 directly inhibiting GPX4, allowing for an increase in activity of ALOX enzymes that is then utilised by Niclosamide to activate the NRF2 pathway, providing protection to the cells in the proposed manner.

4.6. NRF2 expression was affected in all cell lines when treated with Niclosamide

Niclosamide induced an increase in NRF2 expression in SKOV3 cells. As ALOX12 was decreased in these cells, it is possible a different ALOX is responsible for triggering an increase in NRF2. Meanwhile, Niclosamide induced a decrease in NRF2 expression in both TOV112D and OVCAR3 cells. This could be due to an increased cell death when compared to SKOV3 cells, as SKOV3 cells are the least sensitive to Niclosamide.

All three cell lines had an increase in NRF2 expression when they were treated with Erastin. This could be due to Erastin increasing the presence of ROS in the cells, triggering NRF2 activation.

RSL3 induced an increase in NRF2 expression in SKOV3 and OVCAR3 cells, but a decrease in TOV112D cells. The increase in NRF2 expression in SKOV3 and OVCAR3 cells could be, like with Erastin, due to an increase in the ROS produced leading to increased NRF2 activation. It is interesting that this response does not happen in TOV112D cells. This could be due to the lethality of RSL3.

When SKOV3 cells were treated with Erastin and Niclosamide, there was a decrease in NRF2 expression. This implies that an alternative pathway is being utilised to increase GPX4 in this cell line under this condition as both ALOX12 and NRF2 are decreased. It is possible the decrease in ALOX12 itself is the protective mechanism to reduce toxic lipid peroxide production. OVCAR3 cells also show a decrease in NRF2 when treated with Erastin and Niclosamide, however this was expected as there is no protection shown in this cell line. In TOV112D cell, Erastin and Niclosamide induced an increase in NRF2 expression. This could be due to an increase in ROS produced as ALOX12 was not increased in the cell line under this condition or an alternative ALOX enzyme is being utilised.

All three cell lines had increased NRF2 expression when treated with RSL3 and Niclosamide. As ALOX12 was increased under these conditions it is possible that this is what is triggering increased NRF2 expression.

4.7. Niclosamide reduced lipid peroxidation in *SLC7A11* positive cell lines treated with Erastin

For the analysis of lipid peroxidation, only Erastin was used as an inducer of ferroptosis due to the toxicity of RSL3 preventing any usable data. Cells were treated with Niclosamide and Erastin and assessed for lipid peroxidation using Flow Cytometry. Cells were also analysed looking at both live cells and all cells to see the effects of viability on results.

When assessing all SKOV3 cells, an increase in lipid peroxidation was seen when the cells are treated with Erastin. This was expected due to Erastin's function as a ferroptotic inducer which is characterised by the accumulation of toxic lipid peroxides. There is a slight increase with Niclosamide, however the data of note is the decrease in lipid peroxidation when cells were treated with both Erastin and Niclosamide when compared to Erastin-only. This shows Niclosamide's ability to reduce lipid peroxidation, and therefore cell death in SKOV3 cells. In live cells, there was still an increase in lipid peroxidation in cells that are treated with Niclosamide, however there was little to no increase in Erastin-treated cells. This could be due to the toxic role of Erastin, meaning most cells that signal for lipid peroxidation were dead so had been gated out of this data set.

In OVCAR3 cells, there was an increase in lipid peroxidation when cells were treated with Erastin and Niclosamide individually. Also, there was no discernible change in lipid peroxidation in cells that had been treated with Niclosamide and Erastin when compared to those that had been treated with only Erastin. This is concurrent with the cell viability data showing that Niclosamide does not protect OVCAR3 cells from Erastin-induced ferroptotic cell death. Interestingly, there was very little difference between all cells being analysed and live cells only. This is also agreeable with the MTT data as OVCAR3 cells are the most resistant to Erastin so less cell death would have occurred in these samples.

TOV112D cells had increased lipid peroxidation when treated with Erastin, but decreased when treated with Niclosamide. The decrease in lipid peroxidation when treated with Niclosamide is interesting as TOV112D cells are more sensitive to Niclosamide, so it would be expected that they would have a greater effect on the cells. However, there was a decrease in lipid peroxidation in cells that are treated with Niclosamide and Erastin when compared to those treated with just Erastin. As with SKOV3 cells, this aligns with cell viability data showing the resistance Niclosamide provides to these cell lines from ferroptotic cell death. Also following the trend set by SKOV3 cells, there is a difference between lipid peroxidation when all

cells are analysed and when only live cells are analysed. This is once again most likely due to the toxic effect of Erastin, being gated out with the dead cells.

4.8. Niclosamide is a confirmed mitochondrial uncoupler and effected basal respiration of ovarian cancer cells

The XF Mito Stress Test was used to assess oxidative phosphorylation and Niclosamide's role as a mitochondrial uncoupler. Across all three cell lines, Niclosamide led to a reduced effect by FCCP. This shows its effect as a mitochondrial uncoupler. Interestingly, Niclosamide had the biggest effect on FCCP in OVCAR3 cells, which Niclosamide does not provide resistance to. In both SKOV3 cells and OVCAR3 cells, Niclosamide caused an increase in basal respiration (0.3 µM of Niclosamide to a greater extent in OVCAR3 cells). This increase could be due to a higher strain on the protonmotive forces needed to produce ATP while Niclosamide is acting as a mitochondrial uncoupler, as the cell viability data showed that cells were dying at these concentrations. Increasing concentrations of Niclosamide caused a decrease in basal respiration in TOV112D cells. As cell viability data showed that TOV112D cell also die at these concentrations of Niclosamide, this could be due to their increased sensitivity to Niclosamide and therefore increased cell death.

It is also important to note that SKOV3 cells did not respond as expected when FCCP was injected into the samples. This could be due to the lack of pyruvate in the growth media due to pyruvate having an effect on lipid peroxidation as it acts as a scavenger of ROS (Lopalco et al., 2016). This lack of pyruvate transport allows the cells to utilise alternative pathways involving the use of lipids and glutamine to regulate the tricarboxylic acid cycle (Martinez-Zamora et al., 2015).

In TOV112D cells and OVCAR3 cells, Erastin caused a decrease in basal respiration, while it caused an increase in SKOV3 cells. As with Niclosamide, these increases and decreases in basal respiration could be due to increased strain on maintaining the proton gradient and reduced cell function, respectively. Erastin also caused a decreased effect when cells were treated with FCCP. This disruption was weakest in OVCAR3 cells which are the most resistant to Erastin. This disruption of mitochondrial

gradients could be due to Erastin's effects on VDAC. The opening of VDAC by Erastin could contribute to the effect of mitochondrial uncoupling, leading to the decreased potency of FCCP in these samples. This is due to the flux of Ca^{2+} caused by the opening of VDAC.

When TOV112D cells were treated with Niclosamide and Erastin, the basal respiration of the cells increased at the lowest concentration of Niclosamide and then decreased at the higher concentration, when compared to cells just treated with Erastin. In SKOV3 cells under these conditions, basal respiration increased at 0.3 µM Niclosamide and was increased but to a lesser at 0.6 µM. The same can be seen in OVCAR3 cells. This implies that basal respiration is not necessarily linked to the rescue the Niclosamide provides these cells from ferroptotic cell death but gives a representation of their metabolic function under these conditions.

5. Conclusion

This data confirms that Niclosamide provided resistance to ferroptosis in some ovarian cancer cells. Data retrieved using the Mito Stress Test confirms that Niclosamide was acting as a mitochondrial uncoupler. Western blot data indicates that ALOX12 could be involved in the resistance of TOV112D cells, but not in SKOV3 and OVCAR3 cells and that GPX4 expression was consistent with the viability data produced. NRF2 was also shown to be affected by Niclosamide. Flow cytometry data showed that lipid peroxidation was decreased by Niclosamide in cells that it provided resistance to when also treated with Erastin. Overall, this data gives an idea of how Niclosamide is affecting these cells and how it is disrupting the ferroptotic pathway as a mitochondrial uncoupler. More research needs to be done to find the link between uncoupling and NRF2 activation where ALOX12 was not affected. This could be achieved by possibly investigating alternative ALOX enzymes such as ALOX5 which has been shown to be induced by Niclosamide or ALOX15 which is also confirmed to be involved with Ferroptosis (Kumar et al., 2018; Shintoku et al., 2017). Further research also needs to be completed to assess the effect of *SLC7A11* knockout using siRNA and PCR on susceptibility to Niclosamide and expression of ALOXs.

6. Appendix

Appendix A. Western Blots (1-3) showing GPX4 and ALOX12 protein expression in SKOV3 cells using β-actin as a control. Blots were cut and pieces probed individually.

1)

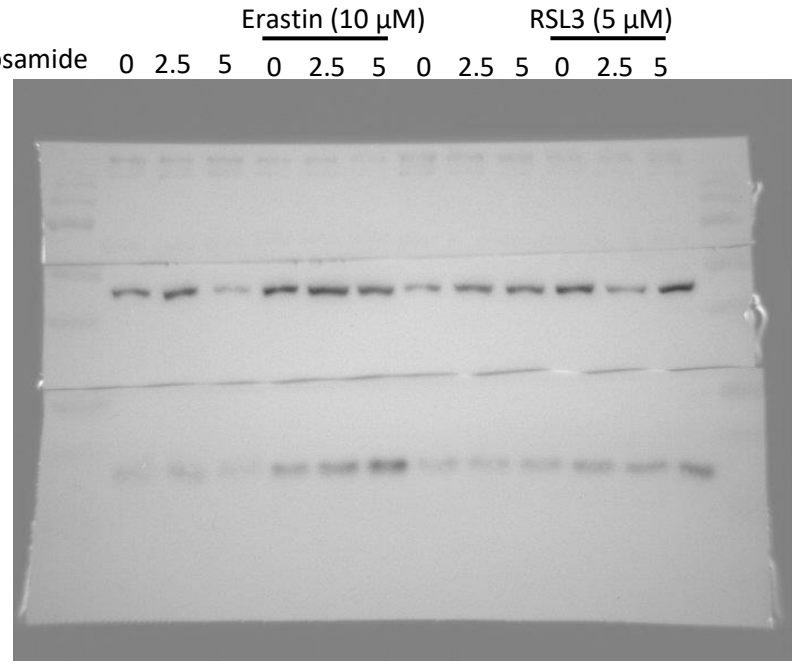

2)

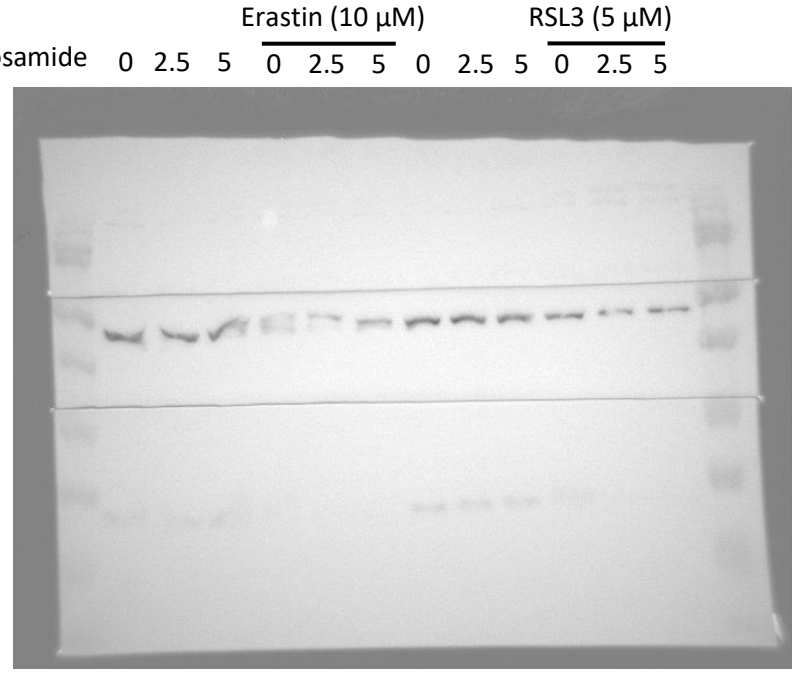

3)

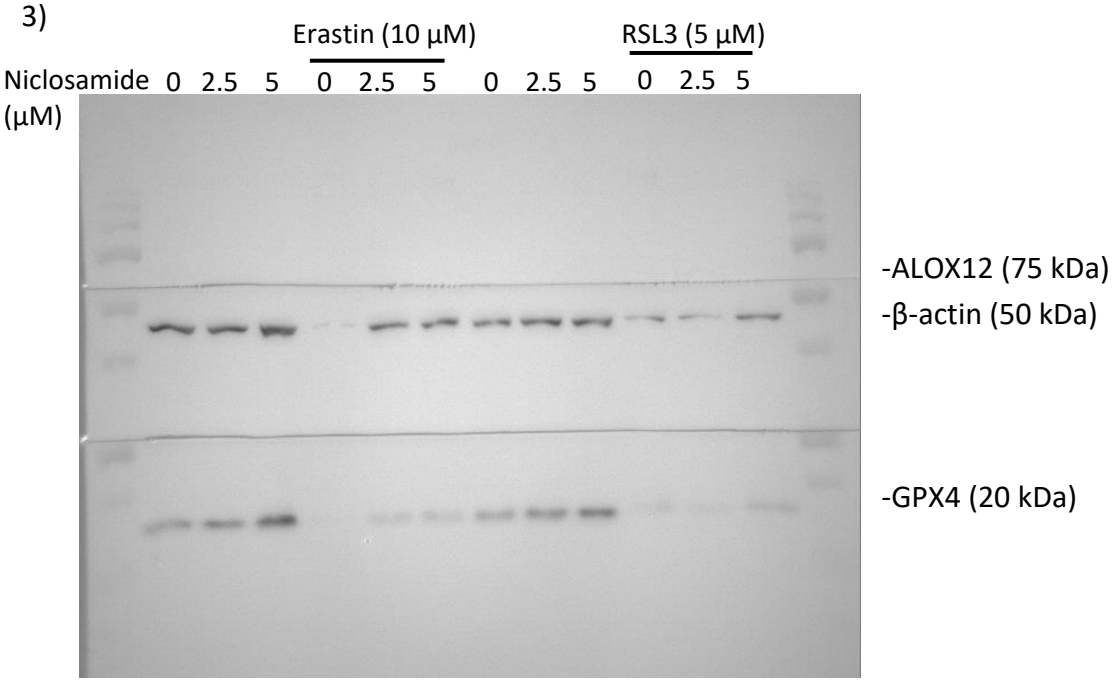

Appendix B. Western Blots (1-4) showing GPX4 and ALOX12 protein expression in OVCAR3 cells using β-actin as a control. Blots were cut and pieces probed individually.

1)

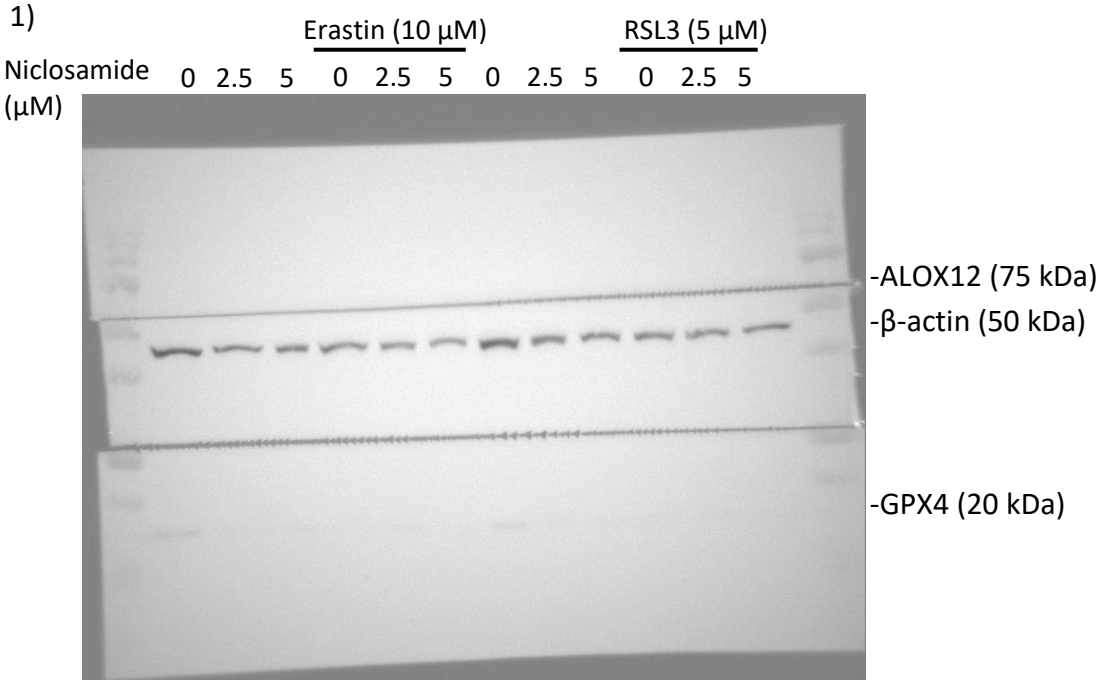

2)

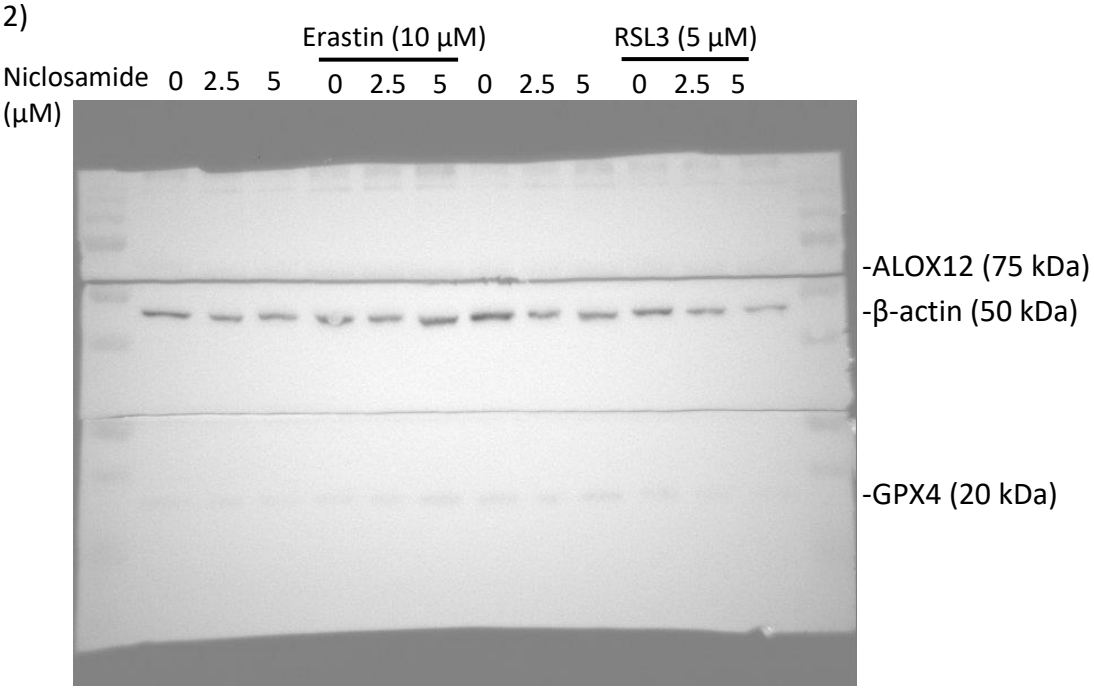
Erastin (10 μM)
RSL3 (5 μM)
Niclosamide (μM)
0 2.5 5 0 2.5 5 0 2.5 5 0 2.5 5
-ALOX12 (75 kDa)
-β-actin (50 kDa)
-GPX4 (20 kDa)

3)

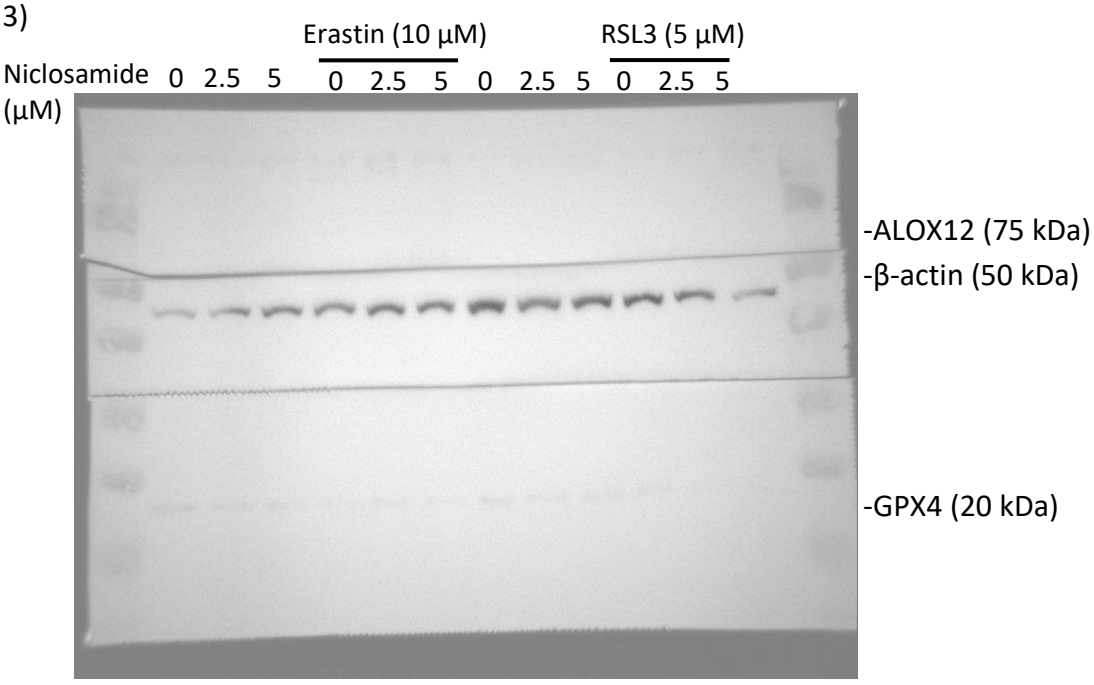
Erastin (10 μM)
RSL3 (5 μM)
Niclosamide (μM)
0 2.5 5 0 2.5 5 0 2.5 5 0 2.5 5
-ALOX12 (75 kDa)
-β-actin (50 kDa)
-GPX4 (20 kDa)

4)

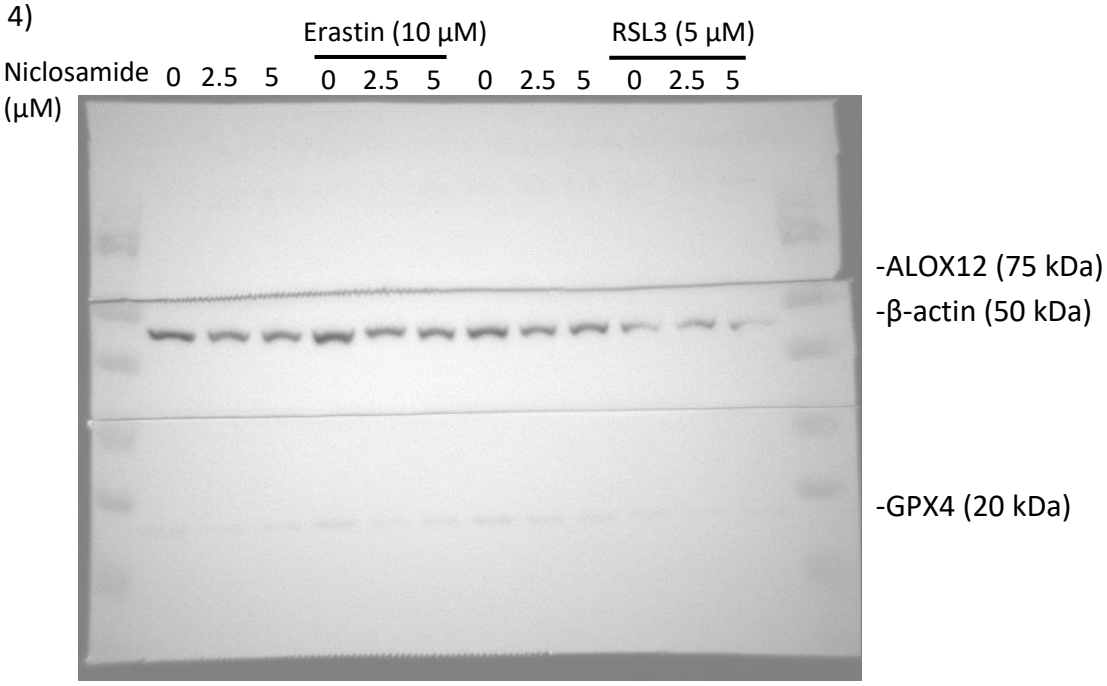

Appendix C. Western Blots (1-3) showing GPX4 and ALOX12 protein expression in TOV112D cells using β-actin as a control. Blots were cut and pieces probed individually.

1)

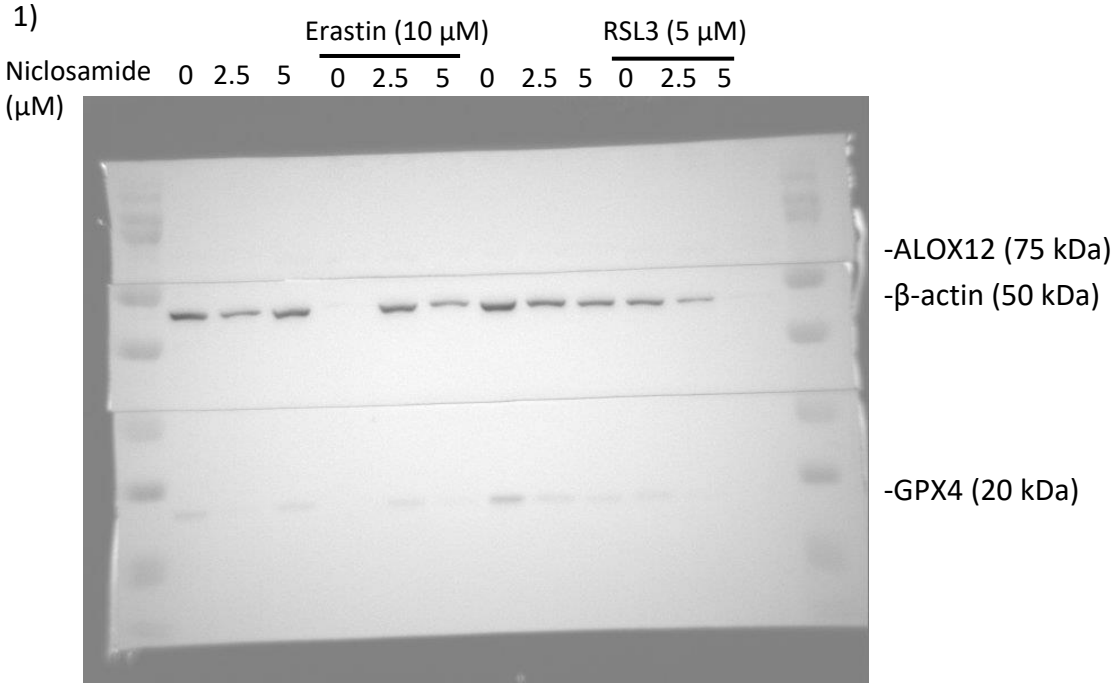

2)

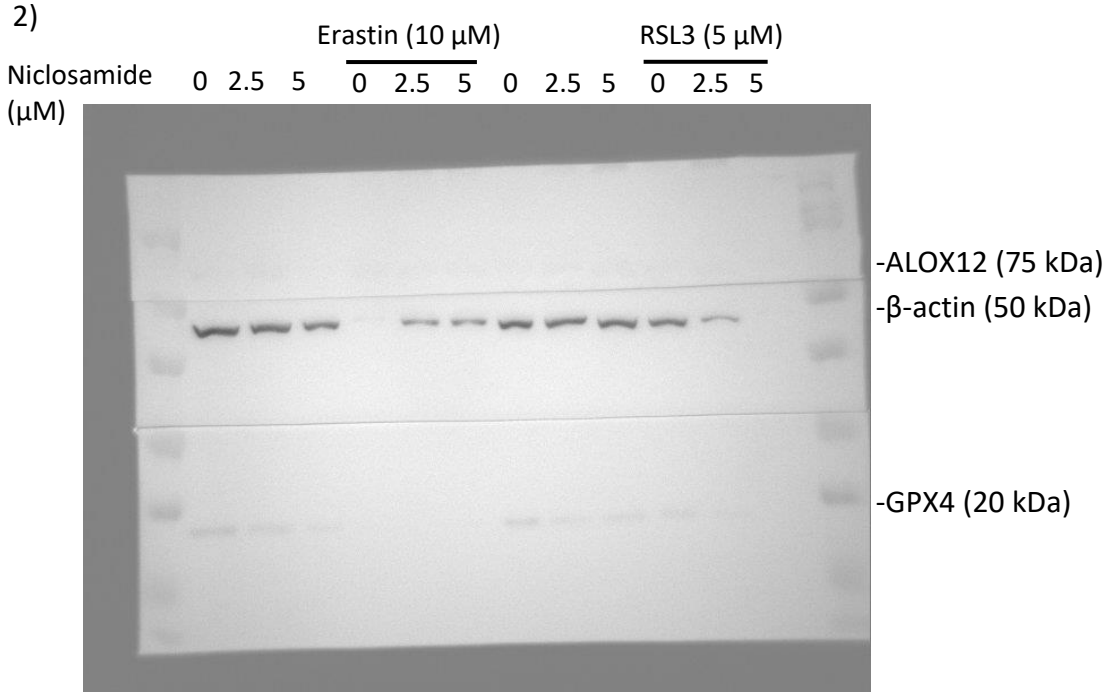
Erastin (10 μM)
RSL3 (5 μM)
Niclosamide (μM)
0 2.5 5 0 2.5 5 0 2.5 5 0 2.5 5
-ALOX12 (75 kDa)
-β-actin (50 kDa)
-GPX4 (20 kDa)

3)

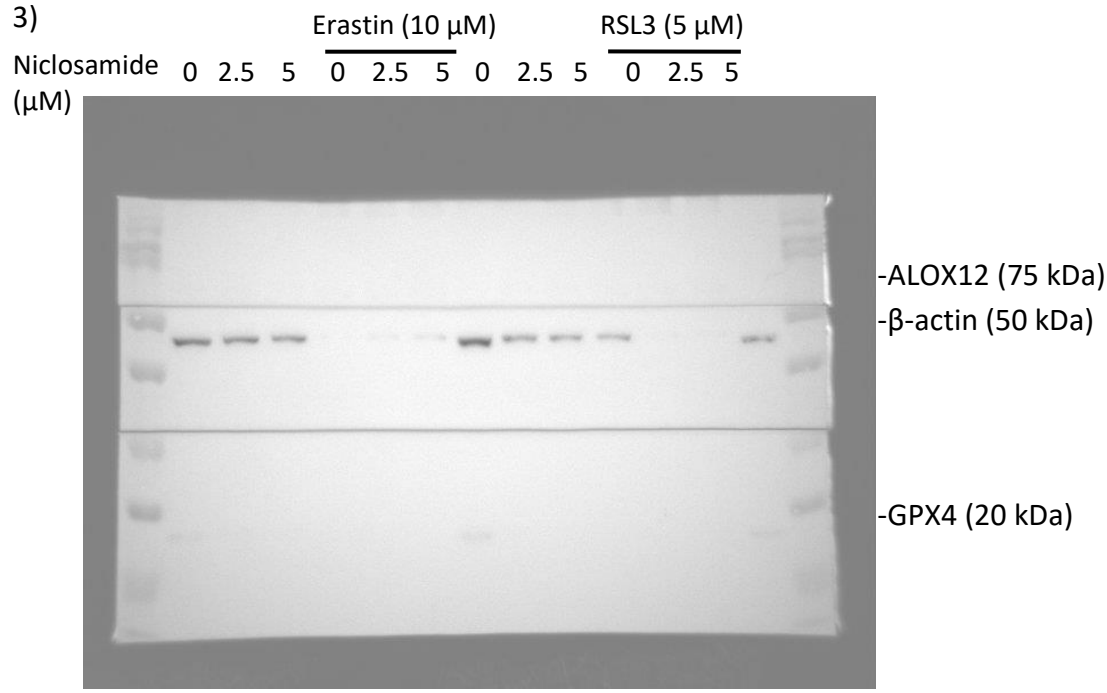
Erastin (10 μM)
RSL3 (5 μM)
Niclosamide (μM)
0 2.5 5 0 2.5 5 0 2.5 5 0 2.5 5
-ALOX12 (75 kDa)
-β-actin (50 kDa)
-GPX4 (20 kDa)

Appendix D. Western Blots (1a-4b) showing NRF2 protein expression in SKOV3 cells with and the same blot stripped and re-probed for α-tubulin.

V: Vehicle
N: Niclosamide (5 µM)
M: Niclosamide (5 µM) + MG-132 (25 µM)

1a)

Erastin (10 µM) RSL3 (5 µM)

V N M V N M V N M V N M

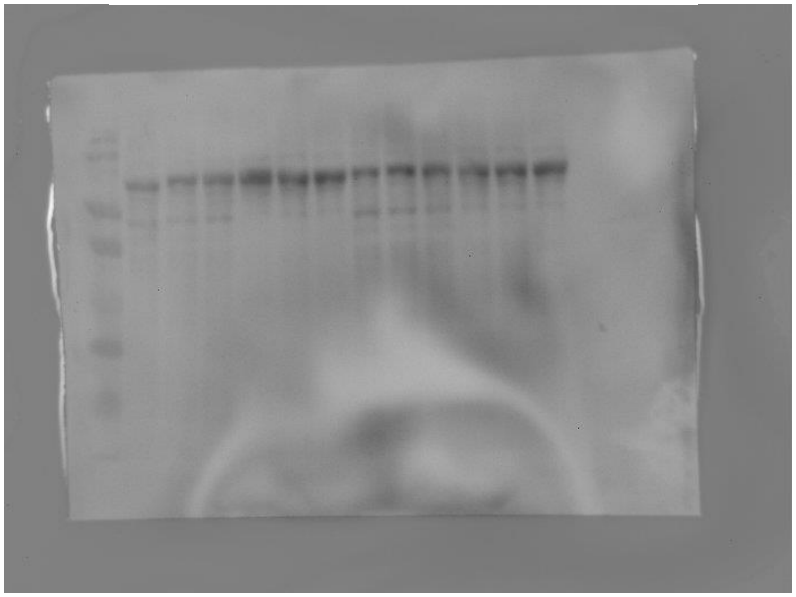

-NRF2 (75 kDa)

1b)

Erastin (10 µM) RSL3 (5 µM)

V N M V N M V N M V N M

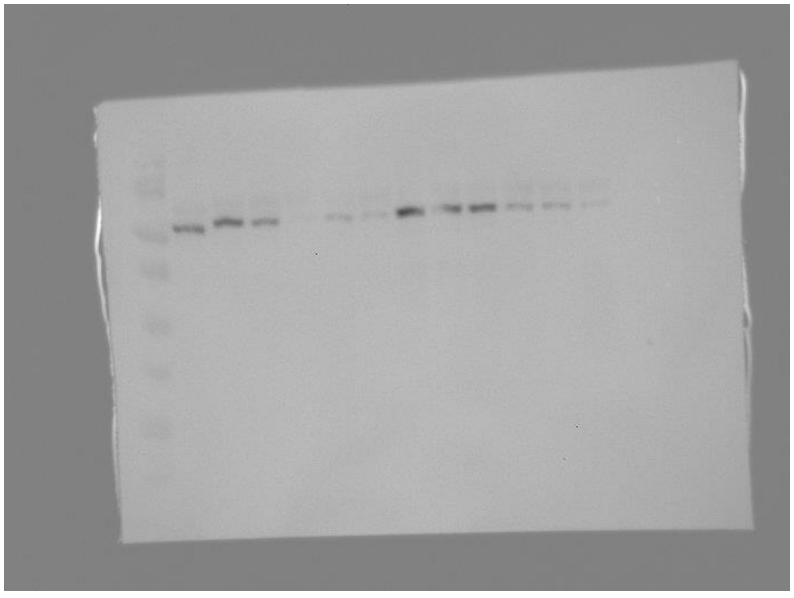

-α-tubulin (50 kDa)

2a)

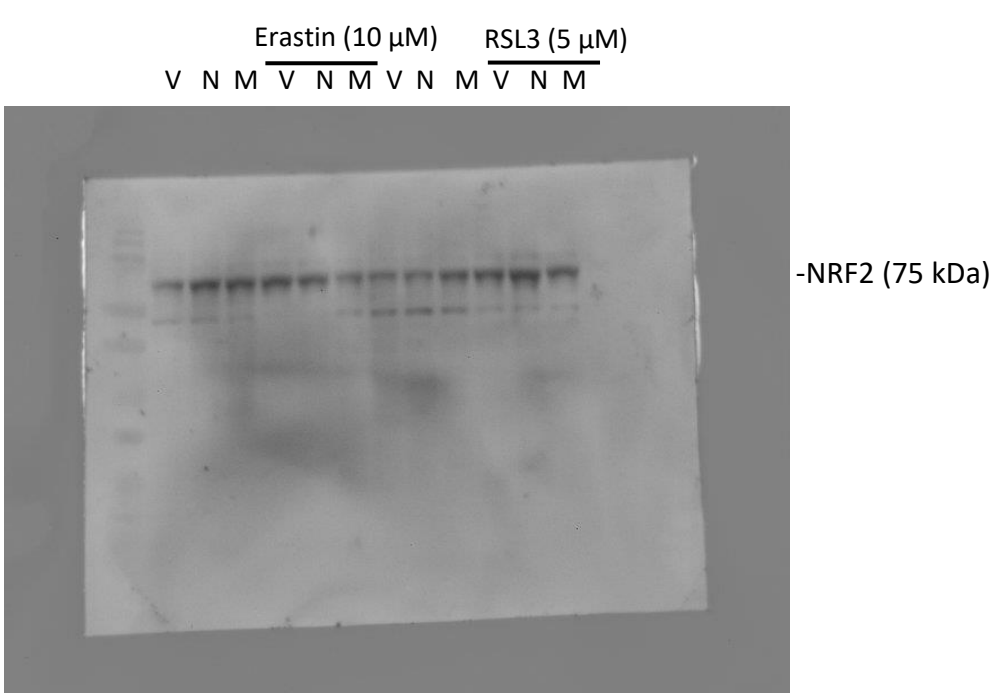
Erastin (10 µM)
RSL3 (5 µM)
V N M V N M V N M V N M
-NRF2 (75 kDa)

2b)

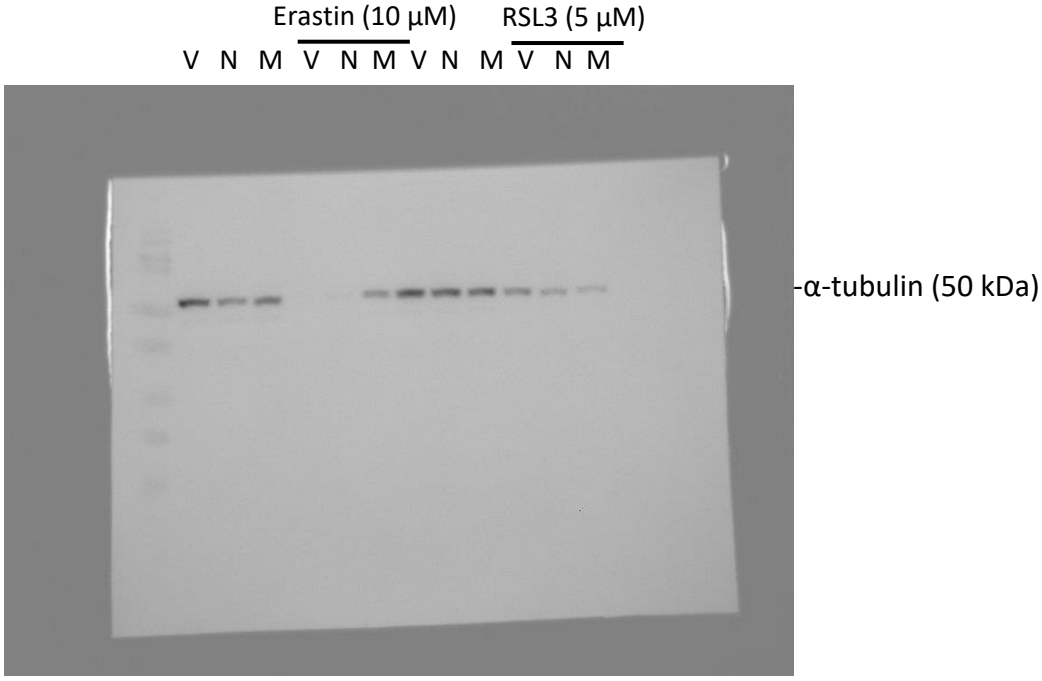
Erastin (10 µM)
RSL3 (5 µM)
V N M V N M V N M V N M
-α-tubulin (50 kDa)

3a)

Erastin (10 μM) RSL3 (5 μM)

V N M V N M V N M V N M

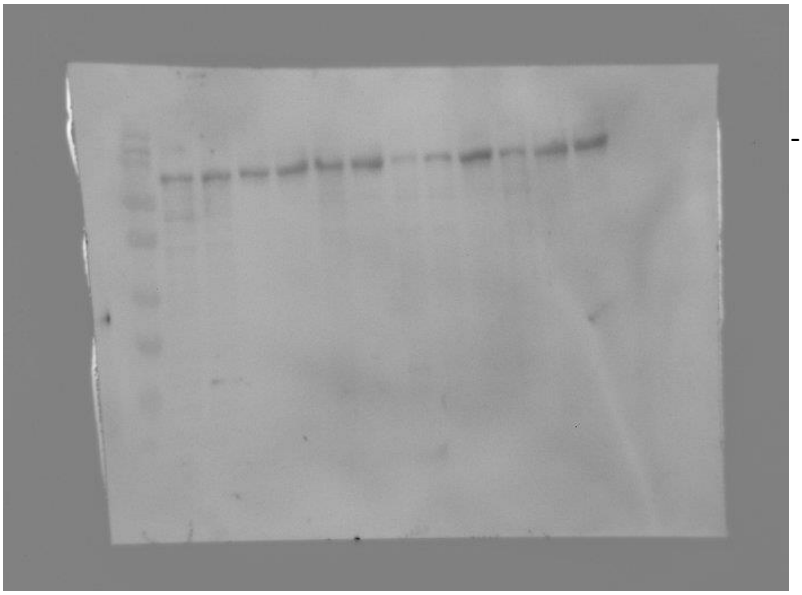

-NRF2 (75 kDa)

3b)

Erastin (10 μM) RSL3 (5 μM)

V N M V N M V N M V N M

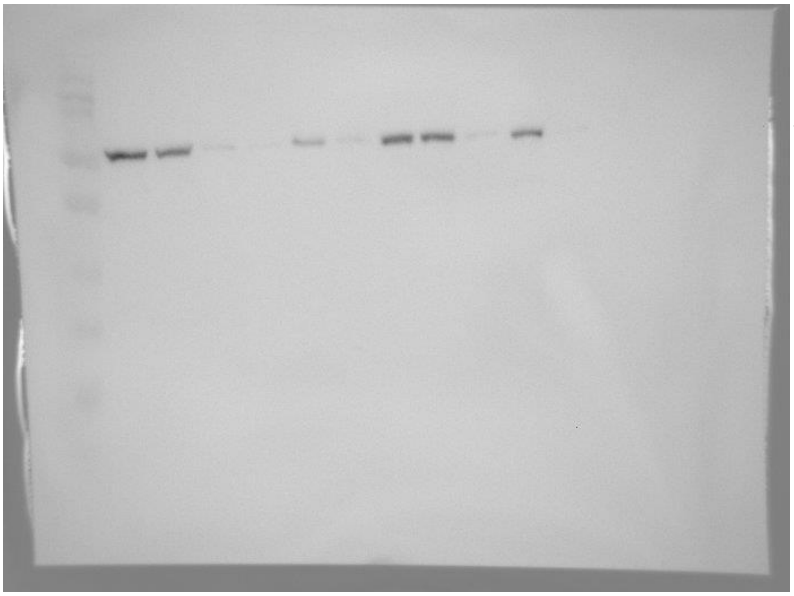

-α-tubulin (50 kDa)

4a)

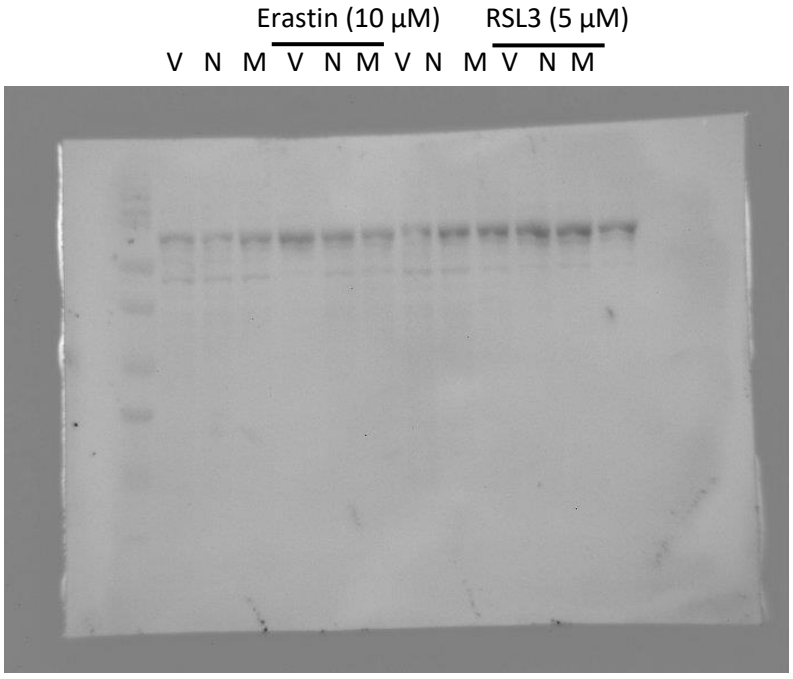
Erastin (10 µM)
RSL3 (5 µM)
V N M V N M V N M V N M
-NRF2 (75 kDa)

4b)

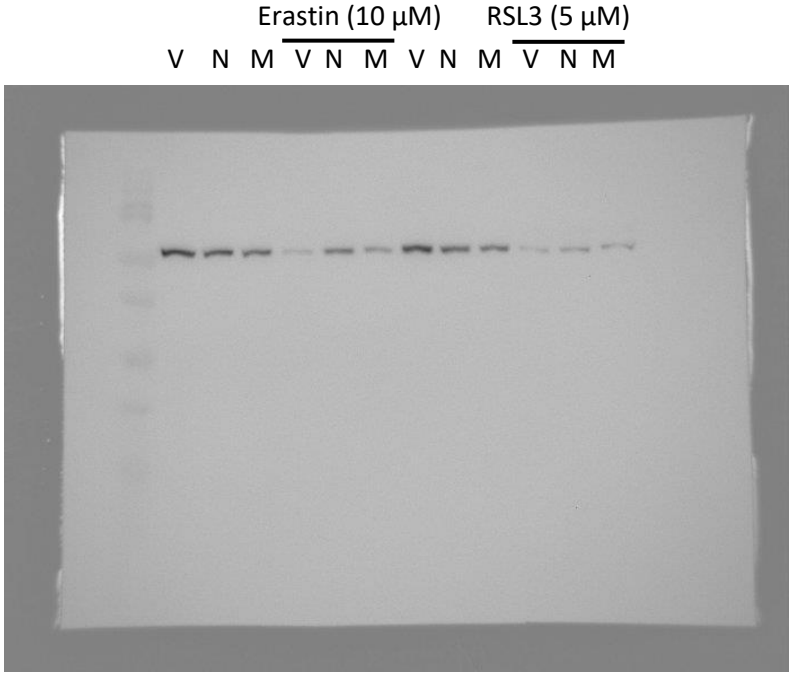
Erastin (10 µM)
RSL3 (5 µM)
V N M V N M V N M V N M
-α-tubulin (50 kDa)

Appendix E. Western Blots (1a-3b) showing NRF2 protein expression in OVCAR3 cells, and the same blot stripped and re-probed for α-tubulin.

1a)

Erastin (10 µM) RSL3 (5 µM)

V N M V N M V N M V N M

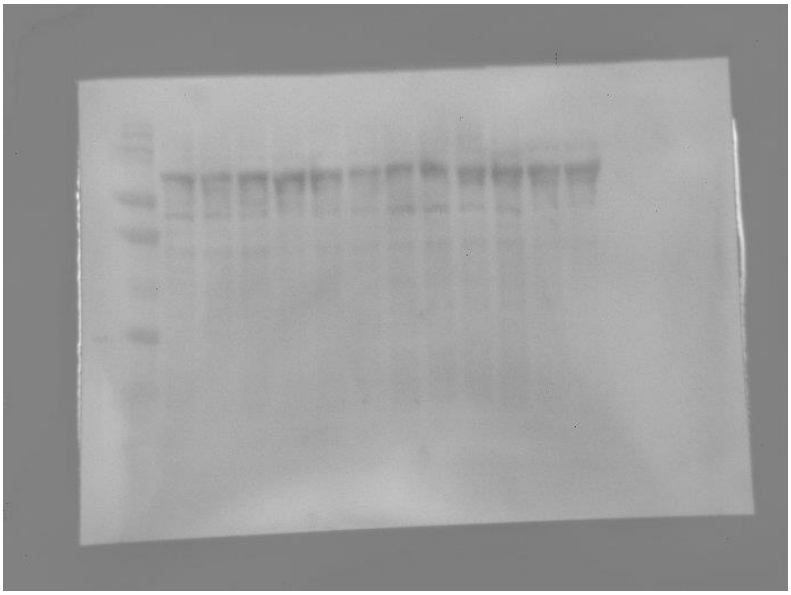

-NRF2 (75 kDa)

1b)

Erastin (10 µM) RSL3 (5 µM)

V N M V N M V N M V N M

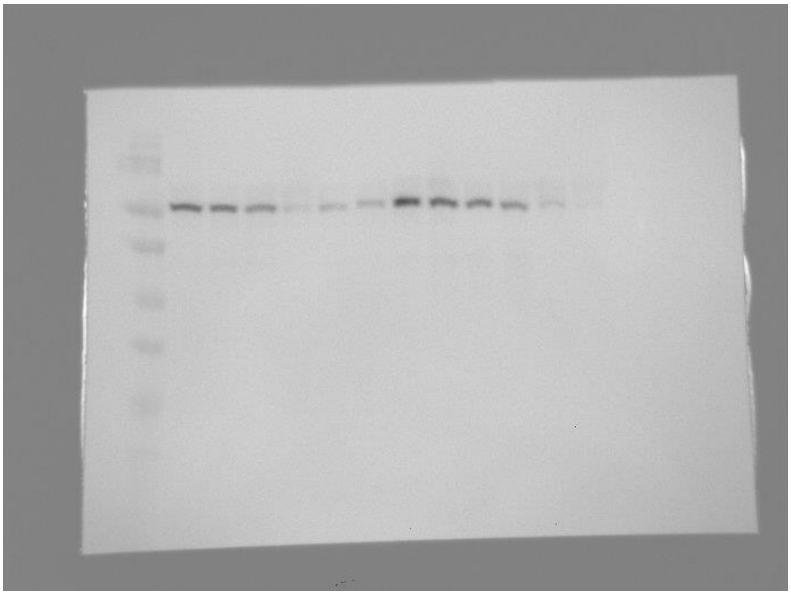

-α-tubulin (50 kDa)

2a)

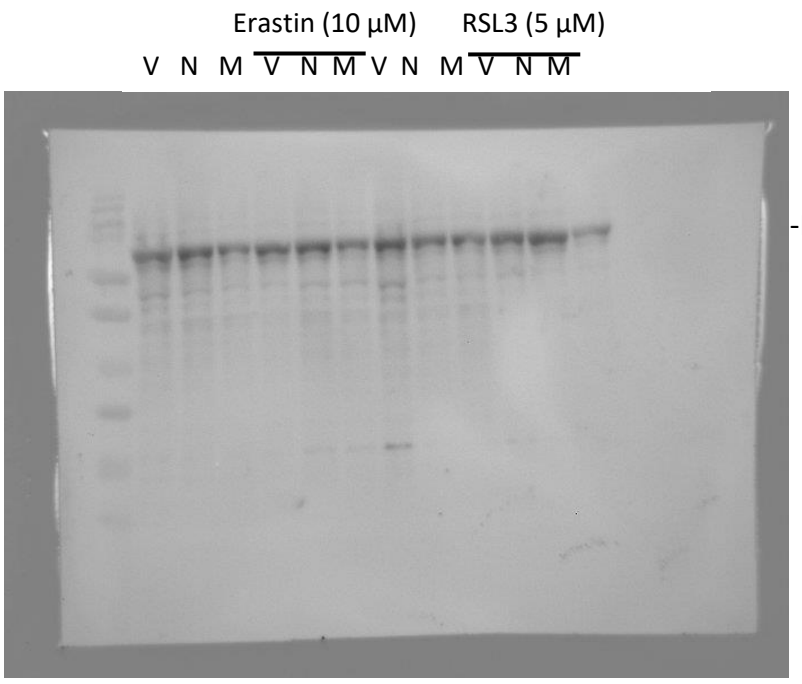
Erastin (10 µM)
RSL3 (5 µM)
V N M V N M V N M V N M
-NRF2 (75 kDa)

2b)

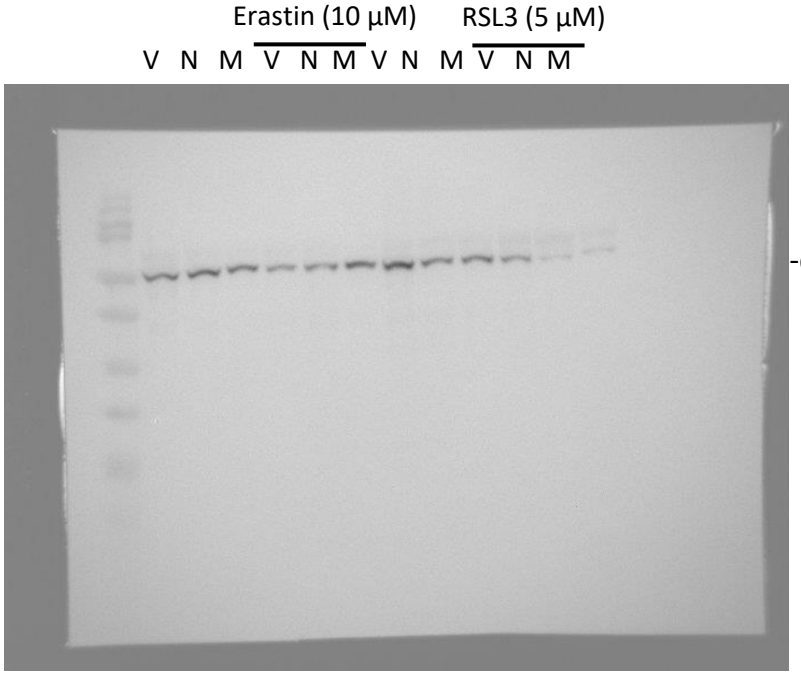
Erastin (10 µM)
RSL3 (5 µM)
V N M V N M V N M V N M
-α-tubulin (50 kDa)

3a)

Erastin (10 µM) RSL3 (5 µM)

V N M V N M V N M V N M

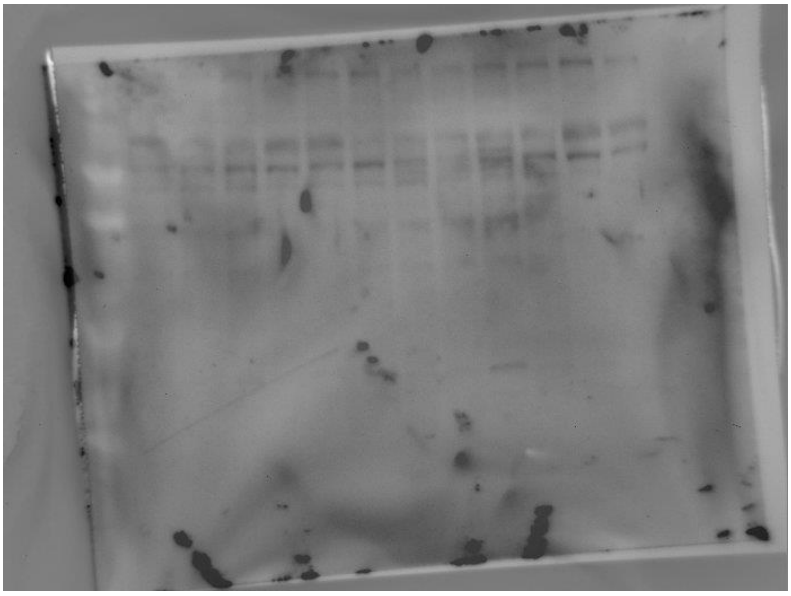

-NRF2 (75 kDa)

3b)

Erastin (10 µM) RSL3 (5 µM)

V N M V N M V N M V N M

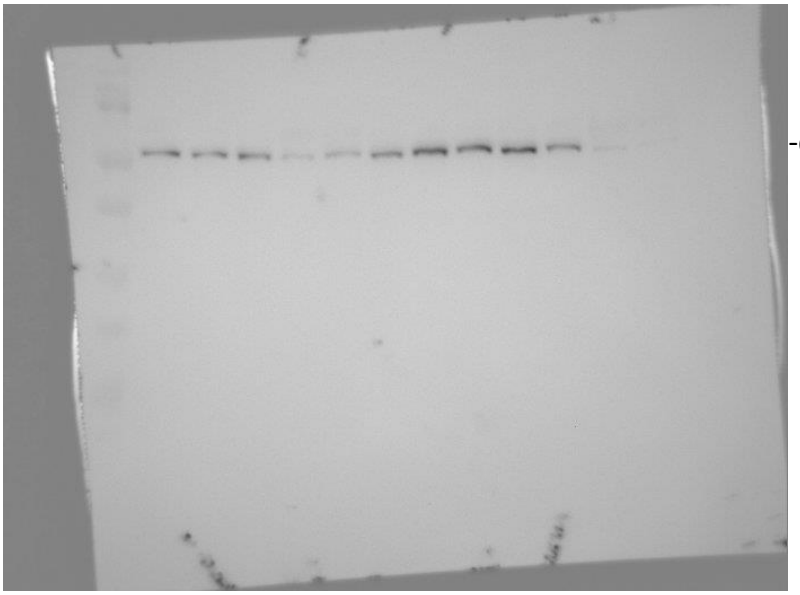

-α-tubulin (50 kDa)

Appendix F. Western Blots (1a-3b) showing NRF2 protein expression in TOV112D cells, and the same blot stripped and re-probed for α-tubulin.

1a)

Erastin (10 μM) RSL3 (5 μM)

V N M V N M V N M V N M

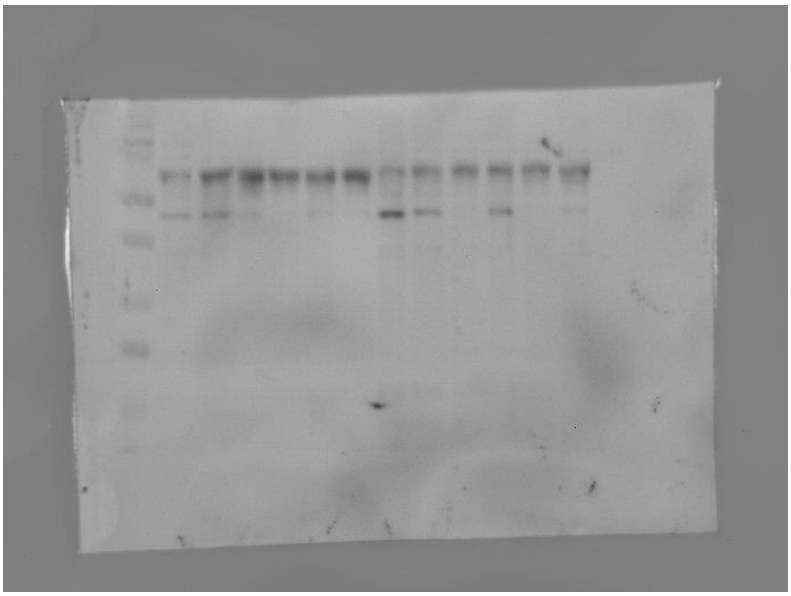

-NRF2 (75 kDa)

1b)

Erastin (10 μM) RSL3 (5 μM)

V N M V N M V N M V N M

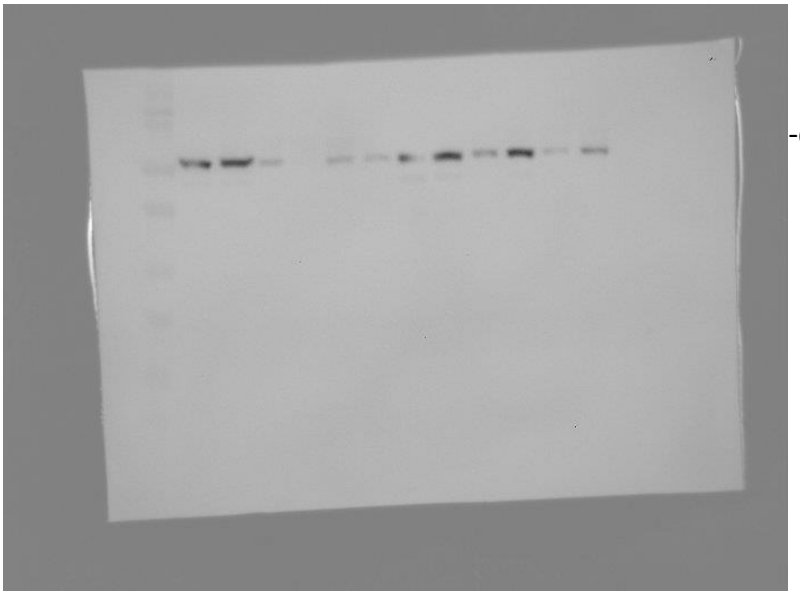

-α-tubulin (50 kDa)

2a)

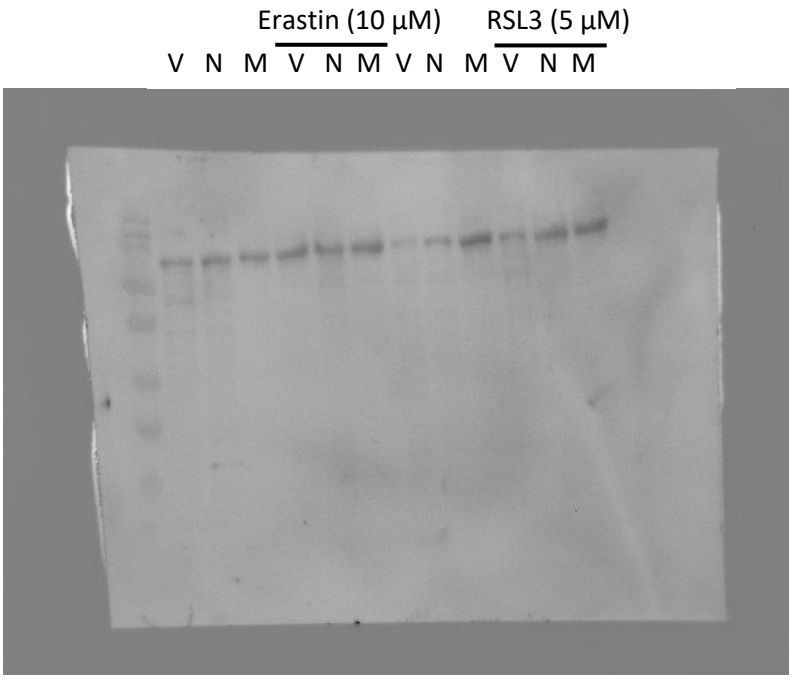
Erastin (10 µM)
RSL3 (5 µM)
V N M V N M V N M V N M
-NRF2 (75 kDa)

2b)

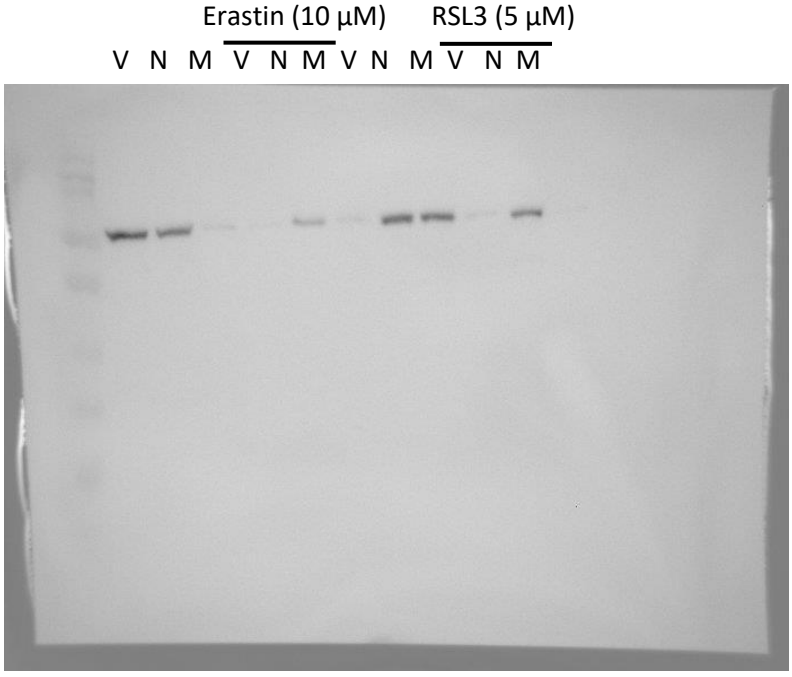
Erastin (10 µM)
RSL3 (5 µM)
V N M V N M V N M V N M
-α-tubulin (50 kDa)

3a)

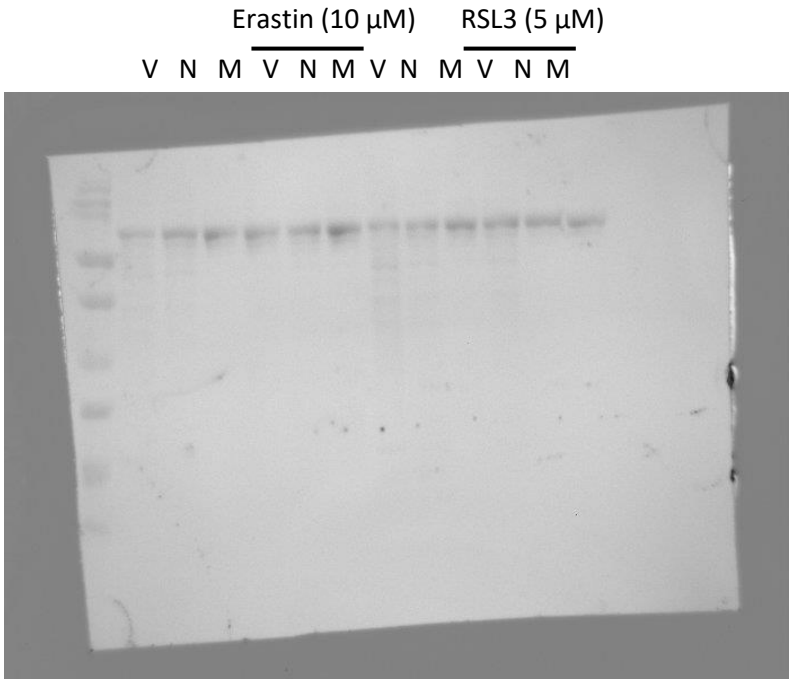

-NRF2 (75 kDa)

3b)

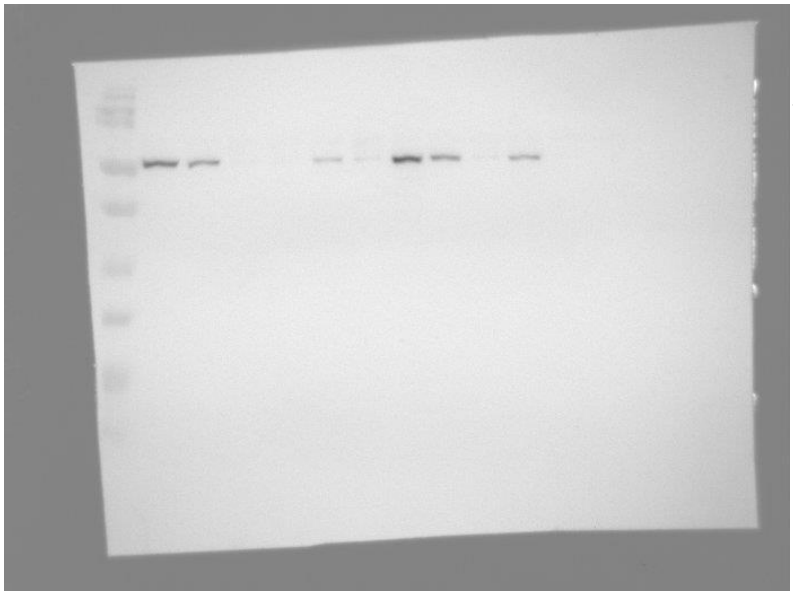

-α-tubulin (50 kDa)

7. Bibliography

Amara, C. E., Shankland, E. G., Jubrias, S. A., Marcinek, D. J., Kushmerick, M. J., & Conley, K. E. (2007). Mild mitochondrial uncoupling impacts cellular aging in human muscles in vivo. *Proceedings of the National Academy of Sciences of the United States of America*, *104*(3), 1057–1062.

Angeli, J. P. F., Schneider, M., Proneth, B., Tyurina, Y. Y., Tyurin, V. A., Hammond, V. J., … Conrad, M. (2014). Inactivation of the ferrroptosis regulator Gpx4 triggers acute renal failure in mice. *Nature Cell Biology*, *16*(12), 1180–1191.

Apter, D., & Vihko, R. (1983). Early menarche, a risk factor for breast cancer, indicates early onset of ovulatory cycles. *The Journal of Clinical Endocrinology and Metabolism*, *57*(1), 82–86.

Auner, V., Kriegshauser, G., Tong, D., Horvat, R., Reinhaller, A., Mustea, A., & Zeillinger, R. (2009). KRAS mutation analysis in ovarian samples using a high sensitivity biochip assay. *BMC Cancer*, *9*, 111.

Ayala, A., Munoz, M. F., & Arguelles, S. (2014). Lipid Peroxidation: Production, Metabolism , and Signaling Mechanisms of Malondialdehyde and 4-Hydroxy-2-Nonenal. *Oxidative Medicine and Cellular Longevity*, *360438*.

Babaier, A., & Ghatage, P. (2020). Mucinous Cancer of the Ovary: Overview and Current Status. *Diagnostics*, *10*(1), 52.

Bannai, S. (1986). Exchange of Cystine and Glutamate across Plasma Membrane of Human Fibroblasts. *Journal of Biological Chemistry*, *261*(5), 2256–2263.

Bashashati, A., Ha, G., Tone, A., Ding, J., Prentice, L. M., Roth, A., … Shah, S. P. (2013). Distinct evolutionary trajectories of primary high-grade serous ovarian cancers revealed through spatial mutational profiling. *Journal of Pathology*, *231*(1), 21–34.

Basta, A., Bidzinski, M., Bienkiewicz, A., Blecharz, P., Bodnar, L., Jack, R., … Madry, R. (2015). Recommendation of the Polish Society of Oncological Gynaecology on the diagnosis and treatment of epithelial ovarian cancer. *Oncology in Clinical Practice*, *11*(5), 233–243.

Bayani, J., Paderova, J., Murphy, J., Rosen, B., Zielenska, M., & Squire, J. A. (2008). Distinct patterns of structural and nnumerical chromosomal instability charaterize sporadic ovarian cancer. *Neoplasia*, *10*(10), 1057–1065.

Bersuker, K., Hendricks, J., Li, Z., Magtanong, L., Ford, B., Tang, P. H., … Olzmann, J. A. (2019). The CoQ oxidoreductase FSP1 acts in parallel to GPX4 to inhibit ferroptosis. *Nature*, *575*(7784), 688–692.

Blaikie, F. H., Brown, S. E., Samuelsson, L. M., Brand, M. D., Smith, R. A. J., & Murphy, M. P. (2006). Targeting dinitrophenol to mitochondria: Limitations to the development of a self-limiting mitochondrial protonophore. *Bioscience Reports*, *26*, 231–243.

Borgese, N., Aggujaro, D., Carrera, P., Pietrini, G., & Bassetti, M. (1996). A role for N-myristoylation in protein targeting: NADH-Cytochrome b5 reductase requires myristic acid for association with outer mitochondrial but not ER membranes. *The Journal of Cell Biology*, *135*, 1501–1513.

Brilhante, A. V. M., Augusto, K. L., Portela, M. C., Sucupira, L. C. G., Oliveira, L. A. F., Pouchaim, A. J. M. V., … Sobreira, L. R. P. (2017). Endometriosis and ovarian cancer: an integrative review (Endometriosis and Ovarian Cancer). *Asian Pacific Journal of Cancer Prevention*, *18*(1), 11–16.

Cancer Research UK. (2019). Ovarian cancer incidence statistics | Cancer Research UK. Retrieved November 13, 2019, from https://www.cancerresearchuk.org/health-professional/cancer-statistics/statistics-by-cancer-type/ovarian-cancer/incidence#ref-5

Casagrande, J. T., Louie, E. W., Pik, M. C., Ross, R. K., & Henderson, B. E. (1979). "Incessant ovulation" and ovarian cancer. *The Lancet*, *2*(8135), 170–173.

Christensen, H. N. (1990). Role of amino acid transport and countertransport in nutrition and metabolism. *Physiological Reviews*, *70*(1), 43–77.

Chu, B., Kon, N., Chen, D., Li, T., Liu, T., Jiang, L., … Gu, W. (2019). ALOX12 is required for p53-mediated tumor suppression through a distinct ferroptosis pathway. *Nature Cell Biology*, *21*(5), 579–591.

Clark, J. D., Lin, L., Kriz, R. W., Ramesha, C. S., Sultzman, L. A., Lin, A. Y., … Knopf, J. L. (1991). A novel arachidonic acid-selective cytosolic PLA2 contains a Ca2+-dependent translocation domain with homology to PKC and GAP. *Cell*, *65*, 1043–1051.

Coburn, S. B., Bray, F., Sherman, M. E., & Trabert, B. (2017). International patterns and trends in ovarian cancer incidence, overall and by histological subtype.

International Journal of Cancer, *140*, 2451–2460.

Colombini, M. (2004). VDAC: The channel at the interface between mitochondria and the cytosol. In *Molecular and Cellular Biochemistry*, *256,* 107-115.

Conrad, M., Kagan, V. E., Bayir, H., Pagnussat, G. C., Head, B., Traber, M. G., & Stockwell, B. R. (2018). Regulation of lipid peroxidation and ferroptosis in diverse species. *Genes & Development*, *32*(9–10), 602–619.

Cont, N. T., Ferrero, A., Peccatori, F. A., D'Alonzo, M., Codacci-Pisanelli, G., Colombo, N., & Biglia, N. (2015). Medical treatment of early stage and rare histological variants of epithelial ovarian cancer. *Ecancermedicalscience*, *9*, 584.

Corsello, S. M., Nagari, R. T., Spangler, R., Rossen, J., Kocak, M., Bryan, J., … Golub, T. (2019). Non-oncology drugs are a source of previously unappreciated anti-cancer activity. *BioRxiv*.

Cortez, A. J., Tudrej, P., Kujawa, K. A., & Lisowska, K. M. (2018). Advances in ovarian cancer therapy. *Cancer Chemotherapy and Pharmacology*, *81*, 17–38.

Coscia, F., Watters, K. M., Curtis, M., Eckert, M. A., Chiang, C. Y., Tyanova, S., … Mann, M. (2016). Integrative proteomic profiling of ovarian cancer cell lines reveals precursor cell associated proteins and functional status. *Nature Communications*, *7*.

Cozza, G., Rossetto, M., Bosello-Travain, V., Maiorino, M., Roveri, A., Toppo, S., … Ursini, F. (2017). Glutathione peroxidase 4-catalyzed reduction of lipid hydroperoxides in membranes: The polar head of the membrane phospholipids binds the enzyme and addresses the fatty acid hydroperoxide group toward the redox center. *Free Radical Biology and Medicine*, *112*, 1–11.

Cramer, D. W., & Welch, W. R. (1983). Determinants of Ovarian Cancer Risk. II. Inferences Regarding Pathogenesis. *Journal of the National Cancer Institution*, *71*(4), 717–721.

Cullinan, S. B., Gordan, J. D., Jin, J., Harper, J. W., & Dielh, J. A. (2004). The Keap1-BTB protein is an adaptor that bridges Nrf2to a Cul3-Based E3 ligase: Oxidative stress sensing by a Cul3-Keap1 ligase. *Molecular and Cellular Biology*, *24*(19), 8477–8486.

DeHart, D. N., Fang, D., Heslop, K., Li, L., Lemasters, J. J., & Maldonado, E. N. (2018).

Opening of voltage dependent anion channels promotes reactive oxygen species generation, mitochondrial dysfunction and cell death in cancer cells. *Biochemical Pharmacology*, *148*, 155–162.

Demine, S., Renard, P., & Arnould, T. (2019). Mitochondrial uncoupling: A key controller of biological processes in physiology and diseases. *Cells*, *8*.

Dempster, J. M., Rossen, J., Kazachkova, M. B., Pan, J., Kugener, G., Root, D., & Tsherniak, A. (2019). Extracting biological insights from the project achilles genome-scale CRISPR screens in cancer cell lines. *BioRxiv*.

Deng, J., Wang, L., Chen, H., Hao, J., Ni, J., Chang, L., … Li, Y. (2016). Targeting epithelial-mesenchymal transition and cancer stem cells for chemoresistant ovarian cancer. *Oncotarget*, *7*(34), 55771–55788.

Depmap, & Broad. (2021). *DepMap 21Q2 Public*.

Di Nicola, V. (2019). Omentum a powerful biological source in regenerative surgery. *Regenerative Therapy*, *11*, 182–191.

Dinkova-Kostova, A. T., Holtzclaw, W. D., Cole, R. N., Itoh, K., Wakabayashi, N., Katoh, Y., … Talalay, P. (2002). Direct evidence that sulfhydryl groups of Keap1 are the sensors regulating induction of phase 2 enzymes that protect against carcinogens and oxidants. *Proceedings of the National Academy of Sciences of the United States of America*, *99*(18), 11908–11913.

Dixon, S. J., Lemberg, K. M., Lamprecht, M. R., Skouta, R., Zaitsev, E. M., Gleason, C. E., … Stockwell, B. R. (2012). Ferroptosis: An iron-dependent form of nonapoptotic cell death. *Cell*, *149*(5), 1060–1072.

Dodson, M., Castro-Portuguez, R., & Zhang, D. D. (2019). NRF2 plays a critical role in mitigating lipid peroxidation and ferroptosis. *Redox Biology*, *23*, 101107.

Doll, S., Freitas, F. P., Shah, R., Aldrovandi, M., da Silva, M. C., Ingold, I., … Conrad, M. (2019). FSP1 is a glutathione-independent ferroptosis suppressor. *Nature*, *575*(7784), 693–698.

Dolma, S., Lessnick, S. L., Hahn, W. C., & Stockwell, B. R. (2003). Identification of genotype-selective antitumor agents using synthetic lethal chemical screening in engineered human tumor cells. *Cancer Cell*, *3*(3), 285–296.

du Bois, A., Reuss, A., Pujade-Lauraine, E., Harter, P., Ray-Coquard, I., & Pfisterer, J. (2009). Role of surgical outcome as prognostic factor in advanced epithelial

ovarian cancer: a combined exploratory analysis of 3 prospectively randomized phase 3 multicenter trials: by the Arbeitsgemeinschaft Gynarkologische Onkologie Studiengruppe Ovarialkarzin. *Cancer*, *115*(6), 1234–1244.

El-Osta, H., Falchook, G., Tsimberidou, A., Hong, D., Naing, A., Kim, K., … Kurzrock, R. (2011). BRAF mutations in advanced cancers: Clinical characteristics and outcomes. *PLoS One*, *6*(10), e25806.

Foley, O. W., Rauh-Hain, J. A., Del Carmen, M. G., & Marcela, G. (2013). Recurrent epithelial ovarian cancer: An update on treatment. *Oncology*, *27*(4), 288–294.

Frayha, G. J., Smyth, J. D., Gobert, J. G., & Savel, J. (1997). The mechanism of action of antiprotozoal and anthelmintic drugs in man. *Genetic Pharmacology*, *28*(1), 273–299.

Friedmann-Morvinski, D., & Verma, I. M. (2014). Dedifferentiation and reprogramming: origins of cancer stem cells. *EMBO Reports*, *15*(3), 244–253.

Gaschler, M. M., & Stockwell, B. R. (2017). Lipid peroxidation in cell death. *Biochemical and Biophysical Research Communications*, *15*(482), 149–425.

Gu, Y., Mohammad, I. S., & Liu, Z. (2020). Overview of the STAT-3 signalling pathway in cancer and the development of specific inhibitors. *Oncology Letters*, *19*(4), 2585–2594.

Habib, E., Linher-Melville, K., Lin, H., & Singh, G. (2015). Expression of xCT and acivity of system xc- are regulated by NRF2 in human breast cancer cells in response to oxidative stress. *Redox Biology*, *5*, 33–42.

Hao, S., Liang, B., Huang, Q., Dong, S., Wu, Z., He, W., & Shi, M. (2018). Metabolic networks in ferroptosis (Review). *Oncology Letters*, *15*, 5405–5411.

Haslehurst, A. M., Koti, M., Dharsee, M., Nuin, P., Evans, K., Geraci, J., … Feilotter, H. (2012). EMT transcription factors snail and slug directly contribute to cisplatin resistance in ovarian cancer. *BMC Cancer*, *12*(91).

Horvath, T. L., Diano, S., & Barnstable, C. (2003, June 15). Mitochondrial uncoupling protein 2 in the central nervous system: Neuromodulator and neuroprotector. *Biochemical Pharmacology*, *65*, 1917–1921.

Huang, X., Liang, Y., Qing, Y., Chen, D., & Shi, N. (2019). Proteasome inhibition by MG-132 protects against deltamethrin-induced apoptosis in rat hippocampus. *Life Sciences*, *220*, 76–83.

Itoh, K., Chiba, T., Takahashi, S., Ishii, T., Igarashi, K., Katoh, Y., … Nabeshima, Y. (1997). An NRF2/Small maf heterodimer mediates the induction of phase II detoxifying enzyme genes through antioxidant response elements. *Biochemical and Biophysical Research Communications*, *236*, 313–322.

Itoh, K., Wakabayashi, N., Katoh, Y., Ishii, T., Igarashi, K., Engel, J. D., & Yamamoto, M. (1999). Keap1 represses nuclear activation of antioxidant responsive elements be Nrf2 thorugh binding to the amino-terminal Neh2 domain. *Genes & Development*, *13*(1), 76–86.

Ivanov, I., Kuhn, H., & Heydeck, D. (2015). Structural and functional biology of arachidonic acid 15-lipoxygenase-1 (ALOX15). *Gene*, *573*(1), 1–32.

Jacobs, I., & Lancaster, J. (1996). The molecular genetics of sporadic and familial epithelial ovarian cancer. *International Journal of Gynecological Cancer*, *6*(5), 337–355.

Jain, R. K. (2014). Antiangiogenesis strategies revisited: from starving tumors to alleviating hypoxia. *Cancer Cell*, *26*(5), 605–622.

Jiang, L., Kon, N., Li, T., Wang, S., Su, T., Hibshoosh, H., … Gu, W. (2015). Ferroptosis as a p53-mediated activity during tumour suppression. *Nature*, *520*(7545), 57–62.

Jordan, S. J., Webb, P. M., & Green, A. C. (2005). Height, age at menarche, and risk of epithelial ovarian cancer. *Cancer Epidemiology, Biomarkers and Prevention*, *14*(8), 2045–2048.

Jurgeit, A., McDowell, R., Moese, S., Meldrum, E., Schwendener, R., & Greber, U. F. (2012). Niclosamide is a proton carrier and targets acidic endosomes with broad antiviral effects. *PLoS Pathogens*, *8*(10), e1002976.

Kim, S., Han, Y., Kim, S. I., Kim, H.-S., Kim, S. J., & Song, Y. S. (2018). Tumor evolution and chemoresistance in ovarian cancer. *Npj Precision Oncology*, *2*(1).

Kralickova, M., Lagana, A. S., Ghezzi, F., & Vetvicka, V. (2020). Endometriosis and risk of ovarian cancer: what do we know? *Archives of Gynechology and Obstetrics*, *301*, 1–10.

Kramer, R. M., & Sharp, J. D. (1997). Structure, function and regulation of Ca2+-sensitive cytosolic phospholipase A2 (cPLA2). *FEBS Letter*, *410*, 49–53.

Kuhn, H., Banthiya, S., & van Leyen, K. (2014). Mammalian lipoxygenases and their

biological relevance. *Biochimica et Biophysica Acta*, *1851*(4), 308–330.

Kumar, R., Coronel, L., Somalanka, B., Raju, A., Aning, O. A., An, O., … Cheok, C. F. (2018). Mitochondrial uncoupling reveals a novel therapeutic opportunity for p53-defective cancers. *Nature Communications*, *9*(1).

Kurman, R. J., & Shih, I. M. (2010). The origin and pathogenesis of epithelial ovarian cancer: A proposed unifying theory. *American Journal of Surgical Pathology*, *34*(3), 433–443.

Kurrey, N. K., Jalgaonkar, S. P., Joglekar, A. V., Ghanate, A. D., Chaskar, P. D., Doiphode, R. Y., & Bapat, S. A. (2009). Snail and slug mediate radioresistance and chemoresistance be antagonizing p53-mediated apoptosis and aquiring a stem-like phenotype in ovarian cancer cells. *Stem Cells*, *27*(9), 2059–2068.

Kurz, T., Gustafsson, B., & Brunk, U. T. (2006). Intralysosomal iron chelation protects against oxidative stress-induced cellular damage. *The FEBS Journal*, *273*(13), 3106–3117.

Labidi-Galy, S. I., Papp, E., Hallberg, D., Niknafs, N., Adleff, V., Noe, M., … Velculescu, V. E. (2017). High grade serous ovarian carcinomas originate in the fallopian tube. *Nature Communications*, *8*(1).

Lamouille, S., Xu, J., & Derynck, R. (2014). Molecular mechanisms of epithelial-mesenchymal transition. *Nature Reviews Molecular Cell Biology*, *15*(3), 178–196.

Latreche, L., Duhieu, S., Touat-Hamici, Z., Jean-Jean, O., & Chavatte, L. (2012). The differential expression of glutathione peroxidase 1 and 4 depends on the nature of the SECIS element. *RNA Biology*, *9*(5), 681–690.

Latunde-Dada, G. O. (2017). Ferroptosis: Role of lipid peroxidation, iron and ferritinophagy. *BBA - General Subjects*, *1861*, 1893–1900.

Li, C., Deng, X., Xie, X., Liu, Y., Angeli, J. P. F., & Lai, L. (2018). Activation of glutathione peroxidase 4 as a novel anti-inflammatory strategy. *Frontiers in Pharmacology*, *9*(1120), 1–12.

Lim, D., Murali, R., Murray, M. P., Veras, E., Park, K. J., & Soslow, R. A. (2016). Morphological and immunohistochemical re-evaluation of tumors initially diagnosed as ovarian endometrioid carcinoma with emphasis on high-grade tumors. *American Journal of Surgical Pathology*, *40*(3), 302–312.

Liu, C., Lou, W., Zhu, Y., Nadiminty, N., Schwatz, C. T., Evans, C. P., & Gao, A. C. (2014). Niclosamide inhibits androgen receptor variants expression and overcomes enzalutamide resistance in castration-resistant prostate cancer. *Clinical Cancer Research*, *20*(12), 3198–3210.

Liu, J. F., Konstantinopoulos, P. A., & Matulonis, U. A. (2014). PARP inhibitors in ovarian cancer: Current status and future promise. *Gynecologic Oncology*, *133*(2), 362–369.

Lopalco, A., Dalwadi, G., Niu, S., Schowen, R. L., Douglas, J., & Stella, V. J. (2016). Mechanism of decarboxylation of pyruvic acid in the presence of hydrogen peroxide. *Journal of Pharmaceutical Sciences*, *105*(2), 705–713.

Magtanong, L., Ko, P. J., To, M., Cao, J. Y., Forcina, G. C., Tarangelo, A., … Dixon, S. J. (2019). Exogenous monounsaturated fatty acids promote a ferroptosis-resistant cell state. *Cell Chemical Biology*, *26*(3), 420-432.e9.

Malpica, A., Deavers, M. T., Lu, K., Bodurka, D. C., Atkinson, E. N., Gershenson, D. M., & Silva, E. G. (2004). Grading ovarian serous carcinoma using two-tier system. *American Journal of Surgical Pathology*, *28*(4), 496–504.

Markowska, A., Sajdak, S., Huczyński, A., Rehlis, S., & Markowska, J. (2018). Ovarian cancer stem cells: A target for oncological therapy. *Advances in Clinical and Experimental Medicine*, *27*(7), 1017–1020.

Martinez-Zamora, A., Meseguer, S., Esteve, J. M., Villaroya, M., Aguado, C., Enriquez, J. A., … Armengod, M. E. (2015). Defective expression of the mitochondrial-tRNA modifying enzyme GTPBP3 triggers AMPK-mediated adaptive responses involving complex I assembly factors, uncoupling protein 2, and the mitochondrial pyruvate carrier. *PLoS One*, *10*(12).

Mashima, R., & Okuyama, T. (2015). The role of lipoxygenases in pathophysiology; new insights and future perspectives. *Redox Biology*, *6*, 297–310.

McHutchison, J. G. (1997). Differential diagnosis of ascites. *Seminars in Liver Disease*, *17*(3), 191–202.

Meng, E., Long, B., Sullivan, P., McClellan, S., Finan, M. A., Reed, E., … Rocconi, R. P. (2012). CD44+/CD24- ovarian cancer cells demonstrate cancer stem cell properties and correlate to survival. *Clinical & Experimental Metastasis*, *29*(8), 939–948.

Meyers, R. M., Bryan, J. G., McFarland, J. M., Weir, B. A., Sizemore, A. E., Xu, H., … Tsherniak, A. (2017). Computational correction of copy number effect improves specificity of CRISPR-CAS9 essentiality screens in cancer cells. *Nature Genetics*, *49*, 1779–1784.

Moi, P., Chan, K., Asunis, I., Cao, A., & Kan, Y. W. (1994). Isolation of NF-E2-related factor 2 (Nrf2), a NF-E2-like basic leucine zipper transcriptional activator that binds to the tandem NF-E2/AP1 repeat of the beta-globin locus control region. *Proceedings of the National Academy of Sciences of the United States of America*, *91*(21), 9926–9930.

Momenimovahed, Z., Tiznobaik, A., Taheri, S., & Salehiniya, H. (2019). Ovarian cancer in the world: Epidemiology and risk factors. *International Journal of Women's Health*, *11*, 287–299.

Moreni-Bueno, G., Gamallo, C., Perez-Gallego, L., de Mora, J. C., Suarez, A., & Palacios, J. (2001). beta-Catenin expression pattern, beta-catenin gene mutations, and microsatellite instability in endometrioid ovarian carcinomas and syncronous endometrial carcinomas. *Diagnostic Molecular Pathology*, *10*(2), 116–122.

Nagahora, Z., Yamada, H., Kikuchi, S., Hakozaki, M., & Yano, A. (2017). Nrf2 activation by 5-lipoxygenase metabolites in human umbilical vascular endothelial cells. *Nutrients*, *9*(9), 1001.

Naser, M., Mehrnoosh, S., Hassan, E., Hajar, N., Mehdi, S., Mohsen, S., … Mehdi, A. (2016). A review on iron chelators in treatment of iron overload syndromes. *International Journal of Hematology-Oncology and Stem Cell Research*, *10*(4), 239–247.

Newcomer, M. E., & Brash, A. R. (2015). The structural basis for specificity in lipoxygenase catalysis. *Protein Science*, *24*(3), 298–309.

Nguyen, T., Nioi, P., & Pickett, C. B. (2009). The NRF2-antioxidant response element signalling pathway and its activation by oxidative stress. *Journal of Biological Chemistry*, *284*(20), 13291–13295.

Nieman, K. M., Kenny, H. A., Penicka, C. V., Ladanyi, A., Buell-Gutbrod, R., Zillhardt, M. R., … Lengyel, E. (2011). Adipocytes promote ovarian cancer metastasis and provide energy for rapid tumor growth. *Nature Medicine*, *17*(11), 1498–1503.

Nowicka, A., Marini, F. C., Solley, T. N., Elizondo, P. B., Zhang, Y., Sharp, H. J., … Klopp, A. H. (2013). Human Omental-Derived Adipose Stem Cells Increase Ovarian Cancer Proliferation, Migration and Chemoresistance. *PLoS One*, *8*(12), e81859.

Okuda, T., Otsuka, J., Sekizawa, A., Saito, H., Makino, R., Kushima, M., … Okai, T. (2003). p53 mutations and overexpression affect prognosis of ovarian endometrioid cancer but not clear cell cancer. *Gynecologic Oncology*, *88*(3), 318–325.

Paranscandola, J. (1974). Dinitrophenol and Bioenergetics: An Historical Persepctive. *Molecular and Cellular Biocemistry*, *5*(1–2), 69–77.

Petri, S., Korner, S., & Kiaei, M. (2012). Nrf2/ARE signaling pathway: Key mediator in oxidative stress and potential therapeutic target in ALS. *Neurology Research International*.

Pozdeyev, N., Yoo, M., Mackie, R., Schweppe, R. E., Tan, A. C., & Haugen, B. R. (2016). Intergrating heterogenous drug sensitivity data from cancer pharmacogenomic studies. *Oncotarget*, *7*(32), 51619–51625.

Ramus, S. J., & Gayther, S. A. (2009). The contribution of BRCA1 and BRCA2 to ovarian cancer. *Molecular Oncology*, *3*(2), 138.

Ratner, E., Lu, L., Boeke, M., Barnett, R., Nallur, S., Chin, L. J., … Weidhaas, J. B. (2010). A KRAS-variant in ovarian cancer acts as a genetic marker of cancer risk. *Cancer Research*, *70*(16), 6509–6515.

Reid, B. M., Permuth, J. B., & Sellers, T. A. (2017). Epidemiology of ovarian cancer: a review. *Cancer Biology & Medicine*, *14*(1), 9.

Ren, X., Duan, L., He, Q., Zhang, Z., Zhou, Y., Wu, D., … Ding, K. (2010). Identification of niclosamide as a new small-molecule inhibitor of the STAT3 signaling pathway. *ACS Medicinal Chemistry Letters*, *1*(9), 454–459.

Rosen, D. G., Yang, G., Liu, G., Mercado-Uribe, I., Chang, B., Xiao, X. (Sherry), … Liu, J. (2009). Ovarian cancer: pathology, biology, and disease models. *Frontiers in Bioscience : A Journal and Virtual Library*, *14*(6), 2089.

Rosencrans, W. M., Rajendran, M., Bezrukov, S. M., & Rostovtseva, T. K. (2021). VDAC regulation of mitochondrial calcium flux: From channel biophysics to disease. *Cell Calcium*, *94*, 102356.

Sato, H., Tamba, M., & Bannai, S. (1999). Cloning and expression of a plasma membrane cystine/glutamate exchange transporter composed of two distinct proteins. *Journal of Biological Chemistry*, *274*(17), 11455–11458.

Sato, M., Kusumi, R., Hamashima, S., Kobayashi, S., Sasaki, S., Komiyama, Y., … Sato, H. (2018). The ferroptosis inducer erastin irreversibly inhibits system xc- and synergizes with cisplatin to increase cisplatin's cytotoxicity in cancer cells. *Scientific Reports*, *8*(1).

Shin, D., Kim, E. H., Lee, J., & Roh, J. (2018). Nrf2 inhibition reverses resistance to GPX4 inhibitor-induced ferroptosis in head and neck cancer. *Free Radical Biology and Medicine*, *129*, 454–462.

Shintoku, R., Takigawa, Y., Yamada, K., Kubota, C., Yoshimoto, Y., Takeuchi, T., … Torii, S. (2017). Lipoxygenase-mediated generation of lipid peroxides enhances ferroptosis induced by erastin and RSL3. *Cancer Science*, *108*(11), 2187–2194.

Silva, I. A., Bai, S., McLean, K., Yang, K., Griffith, K., Thomas, D., … Buckanovich, R. J. (2011). Aldehyde dehydrogenase in combination with CD133 defines angiogenic ovarian cancer stem cells that portend poor patient survival. *Cancer Research*, *71*(11), 3991–4001.

Singer, G., Oldt, R., Cohen, Y., Wang, B. G., Sidransky, D., Kurman, R. J., & Shih, I. (2003). Mutations in BRAF and KRAS chacterize the development of low-grade ovarian serous carcinomas. *Journal of the National Cancer Institute*, *95*(6), 484–486.

Singer, G., Stohr, R., Cope, L., Dehari, R., Hartmann, A., Cao, D., … Shih, I. (2005). Patterns of p53 mutations separate ovarian serous borderline tumors an low- and high-grade carcinomas and provide support for a new model of ovarian carcinogenesis: a mutational analysis with immunohistochemical correlation. *American Journal of Surgical Pathology*, *29*(2), 218–224.

Skouta, R., Dixon, S. J., Wang, J., Dunn, D. E., Orman, M., Shimada, K., … Stockwell, B. R. (2014). Ferrostatins inhibit oxidative lipid damage and cell death in diverse disease models. *Journal of the American Chemical Society*, *136*(12), 4551–4556.

Stockwell, B. R., Friedmann Angeli, J. P., Bayir, H., Bush, A. I., Conrad, M., Dixon, S. J., … Zhang, D. D. (2017, October 5). Ferroptosis: A regulated cell death nexus

linking metabolism, redox Bibology, and disease. *Cell*, *171*, 273–285.

Sui, X., Zhang, R., Liu, S., Duan, T., Zhai, L., Zhang, M., … Xie, T. (2018). RSL3 drives ferroptosis through GPX4 inactivation and ros production in colorectal cancer. *Frontiers in Pharmacology*, *9*.

Sun, X., Ou, Z., Chen, R., Niu, X., Chen, D., Kang, R., & Tang, D. (2016). Activation of the p62-Keap1-NRF2 pathway protects against ferroptosis in hepatocellular carcinoma cells. *Hepatology*, *63*(1), 173–184.

Tan, D. S. P., & Kaye, S. (2007). Ovarian clear cell adenocarcinoma: a continuing enigma. *Journal of Clinical Pathology*, *60*(4), 355–360.

Tao, H., Zhang, Y., Zeng, X., Shulman, G. I., & Jin, S. (2014). Niclosamide ethanolamine-induced mild mitochondrial uncoupling improves diabetic symptoms in mice. *Nature Medicine*, *20*, 1263–1269.

Tarasov, A. I., Griffiths, E. J., & Rutter, G. A. (2012). Regulation of ATP production by mitochondrial Ca2+. *Cell Calcium*, *52*(1), 28–35.

Tenti, P., Aguzzi, A., Riva, C., Usellini, L., Zappatore, R., Bara, J., … Solcia, E. (1992). Ovarian mucinous tumors frequently express markers of gastric, intestinal, and pancreatobiliary epithelial cells. *Cancer*, *69*(8), 2131–2142.

Testa, U., Petrucci, E., Pasquini, L., Castelli, G., & Pelosi, E. (2018). Ovarian cancers: Genetic abnormalities, tumor heterogeneity and progression, clonal evolution and cancer stem cells. *Medicines*, *5*(1), 16.

Tonelli, C., Chio, I. I. C., & Tuveson, D. A. (2018). Transcriptional regulation by NRF2. *Antioxidants & Redon Signaling*, *29*(17), 1727–1745.

Turashvili, G., Grisham, R. N., Chiang, S., Delair, D. F., Park, K. J., Soslow, R. A., & Murali, R. (2018). BRAFV600E mutations and immunihistochemical expression of VE1 protein in low-grade serous neoplasms of the ovary. *Histopathology*, *73*(3), 438–443.

Vaughan, S., Coward, J. I., Bast, R. C., Berchuck, A., Berek, J. S., Brenton, J. D., … Balkwill, F. R. (2011, October 23). Rethinking ovarian cancer: Recommendations for improving outcomes. *Nature Reviews Cancer*, *11*, 719–725.

Yaginuma, Y., & Westphal, H. (1992). Abnormal structure and expression of the p53 gene in human ovarian carcinoma cell lines. *Cancer Research*, *52*(15).

Yagoda, N., Von Rechenberg, M., Zaganjor, E., Bauer, A. J., Yang, W. S., Fridman, D. J., … Stockwell, B. R. (2007). RAS-RAF-MEK-dependent oxidative cell death involving voltage-dependent anion channels. *Nature*, *447*(7146), 864–868.

Yang, W. S., Kim, K. J., Gaschler, M. M., Patel, M., Shchepinov, M. S., & Stockwell, B. R. (2016). Peroxidation of polyunsaturated fatty acids by lipoxygenases drives ferroptosis. *Proceedings of the National Academy of Sciences of the United States of America*, *113*(34), E4966–E4975.

Yang, W. S., & Stockwell, B. R. (2008). Synthetic lethal screening identifies compounds activating iron-dependent, nonapoptotic cell death in oncogenic-RAS-harboring cancer cells. *Chemistry and Biology*, *15*(3), 234–245.

Yap, T. A., Shandu, S. K., Carden, C. P., & de Bono, J. S. (2011). Poly(ADP-ribose) poymerase (PARP) inhibitors: Exploiting a synthetic lethal strategy in the clinic. *CA: A Cancer Journal for Clinicians*, *61*(1), 31–49.

Yin, H., Xu, L., & Porter, N. A. (2011). Free radical lipid peroxidation: Mechanisms and analysis. *Chemical Reviews*, *111*(10), 5944–5972.

Zhang, J., Guo, X., Chang, D. Y., Rosen, D. G., Mercado-Uribe, I., & Liu, J. (2012). CD133 expression associated with poor prognosis in ovarian cancer. *Modern Pathology*, *25*(3), 456–464.

Zhang, Y., Cao, L., Nguyen, D., & Lu, H. (2016). TP53 mutations in epithelial ovarian cancer. *Translational Cancer Research*, *5*(6), 650–663.

Zilka, O., Shah, R., Li, B., Friedmann Angeli, J. P., Griesser, M., Conrad, M., & Pratt, D. A. (2017). On the mechanism of cytoprotection by Ferrostatin-1 and Liproxstatin-1 and the role of lipid peroxidation in Ferroptotic cell death. *ACS Central Science*, *3*(3), 232–243.